ABSTRACT

GREGORY, JOSEPH WILLIAM. Identification of Statistical Energy Analysis Parameters from Measured Data. (Under the Direction of Dr. Richard F. Keltie)

An approach for identifying statistical energy analysis (SEA) parameters from experimental investigation is presented. Specifically, a power flow realization method (PRM) and statistical energy analysis model improvement (SMI) technique using transient time-domain vibration measurements are derived. The efforts are refined and validated using a range of test simulations, and then with true physical tests conducted on both simple and complex structures. Experimentation is also used to define the necessary input power measurements, response energy measurements, and data processing techniques necessary for successful PRM/SMI.

It is found that utilization of time domain data allows for an over-determined power balance providing favorable numerical conditions for the identification. In fact, it is observed that a full matrix of measured inputs and outputs is not necessarily required for successful identification as is the case with current methods. Additionally, useful insight into system dimensionality is obtained during the identification process. Furthermore, it is found that the procedure indicates true parameters that are easily distinguished from those associated with noise in the data and, hence, is well suited for this application. Results indicate that the methodology has the potential to significantly enhance standard SEA procedures.

IDENTIFICATION OF STATISTICAL ENERGY ANALYSIS PARAMETERS FROM MEASURED DATA

By

JOSEPH WILLIAM GREGORY

A thesis submitted to the Graduate Faculty of

North Carolina State University

in partial fulfillment of the

requirements for the Degree of

Doctor of Philosophy

DEPARTMENT OF MECHANICAL AND AEROSPACE ENGINEERING

Raleigh

2002

APPROVED BY:

_____	_____
Dr. Harvey Johnson Charlton	Dr. Charles E. Hall, Jr.
_____	_____
Dr. Robert T. Nagel	Dr. Richard F. Keltie Chairman of Advisory Committee

To Ginger

BIOGRAPHY

Joseph William Gregory was born on February 26, 1965 in Newburgh, New York. He graduated in 1983 from the Maple Shade High School in Maple Shade, New Jersey. He received his Bachelor of Science Degree in Mechanical Engineering in 1989 from the University of Massachusetts-Lowell. In 1991, he received his Master of Science Degree in Mechanical Engineering also from the University of Massachusetts-Lowell. The specific focus of his graduate work towards the Master of Science Degree was in acoustics, general vibrations, modal analysis and solid mechanics. Joseph was employed from 1991-1993 for Lockheed Engineering and Sciences, Co. in Hampton, Virginia as a member of the Control-Structures-Interaction Team at the NASA Langley Research Center (Spacecraft Dynamics Branch). From 1994-1997 he was employed at the Electric Boat Division of General Dynamics were he worked in the Structural Acoustics Section and the Advanced Concepts Section. In August 1998, he married Ginger Dobbins. He began doctoral study at North Carolina State University in the fall semester of 1998. Throughout the course of this effort, Joseph worked at the Center for Sound and Vibration under the direction of Dr. Richard F. Keltie and received the degree of Doctor of Philosophy in Mechanical Engineering in the spring semester of 2002.

ACKNOWLEDGEMENTS

The author acknowledges the primary sponsor of this work, the National Science Foundation under Grant No. CMS-9908326. Sincere thanks are given to Vibro-Acoustic Sciences, Inc. for use of their software, Ford Motor Company for their generous donation of a vehicle used as a test-bed in this effort, and the NASA Langley Research Center for use of the system identification software, SOCIT.

Grateful acknowledgment is given to Dr. Richard F. Keltie who has come to be the author's mentor, friend, and inspiration to pursue research challenges. Gratitude is also extended to the members of the advisory committee: Dr. Harvey Johnson Charlton, Dr. Charles E. Hall Jr., and Dr. Robert T. Nagel.

Deep gratitude is given to the author's family for their encouragement, and, finally, to Eric U. and the other friends of Bill W. for, without their help, none of this would be at all possible.

TABLE OF CONTENTS

LIST OF TABLES

LIST OF FIGURES

1 INTRODUCTION

1.1 BACKGROUND

1.1.1 STRUCTURAL DYNAMICS

The subject of structural dynamics involves the study of the response of structures due to dynamic loading. Over the last sixty years, structural dynamic analysis and testing has been successfully incorporated into many engineering efforts including the design of aircraft, spacecraft, automobiles, surface ships, submarines, bridges, dams, buildings, and many others. There are typically three phases involved with a structural dynamic investigation as diagrammed in Figure 1.1. These are: design, analysis, and testing. More recently, additional consideration is sometimes given to the evaluation of control strategies and to the use of a concurrent rather than sequential approach to the investigation.

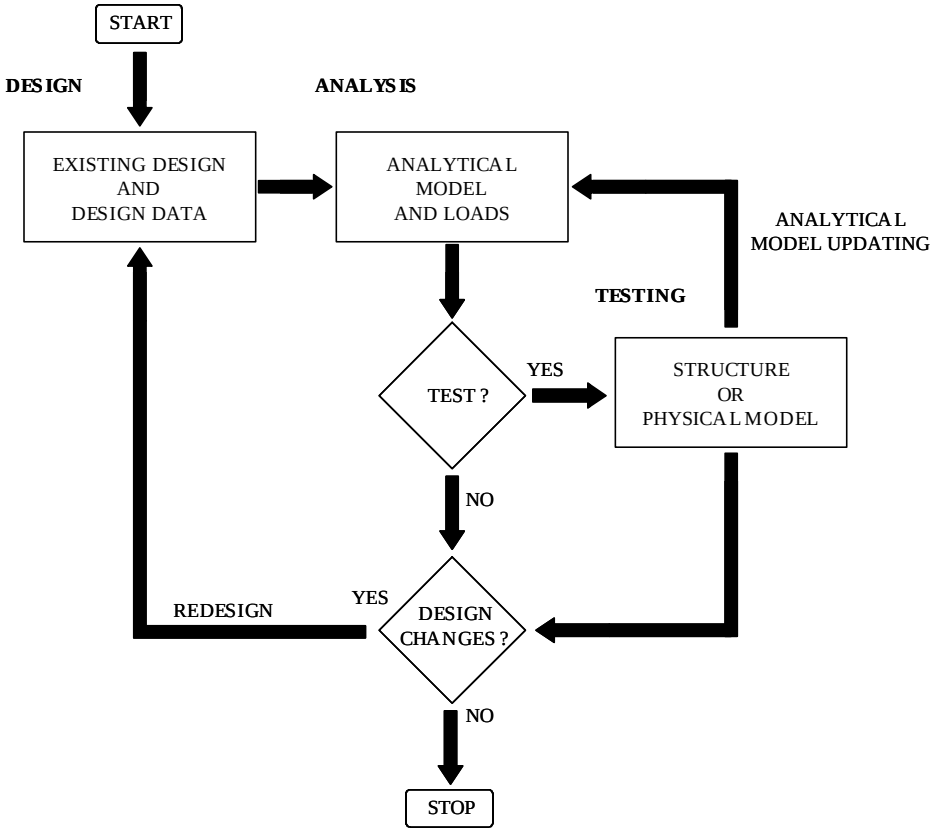

Figure 1.1 Structural Dynamic Investigation

Often, there exist design problems that require a structural dynamic investigation to be linked to an associated structural acoustic study. In these situations, the interaction between structural motion and a connected acoustic field is a key consideration. As a result, the frequency range of interest may be very wide and, in fact, may include the entire bandwidth of human hearing, 20 Hz – 20,000 Hz. Current analysis techniques are applicable only in certain frequency ranges such that assumptions associated with the specific approach are satisfied. As a result, it is usually necessary to divide the analysis into three parts: the low frequency region, the middle frequency region, and the high frequency region. Note, a strict boundary between the regions does not exist and depends, more specifically, on the number of modes that exist in the range of the analysis applied as well as the ratio of the size of the structure to the wavelength of vibration.

At present, it is usually understood that the solution of low frequency problems can be successfully obtained using computational methods. In fact, considerable success has been achieved using Finite Element Analysis (FEA) and the Boundary Element Analysis (BEA) over a wide range of structures and a wide range of geometry from very simple to extremely complex. This result is usually attributed to the extensive research that has been conducted in these areas and to the continued advance of the digital computer. Examples of FEA models are shown in Figure 1.2 and Figure 1.3.

The extension of these computational methods to middle and higher frequencies is problematic. In general, low frequency dynamics involve long wavelengths while high

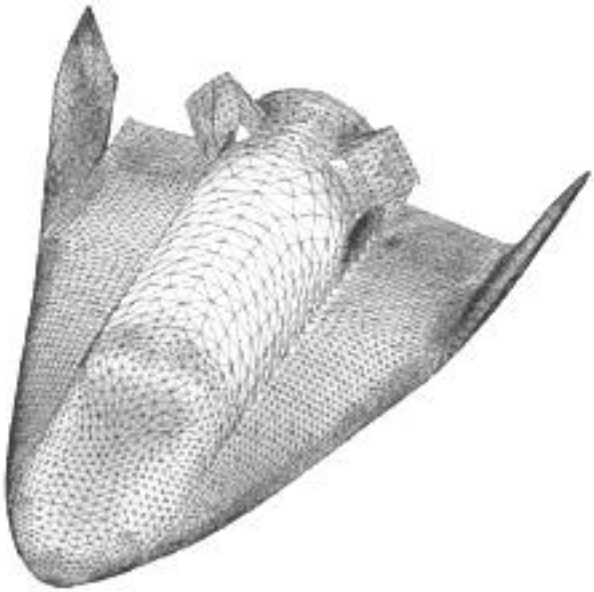

Figure 1.2 FEA Model of Spacecraft Body (National Aerospace Laboratory, NLR)

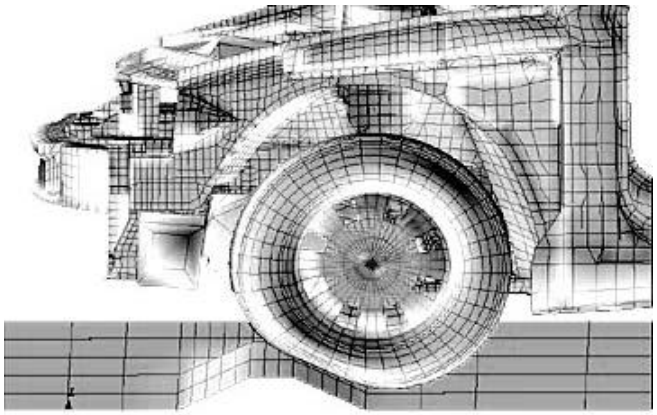

Figure 1.3 FEA Model of Automobile Front End (MSC.Software)

frequency dynamics are associated with short wavelengths. This implies that low frequency models require a relatively coarse breakup or mesh while high frequency models would require a fine mesh. In essence, the extension of the analysis frequency range of a model requires that the mesh be refined at the expense of increasing model size and the subsequent analysis time and expense. Not only does FEA/BEA become computationally unwieldy as frequencies increase, the solution results become less reliable due to uncertainty with respect to the structural properties. Specifically, natural frequencies, modal amplitudes, and damping become highly sensitive to small variations in structural detail and boundary conditions with increasing mode order. Furthermore, for most structures, response at increasingly higher frequencies results from a superposition of an increasingly larger number of modes. Eventually, at high enough frequencies, higher order modes tend to overlap or fall

within one damping bandwidth of one another making it difficult to be certain of even the amount or ordering of natural frequencies. As a result, it has been observed that even similar structural dynamic and structural acoustic systems can exhibit unpredictably different behavior [1,2].

Methods exist for overcoming these difficulties with respect to decreasing the computational demand and increasing the reliability of predictions. These include [2,3]:

- Statistical Energy Analysis (SEA)
- Asymptotic Modal Analysis (AMA)
- General Energy Formulation Method (GEFM)
- Smooth Energy Formulation (SEM)
- Envelope Energy Modeling (EEM)
- Envelope-Phase Energy Modeling (EPHEM)
- Complex Envelope Displacement Analysis (CEDA)
- Mobility Energy Flow Analysis (MEFA)

Some of the listed items are, indeed, similar. Other techniques, including hybrid approaches, do also exist. Statistical Energy Analysis is the specific focus of this investigation; however, the other methods in this list are summarized in Section 1.1.2.

Structural dynamic testing is used most frequently to confirm and update analytical models. In addition, testing can often be utilized to ensure that specifications are met and to provide other information such as details pertaining to loading and constraints on motion. Dynamic scale model tests are often used to confirm analytical models and verify design strategy prior to the construction of a full-scale prototype. A scale model of a propeller being tested in a variable pressure water tunnel is shown in Figure 1.4. Note, a laser doppler sensor measures velocities and hydrophones (not shown) measure flow noise.

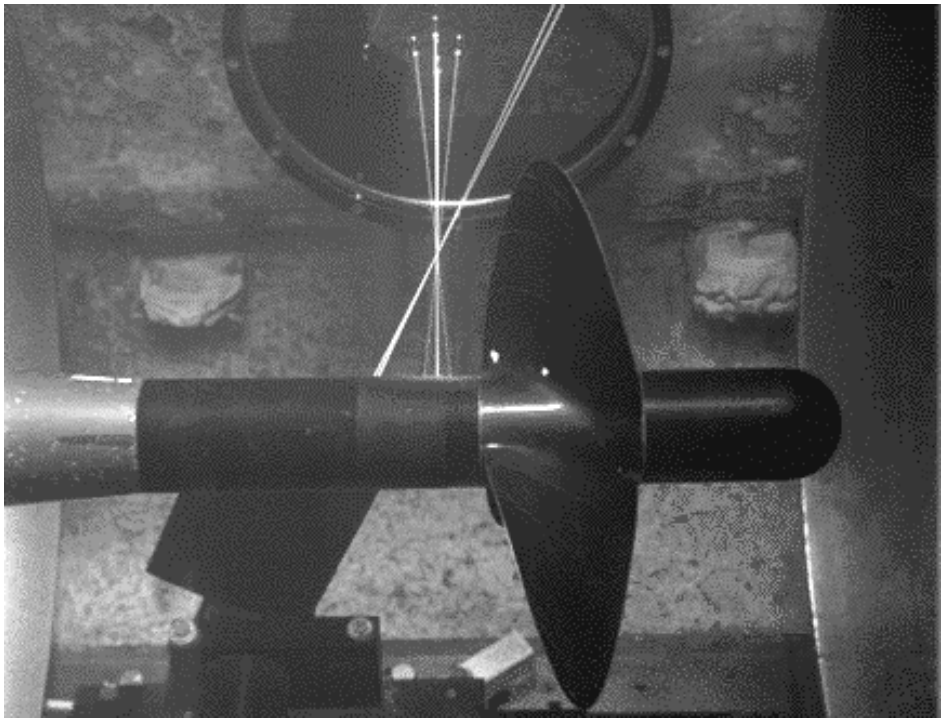

Figure 1.4 Scale Model Test of a Propeller (Naval Surface Warfare Center – Carderock Division)

Full scale testing is also a regular part of a structural dynamic investigation. Ground vibration testing, for example, of the F-22 Raptor fighter aircraft is shown in Figure 1.5.

Figure 1.5 Ground Vibration Test of F-22 Aircraft at Edwards Air Force Base (US Air Force Photo)

Test methods and model correlation/improvement techniques for the low frequency regime are well established and considered, by most, to yield reliable results (even for complex structures) given proper planning and the application of careful, appropriate measurement techniques. Although significant progress has been achieved, a similar reliability and strong history does not exist with respect to the measurement of power and energy quantities at high frequencies nor with respect to SEA model correlation/improvement techniques.

1.1.2 ANALYSIS METHODS

The Statistical Energy Analysis (SEA) method addresses the predictive difficulty by employing a statistical description of the structural and the acoustic parameters. The system is represented by a set of coupled idealized subsystems. Allowing for statistical variation, the parameters of each subsystem are the result of averaging with respect to one of the following: samples of like systems, time, or a frequency band of interest. Hence, the mathematics of the approach is simplified. Analogous to a thermodynamic energy balance, specifically, a set of coupled linear power balance equations is used to represent power dissipation and transfer from the subsystems, which make up the global system. The main assumption is that the power flow between coupled subsystems is proportional to the energy difference in their respective modal energies. Examples of typical idealized subsystems include: beams, plates, shells, cylinders, and various acoustic spaces. More precisely, an SEA subsystem is chosen to represent one wave type (or mode type). Hence, a beam, for example, typically includes a bending wave subsystem, a compression wave subsystem, and a torsion wave subsystem. Furthermore, shear effects can also be represented. A low frequency limit exists in that global modes (typical at lower frequencies) that extend across subsystems are not

represented. Additionally, for band averaging, statistical variance is high since the number of modes in a particular bandwidth of interest at lower frequencies is usually relatively low. For some subsystems, a high frequency limit exists at which a wavelength becomes close to the length scale of a defining section such as plate/shell thickness or beam thickness.

Early efforts applied to the asymptotic behavior of dynamic systems were made by Powell [4] and Skudrzyk [5]. The Asymptotic Modal Analysis (AMA) method, developed by Dowell, Kubota, and others [6,7] is a hybrid of modal analysis and SEA. The approximation occurs by neglecting individual modal character via, specifically, utilization of the asymptote of a subsystem's response due to the superposition of a large number of modes. AMA, unlike SEA, can also predict local areas (within a subsystem) of response amplification. A space averaged AMA formulation, in fact, reduces to the SEA formulation therefore providing a means of systematically examining SEA assumptions. However, with AMA, it is assumed that the analysis frequency band is small enough such that modal character can be considered constant yet wide enough to include many modes. At increasing frequency as modal density increases for most systems, this can result in a requirement for increasingly smaller analysis bands thus complicating the investigation. Furthermore, published data concerning the application of AMA to complex systems is relatively small compared to that for SEA.

The General Energy Formulation Method (GEFM) was developed by Le Bot, Jezequel, and others [8-10] for the prediction of the steady state response of one-dimensional structures. Basically, an exact energy flow formulation from low to high frequency is provided by

representing complex, active and reactive, energy in terms of the total (sum of kinetic and potential) and the Lagrangian (difference between kinetic and potential) densities. Note that, for the SEA approach, since the kinetic and potential energies are assumed equal, the Lagrangian is zero. The advantage of the technique is that spatial variation in the response within a subsystem can be predicted and that different types of boundary conditions can be incorporated. A drawback is that the energy formulation becomes a more mathematically difficult problem than the equation of motion in terms of a displacement variable. For example, for a Bernoulli-Euler beam, instead of a single fourth-order partial differential equation of motion, the energy formulation requires two eighth-order partial differential equations. To overcome some of these difficulties, Le Bot and Jezequel [11] formulated the Simple or Smooth Energy Formulation (SEF) by introducing a smoothing function and performing spatial averaging on a single wavelength basis. Their results, for one-dimensional systems, reduce to the heat (or diffusion) equation lending some credibility to the SEA thermal analogy. Le Bot and Luzzato [12] attempt to extend the SEF model to two-dimensional systems; however, their results, in this case, do not reduce to the heat equation. The extension of the GEM method to more complex structures requires more research. Specifically, energy derivations for higher order structures (plates, shells, etc.) and the development of a method of analyzing coupled structures seem necessary.

Further drawbacks of the described energy methods such as non-linear terms and oscillation of the energy density at high frequencies (not in agreement with the thermal analogy) motivated Carcaterra and Sestieri [13] to formulate the Energy Envelope Method (EEM), which simplifies the energy density formulation by enveloping via Hilbert transform. The

authors [14] also developed the Energy Phase Envelope Method (EPHEM), which is EEM with the addition of an energy phase variable to account for energy discontinuity at boundaries. Several features make EEM and EPHEM attractive. It shows similar behavior to the general energy methods yet eliminates the oscillatory energy density problem and, therefore, allows the use of an existing low frequency FEA model to be used in the EEM model generation. However, published information regarding applications of this method to complex systems is limited.

Carcaterra and Sestieri [15] also developed the Complex Envelope Displacement Analysis (CEDA) technique for one-dimensional systems. Unlike EEM and EPHEM, which are energy formulations, CEDA is formulated by transforming the displacement variable by an enveloping operator. The results are favorable; however, an approach that can handle higher dimensional problems has yet to be presented.

The Mobility Energy Flow Analysis (MEFA) is another modeling method where the global system is divided into subsystems. In this case, energy flow is formulated in terms of the input and transfer mobility functions of the subsystems. The method has its origins in an investigation by Pinnington and White [16] who examined energy transmission in a system comprised of a mass that was spring coupled to a finite beam. The authors were able to obtain expressions for mean and peak energy flows. Additionally, they observed that for frequency average response, the mobility for a beam of infinite extent could be equivalently used to represent the mobility of the finite beam. The method was extended to energy transmission between elements of connected structures, modeled with FEA, by Cushieri [17].

McColum and Cushieri [18] report success using MEFA to represent two coupled plates. They observed that, compared to FEA at high frequency, a computationally simpler model could be formed while still maintaining solution accuracy. The advantage of MEFA, when compared to SEA is that the spatial dependence of the response is provided. Furthermore, there is no need to perform frequency band averaging. Although MEFA appears useful in the middle frequency regime, more effort is required if the technique is to be applied reliably on complex structures.

1.1.3 CONCLUSIONS

Reliable, established methods for the prediction of structural dynamic and structural acoustic response exist only with respect to the low frequency regime. The use of SEA for the prediction of response in the middle to higher frequency regime also has a strong history, dating back to the early 1960's. However, the method was applied to only a narrow range of disciplines, which include aerospace, shipbuilding, and building acoustics. Newer applications of SEA and the application of SEA alternatives, having only been recently studied and, as of yet, have not achieved a similar level of predictive reliability with respect to complex systems. As Sestieri [2] concludes, neither SEA nor the alternatives has reached full acceptance. Similarly, trusted techniques for measurement and analytical/computational model correlation and improvement using measured data also exist only with respect to the low frequency regime. Considerable effort has been made in high frequency methods, yet it is still considered to be in its infancy. In this dissertation, the SEA framework is used because of its strong history, its successes, and fervent industry interest evident from the increasing demand and popularity of the commercially available SEA software.

Furthermore, it is believed that advances related to experimental methods would benefit both established and newer industrial applications of SEA by providing physical insight into modeling techniques and assumptions.

1.2 PREDICTIVE SEA

1.2.1 HISTORY

Statistical Energy Analysis was developed in the early 1960's to address the need to predict the response of launch vehicles to rocket noise and overcome the limitations of computational methods at that time [19]. Early SEA resulted from a collaboration of two independent efforts by Lyon and Maidanik [20] and Smith [21] where the energy exchange of coupled oscillators was examined. This was extended to a structural acoustic analysis of elastic panels by Maidanik [22], Lyon [23], and Manning and Maidanik [24]. SEA applied to connected elastic structures was examined by Lyon and Eichler [25] and Scharton [26]. Significant theoretical refinements, extension to unexplored systems, and the development of complementary methods has occurred. However, the basic SEA theory has changed little since its initial formulation.

1.2.2 COUPLED SYSTEMS

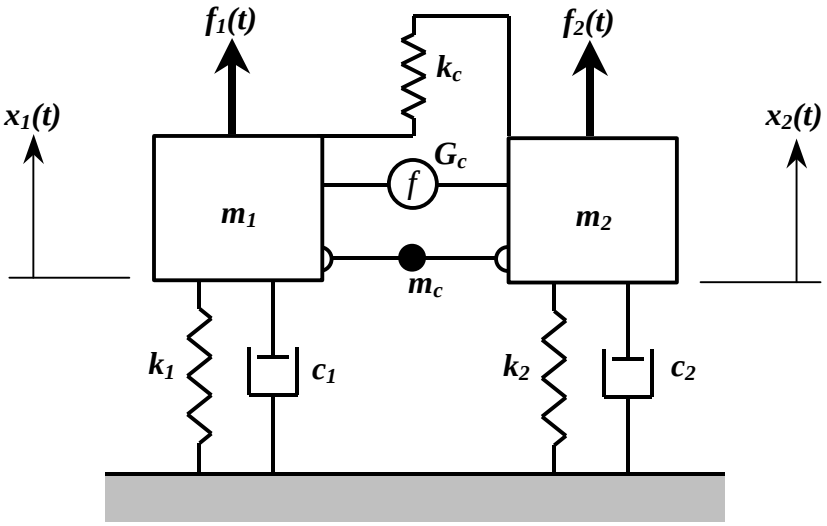

Figure 1.6 Coupled Oscillators

In 1962, Lyon and Maidanik [20] derived what has come to be the basis for the predictive SEA method. Specifically, an expression for the power flow between linearly coupled oscillators was obtained. Two linear oscillators, each comprising a single degree of freedom system with mass, a force-displacement proportional spring, and force-velocity proportional viscous damping, are coupled via spring, mass, and gyroscopic elements as shown in Figure 1.6. The spring constant for the coupling is given by k_c, the mass of the coupling is given by m_c, and the force-velocity constant of proportionality for the gyroscopic coupling is given by G_c.

When subjected to steady state forces, $f_1(t)$ and $f_2(t)$, that are independent stationary random inputs of constant spectral density (white noise), the power flow, P_{12}, between oscillator 1 and oscillator 2 is:

$$P_{12} = b\left(E_1 - E_2\right) \tag{1.1}$$

where, E_1 is the energy of oscillator 1, E_2 is the energy of oscillator 2, and b is a constant of proportionality in terms of the system parameters. Specifically, for this system, b is:

$$b = \frac{m^2\left[D_1 w_2^4 + D_2 w_1^4 + D_1 D_2\left(D_1 w_2^2 + D_2 w_1^2\right)\right] + \left(g^2 + 2mk\right)\left(D_1 w_2^2 + D_2 w_1^2\right) + k^2\left(D_1 + D_2\right)}{\left(1 - m^2\right)\left[\left(w_1^2 - w_2^2\right)^2 + \left(D_1 + D_2\right)\left(D_1 w_2^2 + D_2 w_1^2\right)\right]} \tag{1.2}$$

where,

$$m = \tfrac{1}{4} m_c \sqrt{\left(m_1 + \tfrac{1}{4} m_c\right) \Big/ \left(m_2 + \tfrac{1}{4} m_c\right)} \qquad \text{(1.3a - e)}$$

$$g = G_c \Big/ \sqrt{\left(m_1 + \tfrac{1}{4} m_c\right)\left(m_2 + \tfrac{1}{4} m_c\right)}$$

$$k = k_c \Big/ \sqrt{\left(m_1 + \tfrac{1}{4} m_c\right)\left(m_2 + \tfrac{1}{4} m_c\right)}$$

$$D_i = c_i \Big/ \left(m_i + \tfrac{1}{4} m_c\right)$$

$$w_i^2 = \left(k_i + k_c\right) \Big/ \left(m_i + \tfrac{1}{4} m_c\right)$$

Note that D_i are the modal half power bandwidths and w_i are the blocked natural frequencies computed by constraining the motion of the oscillator not being evaluated.

The following points regarding the power flow result can be made:

1) The power flow is proportional to the difference in the decoupled energies of the oscillators.
2) The power flow is proportional to the difference in the actual energies of the oscillators.
3) The constant of proportionality, b, is dominated by the resonant interaction of the two resonators.
4) b is positive definite implying that the power flows from the more energetic to the less energetic oscillator.
5) b is symmetric with respect to the system parameters. Therefore, the power flow is reciprocal.

Note that the decoupled (blocked) energies are defined by constraining the motion of the oscillator that is not being evaluated. Specifically, for oscillator i the decoupled energy is:

$$E_i = \frac{pS_{f_i}}{D_i\left(m_i + \tfrac{1}{4} m_c\right)} \qquad (1.4)$$

where S_{fi} is the power spectral density of the force, f_i, applied to oscillator i. Remarkably, the power flow proportionality exists also with respect to the actual (coupled) mean total energy, actual mean kinetic energy, or actual mean potential energy. Furthermore, the power flow is dominated by the resonant interaction between the oscillators and is largest when the blocked

natural frequencies, w_1 and w_2, are within a damping bandwidth of one another as shown in Figure 1.7.

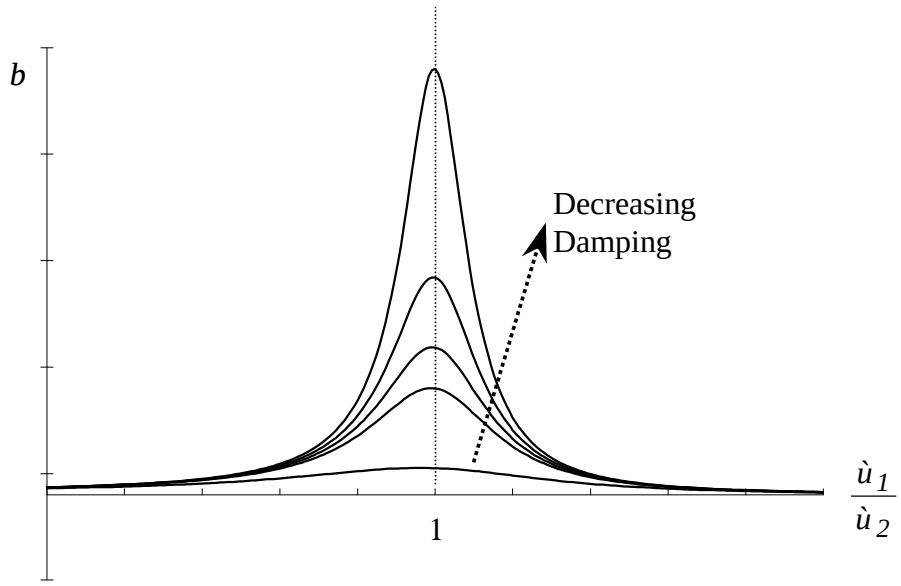

Figure 1.7 Coupling Coefficient

A more detailed depiction of the magnitude of the coupling coefficient as a function of the natural frequency separation as well as the damping bandwidth is shown in Figure 1.8.
As put forth by Lyon [28], the coupled oscillator results can readily be extended to the power flow between coupled multiple degree of freedom subsystems. The approach is to consider the structural dynamics of each subsystem in terms of its respective modal dynamics assuming subsystem 1 is comprised of N_1 similar modes and subsystem 2 is comprised of N_2 similar modes over an analysis frequency interval Dw.

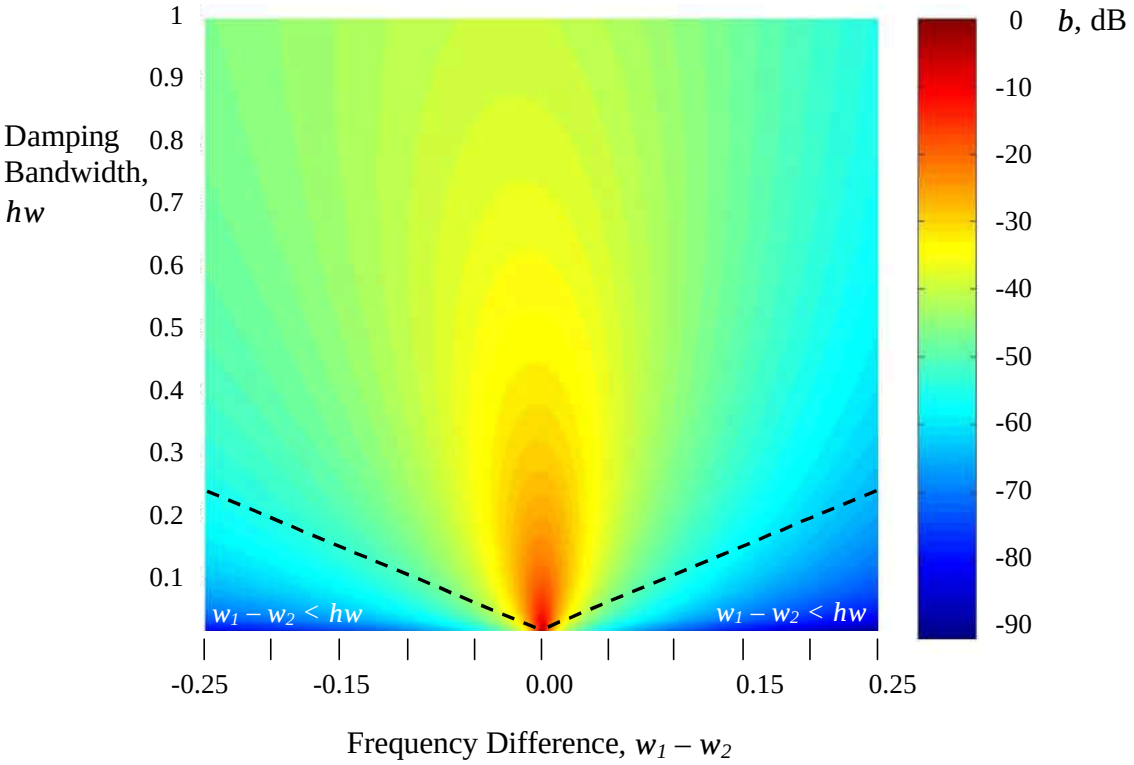

Figure 1.8 Coupling Coefficient Magnitude

The coupling between the two systems is then represented by the interactions of all of the possible mode pairs as shown in Figure 1.9.

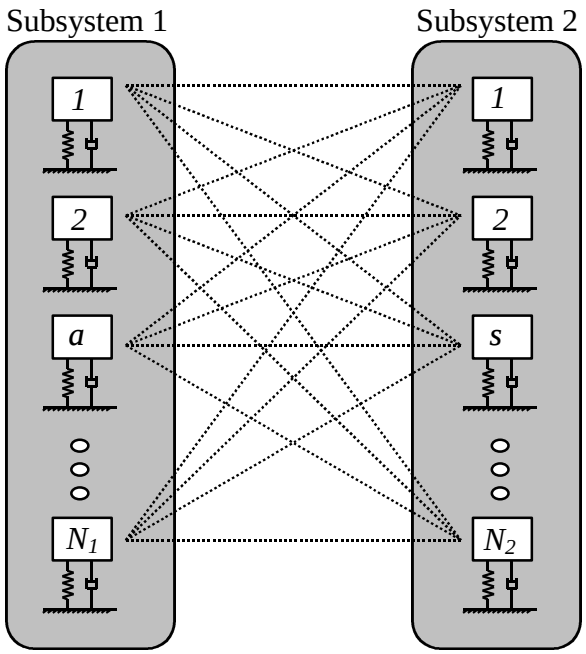

Figure 1.9 Mode Pair Interactions of Coupled Dynamic Systems

The fundamental SEA power flow proportionality can be applied to each mode pair to determine its contribution to the total power flow provided several assumptions are met:

1) The modes of each subsystem have a uniform distribution of natural frequencies over the bandwidth, *Dw*.

2) There is an equipartition of energy over all the modes of each subsystem over *Dw*.

3) The modal amplitudes are incoherent (The modes of a particular subsystem are orthogonal and the inputs are independent) over *Dw*.

4) The damping of the modes in a subsystem is equal over *Dw* (this is merely convenient).

The power flow between mode a of subsystem 1 and mode s of subsystem 2 is the fundamental result in equation 1.1:

$$P_{as} = \langle b_{as} \rangle_{w_a w_s} \left(\frac{E_1}{N_1} - \frac{E_2}{N_2} \right) \tag{1.5}$$

where, the coupling coefficient is an average with respect to the frequencies w_a and w_s. Additionally, since the modes within a subsystem are equally energetic, each mode has a total energy of E_i/N_i. The total power flow from all N_1 modes of subsystem 1 to mode s of subsystem 2 is:

$$P_{1s} = \langle b_{as} \rangle_{w_a w_s} N_1 \left(\frac{E_1}{N_1} - \frac{E_2}{N_2} \right) \tag{1.6}$$

The total power flow from all N_1 modes of subsystem 1 to all N_2 modes of subsystem 2 is:

$$P_{12} = \langle b_{as} \rangle_{w_a w_s} N_1 N_2 \left(\frac{E_1}{N_1} - \frac{E_2}{N_2} \right) \tag{1.7}$$

By defining the coupling loss factors, h_{12} and h_{21}, the overall power flow can be written in its most familiar form:

$$P_{12} = w h_{12} E_1 - w h_{21} E_2 \tag{1.8}$$

where, $h_{12} \circ (1/w) \langle b_{as} \rangle N_2$ and $h_{21} \circ (N_1/N_2) h_{12}$.

The previously listed assumptions and the computation of an average coupling proportionality make up a statistical description of the relevant parameters. Indeed, the word "statistical" in the Statistical Energy Analysis method refers to this. It does not refer to the other reference to a statistical approach, inherent in the choice of white noise inputs. In fact, statistically random forcing is not strictly necessary; even pure tone inputs can be analyzed provided a significant number of modes participate in the response [28].

1.2.3 POWER BALANCE

When applied to a network of coupled subsystems, the fundamental SEA power flow relationship can be used to construct a set of steady state power balance equations. For example, a three subsystem SEA model is diagrammed in Figure 1.10.

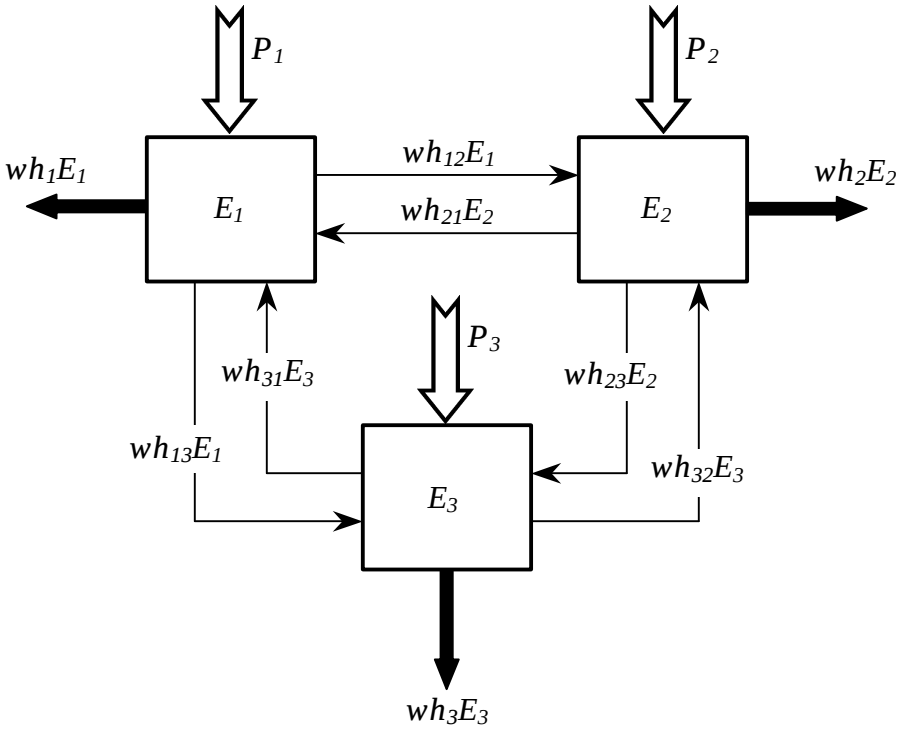

Figure 1.10 Three Subsystem SEA Model

Here, the input powers are P_i, the mean energies of the respective subsystems are E_i, the damping loss factors are h_i, the coupling loss factors are h_{ij}, and the center frequency of the analysis band is w. By considering conservation of energy for each of the three subsystems, three power balance equations can be written:

$$\begin{aligned} w(h_1 + h_{12} + h_{13})E_1 - wh_{21}E_2 - wh_{31}E_3 &= P_1 \\ w(h_2 + h_{21} + h_{23})E_2 - wh_{12}E_1 - wh_{32}E_3 &= P_2 \\ w(h_3 + h_{31} + h_{32})E_3 - wh_{13}E_1 - wh_{23}E_2 &= P_2 \end{aligned} \qquad (1.9a - c)$$

In matrix form, this is:

$$w\begin{bmatrix} (h_1 + h_{12} + h_{13}) & -h_{21} & -h_{31} \\ -h_{12} & (h_2 + h_{21} + h_{23}) & -h_{32} \\ -h_{13} & -h_{23} & (h_3 + h_{31} + h_{32}) \end{bmatrix} \begin{Bmatrix} E_1 \\ E_2 \\ E_3 \end{Bmatrix} = \begin{Bmatrix} P_1 \\ P_2 \\ P_3 \end{Bmatrix} \qquad (1.10)$$

Finally, for a general SEA model comprised of m subsystems, the set of power balance equations becomes:

$$w\begin{bmatrix} h_1 + \sum_{j\neq 1} h_{1j} & -h_{21} & \cdots & -h_{m1} \\ -h_{12} & h_2 + \sum_{j\neq 2} h_{2j} & \cdots & -h_{m2} \\ \vdots & \vdots & \ddots & \vdots \\ -h_{1m} & -h_{2m} & \cdots & h_m + \sum_{j\neq m} h_{mj} \end{bmatrix} \begin{Bmatrix} E_1 \\ E_2 \\ \vdots \\ E_m \end{Bmatrix} = \begin{Bmatrix} P_1 \\ P_2 \\ \vdots \\ P_m \end{Bmatrix} \qquad (1.11)$$

This can be more conveniently written using a symbolic notation for the matrices:

$$w[H]\{E\} = \{P\} \qquad (1.12)$$

where, $[H]$ is the matrix of loss factors, $\{E\}$ is the vector of subsystem energies, and $\{P\}$ is the vector of subsystem input powers. Note that the loss factor matrix is not symmetric. As

a result, power flow is not reciprocal with respect to the total subsystem energies. However, the system can be made symmetric by multiplying each column of the loss factor matrix by the number of modes in the analysis band for the associated subsystem. It then becomes necessary to normalize the total energies by their respective number of modes. The power balance becomes:

$$w\begin{bmatrix} N_1\left(h_1+\sum_{j\neq 1}h_{1j}\right) & -N_2h_{21} & \cdots & -N_mh_{m1} \\ -N_1h_{12} & N_2\left(h_2+\sum_{j\neq 2}h_{2j}\right) & \cdots & -N_mh_{m2} \\ \vdots & \vdots & \ddots & \vdots \\ -N_1h_{1m} & -N_2h_{2m} & \cdots & N_m\left(h_m+\sum_{j\neq m}h_{mj}\right) \end{bmatrix}\begin{Bmatrix} E_1/N_1 \\ E_2/N_2 \\ \vdots \\ E_m/N_m \end{Bmatrix}=\begin{Bmatrix} P_1 \\ P_2 \\ \vdots \\ P_m \end{Bmatrix} \quad (1.13)$$

Since $N_ih_{ij} = N_jh_{ji}$, this system is, indeed, symmetric. The implication, here, is that although reciprocity does not exist with respect to the total energies, power flow reciprocity does exist with respect to the subsystem modal energies, E_i/N_i. Hence, power flows from a subsystem of higher modal energy to a subsystem of lower modal energy. Using symbolic notation, the symmetric power balance can be written:

$$w[K]\{e\}=\{P\} \quad (1.14)$$

where, $[K]$ is the symmetric coupling matrix and $\{e\}$ is a vector of the modal energies. The use of the power balance for predictive SEA is straightforward. A disturbance to the dynamic system, quantified by input power, is multiplied by a computed inverse of the coupling matrix to yield response energies:

$$\{e\} = \frac{1}{w}[K]^{-1}\{P\} \tag{1.15}$$

In practice, the explicit inverse is not usually computed, however. A more computationally efficient method, such as Gauss elimination, is usually implemented.

There exists an especially desirable feature of both the symmetric and non-symmetric forms of the coupling matrix. Specifically, since the inner product $\{u\}^T[K]\{u\}$ (Note, the transpose operator suffices since $[K]$ is real and symmetric) is greater than zero for all $\{u\} \neq \{0\}$, then $[K]$ is positive definite; see, for example, Morse and Feshbach [29]. Furthermore, $[K]$ is diagonally dominant for most lightly coupled systems. As a result, the inversion of the coupling matrix is very well conditioned and relatively insensitive to coupling loss factor error. To illustrate, the quadratic form, $Q(u) = \{u\}^T[K]\{u\}$ is computed for a two-subsystem SEA model:

$$Q(u) = N_1 h_1 u_1^2 + N_2 h_2 u_2^2 + N_1 h_{12}(u_1 - u_2)^2 \tag{1.16}$$

where,

$$\{u\} = \begin{Bmatrix} u_1 \\ u_2 \end{Bmatrix} \tag{1.17}$$

Clearly, $Q(u)$ is greater than zero for any non-trivial u_1 and u_2 indicating that the coupling matrix is positive definite. Additionally, by considering the quadratic form, $Q(u)$, as a radial map to each point on a sphere $\|u\| = 1$, see Figure 1.11, $Q(u)$ is seen to resemble an ellipsoid which also occurs when $[K]$ is positive definite [30]. Note that the ratio of the width along

the u_1 axis to the width along the u_2 axis is equal to the square root of the diagonal elements of the coupling matrix. Also, the directions to maximum and minimum curvature are orthogonal. The distance to these locations are equal to the eigenvalues of the coupling matrix which have been labeled as principal loss factors, h_{p1} and h_{p2}. This applies

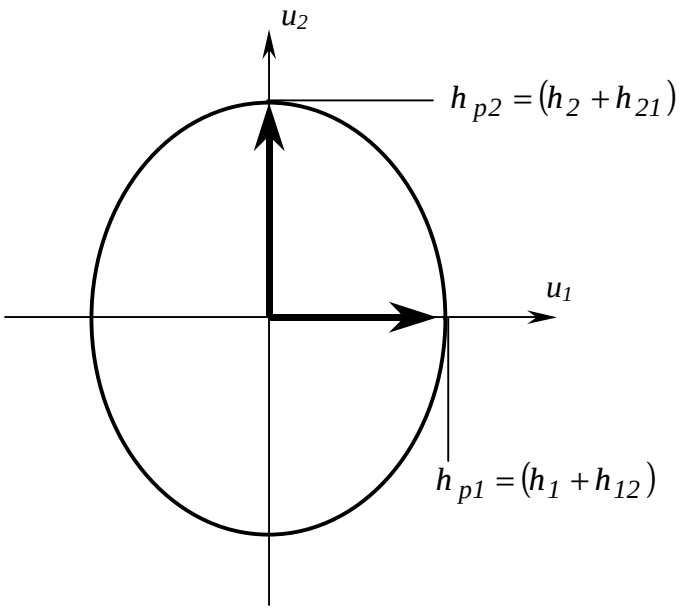

Figure 1.11 Quadratic Form of Two-Subsystem Coupling Matrix

to higher order systems as well by extending the dimensionality of the quadratic form. The representation of the coupling matrix in terms of its eigenpairs is utilized to a great extent in this investigation, especially with respect to transient dynamics, and is further examined in later sections.

Before examining the details of the creation of SEA models, it is worth noting that there exists another symmetric form of the power balance equations common in the literature. Specifically, this involves the conservation of modal power potential. The modal density

(instead of the mode count as in equation 1.13) is used to transform the loss factor matrix into a symmetric form. The modal density is merely the number of modes that exist for that particular subsystem in the analysis frequency range, $n_i = N_i/Dw$. The power balance is:

$$w\begin{bmatrix} n_1\left(h_1+\sum_{j\neq 1}h_{1j}\right) & -n_2h_{21} & \cdots & -n_mh_{m1} \\ -n_1h_{12} & n_2\left(h_2+\sum_{j\neq 2}h_{2j}\right) & \cdots & -n_mh_{m2} \\ \vdots & \vdots & \ddots & \vdots \\ -n_1h_{1m} & -n_2h_{2m} & \cdots & n_m\left(h_m+\sum_{j\neq m}h_{mj}\right) \end{bmatrix} \begin{Bmatrix} E_1/n_1 \\ E_2/n_2 \\ \vdots \\ E_m/n_m \end{Bmatrix} = \begin{Bmatrix} P_1 \\ P_2 \\ \vdots \\ P_m \end{Bmatrix} \tag{1.18}$$

Using symbolic notation, this can be written:

$$[b]\{f\} = \{P\} \tag{1.19}$$

where, $[b]$ is the symmetric modal coupling matrix and $\{f\}$ is a vector of the modal power potentials. Note that the center frequency of the analysis band, w, is incorporated into the modal coupling matrix. Furthermore, the modal coupling matrix, $[b]$, like the coupling matrix, $[K]$, is also positive definite and usually diagonally dominant.

Langley [31] derives general equations for the conservation of vibration energy in multi-coupled structures excited by random excitation. The equations are a symmetric form of the power balance using total energy in a form that resembles the modal power potential, $\{f\}$, defined earlier. The only assumption is that each subsystem is chosen such that the relative modal amplitudes or wave amplitudes are independent of the excitation such that the effective densities are independent of the excitation as described by Finnveden [32] or when

the density is uniform within a subsystem. Note that the first of these follows from the standard SEA assumption of equipartition of modal energy for independent modes (diffuse wave fields). Furthermore, for conservatively coupled systems, the equations reduce to the standard SEA power balance equations provided the driving point Green's function for the coupled structure is approximately equal to that for the uncoupled structure (i.e., weak coupling).

1.2.4 CONCLUSIONS

Statistical Energy Analysis has existed as a tool for predicting the response of engineering structures to dynamic loads for over 40 years. Significant successes have been realized in a few different disciplines. However, the validity of the assumptions made in forming the steady state predictive SEA equations are still open to debate; see, for example, Fahy [1]. The equations, essentially, arise from the extension of results derived for two coupled oscillators and, in particular, two coupled subsystems comprised of independent oscillators. However, as described earlier, the general derivation given by Langley [31] is based on first principles with few assumptions. Although more complicated, the range of applicability of the general power balance given is broader than that of the SEA power balance. Furthermore, if the same assumptions used in the derivation of the SEA power balance are applied to the general power balances, the two are equivalent.

1.3 SEA MODEL DEVELOPMENT

In general, the approach to constructing an SEA model consists of first defining appropriate subsystems, then defining subsystem coupling, and, finally, characterizing external model inputs or excitations. Subsystem breakup is guided by the requirement that modes of a system must be incoherent and equally share energy over the analysis frequency bandwidth as described earlier. In other words, a subsystem represents a collection of similar mode (or wave) types. To illustrate, the subsystem breakup of a structure comprised of two connected plates and a rectangular beam is shown in Figure 1.12.

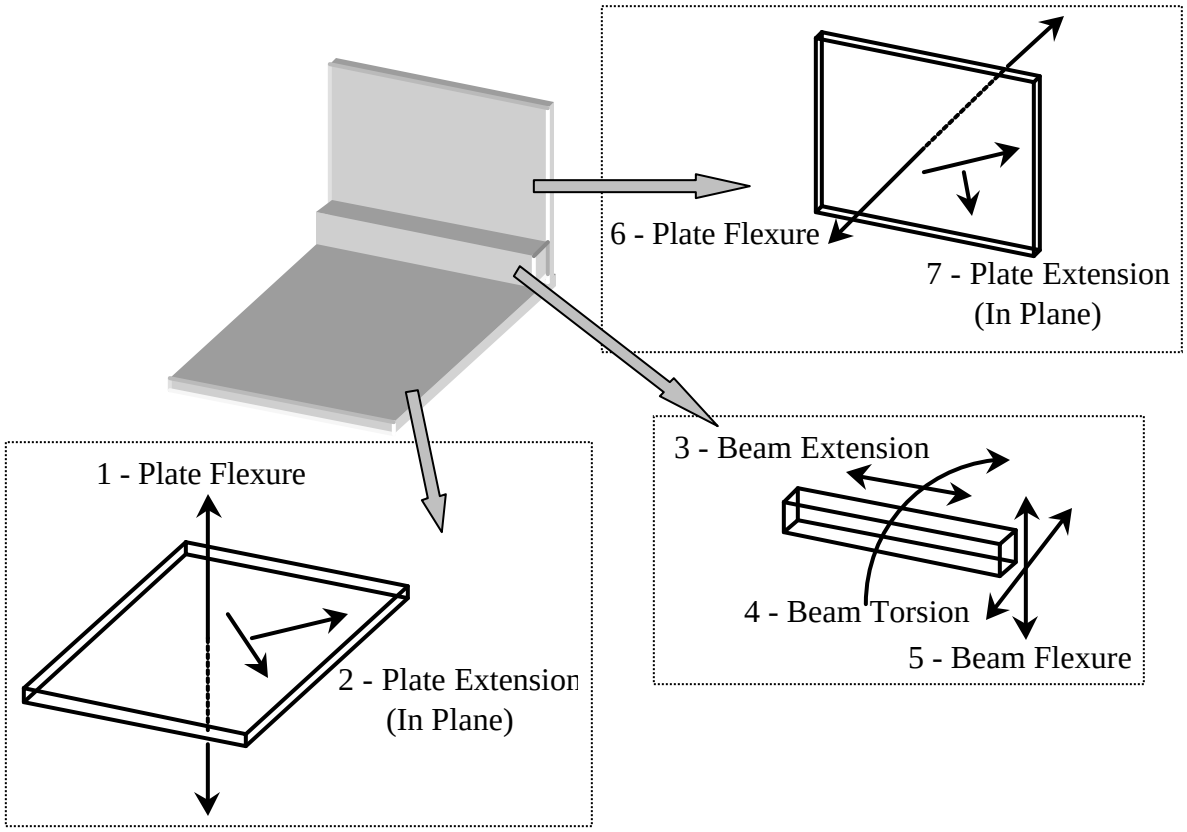

Figure 1.12 Simple Structure Decomposed into SEA Subsystems

Separate subsystems, labeled 1 - 7, are used to represent major mode groups each with a single (energy) degree of freedom as shown. Obviously, modes whose shapes extend across the subsystems are not represented. Typically, the natural frequencies of these global modes define the lower limit of the applicable frequency range. The thrust of SEA modeling is the determination of the elements of the coupling matrix, specifically, mode count (or modal density), damping loss factors, and coupling loss factors for each of the chosen subsystems. To establish the model input, typically, the known excitation such as force must be is converted to an input power. An additional consideration is with respect to post processing. Since, model solution yields response energy, this must usually be related to a particular quantity of interest such as acceleration, velocity, strain, or sound pressure level.

1.3.1 MODAL DENSITY

Modal densities of idealized continuous subsystems such as beams, plates, and acoustic volumes can be readily determined from theoretical equations of motion by examination of the resulting dispersion relation and mode shape geometry. A partial listing is shown in Table 1.1. In this table, L is the beam length, c_L is the longitudinal wave speed, E is the elastic modulus, r is the density, c_T is the torsion wave speed, J is the torsion moment of rigidity, G is the shear modulus, I_p is the polar moment of inertia, w is frequency, k is the radius of gyration, c_B is the bending wave speed, c_g is the shear wave speed, A is the plate surface area, and n is Poisson's ratio. Broader compilations and modal densities of more complex systems based upon theory and semi-empirical data, such as shells and honeycomb panels, can be found in works by Cremer and Heckl [27], Lyon and DeJong [28], Norton [33], Fahy [34], and Hart and Shah [35].

Table 1.1 Modal Densities of Idealized Systems

System	Modal Density, n	Wave Speed
Beam, In plane Extension	$\frac{L}{pc_L}$	$c_L = \sqrt{\frac{E}{r}}$
Beam, Torsion	$\frac{L}{pc_T}$	$c_T = \sqrt{\frac{JG}{rI_p}}$
Beam, Flexure	$\frac{L}{2p\sqrt{wkc_L}} = \frac{L}{2pc_B}$	$c_L = \sqrt{\frac{E}{r}}$, $c_B = \sqrt{wkc_L}$
Beam, Flexure with Shear Effect	$\frac{L\left(\frac{1}{c_B^2} + \frac{2}{c_g^2}\right)}{2p\sqrt{\frac{1}{c_B^2} + \frac{1}{c_g^2}}}$	$c_B = \sqrt{wkc_L}$, $c_g = \sqrt{\frac{G}{rg}}$
Plate, In Plane Extension	$\frac{wA}{2pkc_L^2}$	$c_L = \sqrt{\frac{E}{r\left(1-n^2\right)}}$
Plate, In Plane Shear	$\frac{wA}{2pkc_s^2}$	$c_s = \sqrt{\frac{G}{r}}$
Plate, Flexure	$\frac{A}{4pkc_L}$	$c_L = \sqrt{\frac{E}{r\left(1-n^2\right)}}$
Plate, Flexure with Shear Effect	$\frac{wA\left(\frac{1}{c_B^2} + \frac{2}{c_g^2}\right)}{4pkc_L}$	$c_B = \sqrt{wkc_L}$, $c_g = \sqrt{\frac{G}{rg}}$

Several experimental methods for measuring the modal density are popularly employed. One straightforward method is to count the number of resonance peaks observed in a drive point frequency response function measurement. However, as was mentioned previously, the modal density will be underestimated in frequency ranges where modal overlap exists. A second technique is to conduct a spatial and frequency average mobility measurement. The

modal density can be shown, see Clarkson [36] for example, to be related to the real part of the mobility (conductance):

$$n(w) = \frac{2}{p} m\langle Re(Y)\rangle = \frac{2}{p} m\langle G\rangle \tag{1.20}$$

where, $n(w)$ is the modal density, m is the system mass, and $\langle G\rangle = \langle Re(Y)\rangle$ is the real part of the mobility (conductance, G) that has been averaged in space and frequency.

1.3.2 DAMPING LOSS FACTOR

The definition of damping in a SEA sense in given in equation 1.12. In other words, by considering the steady state power balance for a single isolated subsystem, it can be seen that, $P = whE = 2pfhE$. The input power is equal to the energy dissipated. Furthermore, $2p h$, like efficiency, is the ratio of the input power to the energy dissipated by cycle.

Table 1.2 Damping Measures

Damping Loss Factor, h	h
Critical Damping Ratio, z	$2z$
Quality Factor, Q	$\frac{1}{Q}$
Reverberation Time, T_{60} (f = Frequency, Hz)	$\frac{2.2}{fT_{60}}$
Decay Rate, DR, dB/sec	$\frac{DR}{27.3f}$
Log Decrement, d	$\frac{d}{pf}$
Wave Attenuation, g (c_g = Group Velocity)	$\frac{c_g a}{pf}$
Half Power Bandwidth, $D_{1/2}$	$\frac{D_{1/2}}{f}$
Phase Angle, f	$\tan(f)$
Absorption Coefficient, α (c = Sound Speed) (A = Wall Area) (V = Room Volume)	$\frac{cAa}{8pfV}$

Damping is by no means unique to SEA and no attempt is made here to conduct an exhaustive review of the wealth of pertinent information. Generally, analytical expressions are unavailable for most systems. Typically, one must rely on empirical data or must conduct measurements to obtain damping parameters. Linear viscous damping or an equivalent is by far the most common representation. Numerous

viscous damping descriptors exist and most are simply related as shown in Table 1.2. Two of the most common techniques for measuring damping are decay rate testing and the half power method. Decay rate methods involve acquiring a damping value from the transient free decay of a response measurement. Typically, for frequency average SEA, this requires either pulse or filtered (in the band of interest) noise burst inputs. The response is also filtered in the same bandwidth of interest. The envelope of the free decay is then obtained by time averaging or Hilbert transform. The decay of the envelope can then be simply related to the damping loss factor either manually or by a least squares fit. The drawback is that the subsystem of interest must be isolated from the rest of the dynamic system. Breaking down a complex system under consideration into components or otherwise blocking the other components via mass loading or applied damping is often impractical or unrealistic. Alternatively, an in situ measurement of the damping loss factor may contain some error since not all of the measured loss is dissipative, some of the loss is simply energy transferred to other parts of the system. Furthermore, the method assumes that there truly exists an equipartition of energy and a constant damping value over the measured bandwidth. Use of the decay rate method alone does not allow for a quantified assessment of the degree to which these assumptions are or are not being met.

The half power method is used to acquire a damping measure from the resonance bandwidth (of a measured frequency response function) of a particular mode of interest. Difficulty arises for systems with light damping since a frequency response function measurement must have high resolution and minimal Fourier transform leakage to accurately capture the narrow resonance and its associated half power bandwidth. Additionally, since the half power

method is applied to a single resonance at a time (behaving as a single degree of freedom system in the vicinity of the natural frequency), the technique fails in frequency ranges where significant modal overlap occurs.

The SEA power balance for a single isolated subsystem can be used to infer damping. Solving for the loss factor reveals that $h = P/(wE)$. Thus, by measuring filtered (centered at w) steady state input power and response energy, the loss factor can be computed. Again, however, this requires that the subsystem be practically or virtually isolated.

1.3.3 COUPLING LOSS FACTOR

The coupling loss factor is unique to SEA. Although defined in manner similar to the damping loss factor, the coupling loss factor represents power being transferred from one subsystem to another. The damping loss factor represents power dissipated by a subsystem. Physically, a damping mechanism may actually be a loss to some other medium. However, if the response of the other medium is of no interest, then it is not modeled as a SEA subsystem. The associated coupling loss, therefore, is not represented but it is, instead, incorporated into the damping loss factor.

Coupling loss factors of idealized connections such as point, line, and area junctions can be determined using a mode or wave approach; see, for example, Cremer and Heckl [27], Lyon and Dejong [28], or Fahy [34]. Theoretical values for coupling loss factors are usually derived using the wave approach for semi-infinite systems, which is often simpler. Furthermore, a considerable amount of effort regarding wave transmission across idealized

junctions exists in the literature. This can be readily applied to evaluate coupling loss factors. It is worth noting that SEA coupling parameters can be equivalently formulated using a mobility approach as discussed by Manning [37].

One of the earliest experimental approaches to verifying or identifying coupling loss factors is a method that uses the SEA power balance to solve for the coupling loss factor in terms of the measured subsystem energies and damping losses with respect to a single isolated junction. The approach for two subsystems and a single junction is shown in Figure 1.13. By applying damping to subsystem 2, energy dissipated by subsystem 1 is negligible. Note, also, that only subsystem 1 is excited.

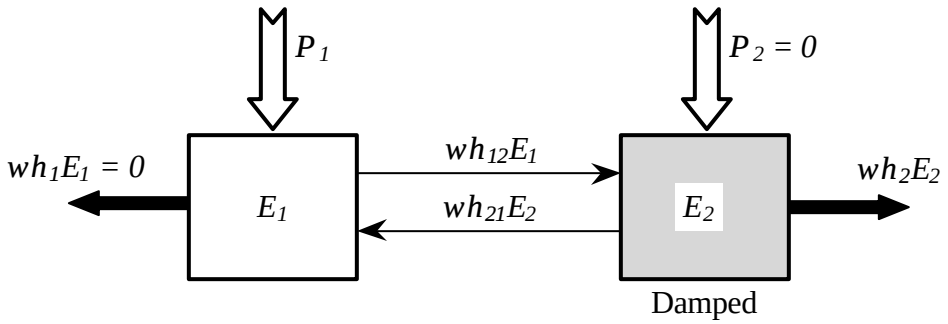

Figure 1.13 Measurement of Coupling Loss

The power balance for subsystem 1 is:

$$wh_{12}E_1 - wh_{21}E_2 = P_1 \tag{1.21}$$

Since the only appreciable energy dissipation occurs at subsystem 2, the input power, P_1 is equal to the power dissipated in subsystem 2, wh_2E_2. Hence, the power balance becomes:

$$wh_{12}E_1 - wh_{21}E_2 = wh_2E_2 \tag{1.22}$$

Using the reciprocity relation, $n_1(w)h_{12} = n_2(w)h_{21}$, and solving for the loss factor yields:

$$h_{12} = \frac{h_2 E_2}{E_1 - \frac{n_1(w)}{n_2(w)} E_2} \tag{1.23}$$

Again, the disadvantage here is that isolation of a single junction is required. This is likely to pose a great challenge if it is to be applied to a structure with any reasonable degree of complexity.

1.3.4 SUMMARY

In summary, the essence of SEA modeling is to evaluate the three main parameters: modal density, damping, and coupling. It is believed that subsystem modal density can be accurately obtained for idealized systems since there is a firm theoretical basis and evidence of positive experimental results as shown by Hart and Shah [35], Clarkson [36], Clarkson and Pope [38], Szechenyi [39], and Keswick and Norton [40]. There is also reason to believe that the computation of theoretical coupling loss factors for idealized systems also maintains a fair degree of accuracy. On the other hand, an experimental approach must usually be taken to obtain damping loss factors for even the simplest systems. Furthermore, for any reasonably complex structure, there is no firm procedure as to how to properly formulate any of the SEA parameters. This and the impracticality of component and/or junction isolation for complex structures suggest that there is a need for improved methods for experimentally

obtaining parameters that, specifically, can be employed in situ. In fact, addressing this need is one of the key focus areas of this dissertation.

1.4 EXPERIMENTAL SEA

A considerably limited amount of research effort has been conducted on experimental SEA. To date, some compelling work has been done mainly on somewhat simple structures; see, for example, Clarkson and Pope [38], Norton and Greenhalgh [41], and Wu et al [42]. However, it seems that further effort is required to examine the possibility and means of establishing a structured approach to the experimental identification of SEA parameters.

As was described previously, the direct measurement of SEA damping and coupling loss factors via subsystem and junction isolation methods is problematic. To overcome this, it seems obvious to attempt a more structured approach by simultaneously identifying all the elements of a coupling matrix from in situ response measurements. In fact, the idea of using the steady state power balance in an inverse manner was considered even early in SEA history. In Lyon and Dejong's text [28], the idea is briefly discussed. Recall that since the coupling matrix, $[b]$ (equation 1.19) for instance, is positive definite and usually diagonally dominant, the process of inverting the matrix is numerically stable.

However, the inversion of a measured response matrix in the form of $\{[b]^{-1}\}^{-1}$ used to reconstruct (or identify) $[b]$ may be numerically unstable. In fact, $\{[b]^{-1}\}^{-1}$ is extremely ill-conditioned for dynamic systems with moderate to high coupling. Specifically, this occurs whenever the magnitude of the off-diagonal elements of $[b]$ approach that of the diagonal elements, or in other words, when the coupling loss factors become as large as the damping loss factors.

1.4.1 CLASSICAL POWER INJECTION METHOD

The earliest advance, by Bies and Hamid [43], to use the SEA power balance in an inverse manner is the development of the Power Injection Method (PIM). Basically, an experimental identification of loss factors for *m* subsystems is formed by inverting an $m^2 \times m^2$ matrix of measured steady state response energies. To illustrate, the three subsystem SEA model, shown in Figure 1.10, is used. First, the power balance is written for the case in which subsystem 1 is singly excited:

$$w[H]\begin{Bmatrix} E_1^{(1)} \\ E_2^{(1)} \\ E_3^{(1)} \end{Bmatrix} = \begin{Bmatrix} P_1 \\ 0 \\ 0 \end{Bmatrix} \tag{1.24}$$

where, $E_i^{(j)}$ is the response energy of subsystem *i* due to excitation at subsystem *j*. For this size system, the coupling matrix is given by:

$$[H] = \begin{bmatrix} (h_1 + h_{12} + h_{13}) & -h_{21} & -h_{31} \\ -h_{12} & (h_2 + h_{21} + h_{23}) & -h_{32} \\ -h_{13} & -h_{23} & (h_3 + h_{31} + h_{32}) \end{bmatrix} \tag{1.25}$$

Similarly, a power balance can be written for the other two cases where each of the remaining subsystems is singly excited:

$$w[H]\begin{Bmatrix} E_1^{(2)} \\ E_2^{(2)} \\ E_3^{(2)} \end{Bmatrix} = \begin{Bmatrix} 0 \\ P_2 \\ 0 \end{Bmatrix} \quad \text{and} \quad w[H]\begin{Bmatrix} E_1^{(3)} \\ E_2^{(3)} \\ E_3^{(3)} \end{Bmatrix} = \begin{Bmatrix} 0 \\ 0 \\ P_3 \end{Bmatrix} \tag{1.26a \& b}$$

The *m* individual power balance equations are combined into a single $m^2 \times m^2$ matrix equation:

(1.27)

$$w\begin{bmatrix} E_1^{(1)} & E_1^{(1)} & E_1^{(1)} & -E_2^{(1)} & 0 & 0 & -E_3^{(1)} & 0 & 0 \\ 0 & -E_1^{(1)} & 0 & E_2^{(1)} & E_2^{(1)} & E_2^{(1)} & 0 & -E_3^{(1)} & 0 \\ 0 & 0 & -E_1^{(1)} & 0 & 0 & -E_2^{(1)} & E_3^{(1)} & E_3^{(1)} & E_3^{(1)} \\ E_1^{(2)} & E_1^{(2)} & E_1^{(2)} & -E_2^{(2)} & 0 & 0 & -E_3^{(2)} & 0 & 0 \\ 0 & -E_1^{(2)} & 0 & E_2^{(2)} & E_2^{(2)} & E_2^{(2)} & 0 & -E_3^{(2)} & 0 \\ 0 & 0 & -E_1^{(2)} & 0 & 0 & -E_2^{(2)} & E_3^{(2)} & E_3^{(2)} & E_3^{(2)} \\ E_1^{(3)} & E_1^{(3)} & E_1^{(3)} & -E_2^{(3)} & 0 & 0 & -E_3^{(3)} & 0 & 0 \\ 0 & -E_1^{(3)} & 0 & E_2^{(3)} & E_2^{(3)} & E_2^{(3)} & 0 & -E_3^{(3)} & 0 \\ 0 & 0 & -E_1^{(3)} & 0 & 0 & -E_2^{(3)} & E_3^{(3)} & E_3^{(3)} & E_3^{(3)} \end{bmatrix} \begin{Bmatrix} h_1 \\ h_{12} \\ h_{13} \\ h_{21} \\ h_2 \\ h_{23} \\ h_{31} \\ h_{32} \\ h_3 \end{Bmatrix} = \begin{Bmatrix} P_1 \\ 0 \\ 0 \\ 0 \\ P_2 \\ 0 \\ 0 \\ 0 \\ P_3 \end{Bmatrix}$$

Finally, equation 1.27 is solved to obtain the vector of loss factors by inverting the matrix of measured energies and then post multiplying by the vector of input powers.

Several drawbacks inherent to classical PIM are obvious. The dimension of the energy matrix increases with the square of the number of subsystems resulting in a substantial rise in computation time with increasing system complexity. Furthermore, the energy matrix has a tendency to be ill-conditioned due to the presence of significantly large off-diagonal terms. In fact, in this formulation, drive point energies, which tend to be the largest, are not restricted to the diagonal.

1.4.2 IMPROVED POWER INJECTION METHOD

In attempt to overcome the computational difficulty associated with inverting a large energy matrix, Lalor [44] showed that by recombining the components of matrix equation 1.27, the damping loss factors could be separated from the coupling loss factors. The result is a simpler set of equations. Instead of m^2 equations, the system is reduced to m sets of $(m-1)\ x$

(m-1) matrix equations for the coupling loss factors and a single *m x m* equation for the damping loss factors. To illustrate for three subsystems, equation 1.27 is recombined to give:

$$\begin{bmatrix} \left(\frac{E_2^{(2)}}{E_1^{(2)}} - \frac{E_2^{(1)}}{E_1^{(1)}}\right) & \left(\frac{E_3^{(2)}}{E_1^{(2)}} - \frac{E_3^{(1)}}{E_1^{(1)}}\right) \\ \left(\frac{E_2^{(3)}}{E_1^{(3)}} - \frac{E_2^{(1)}}{E_1^{(1)}}\right) & \left(\frac{E_3^{(3)}}{E_1^{(3)}} - \frac{E_3^{(1)}}{E_1^{(1)}}\right) \end{bmatrix} \begin{Bmatrix} h_{21} \\ h_{31} \end{Bmatrix} = \begin{Bmatrix} \frac{P_1}{wE_1^{(1)}} \\ \frac{P_1}{wE_1^{(1)}} \end{Bmatrix} \tag{1.28}$$

$$\begin{bmatrix} \left(\frac{E_1^{(1)}}{E_2^{(1)}} - \frac{E_1^{(2)}}{E_2^{(2)}}\right) & \left(\frac{E_3^{(1)}}{E_2^{(1)}} - \frac{E_3^{(2)}}{E_2^{(2)}}\right) \\ \left(\frac{E_1^{(3)}}{E_2^{(3)}} - \frac{E_1^{(2)}}{E_2^{(2)}}\right) & \left(\frac{E_3^{(3)}}{E_2^{(3)}} - \frac{E_3^{(2)}}{E_2^{(2)}}\right) \end{bmatrix} \begin{Bmatrix} h_{12} \\ h_{32} \end{Bmatrix} = \begin{Bmatrix} \frac{P_2}{wE_2^{(2)}} \\ \frac{P_2}{wE_2^{(2)}} \end{Bmatrix} \tag{1.29}$$

$$\begin{bmatrix} \left(\frac{E_1^{(1)}}{E_3^{(1)}} - \frac{E_1^{(3)}}{E_3^{(3)}}\right) & \left(\frac{E_2^{(1)}}{E_3^{(1)}} - \frac{E_2^{(3)}}{E_3^{(3)}}\right) \\ \left(\frac{E_1^{(2)}}{E_3^{(2)}} - \frac{E_1^{(3)}}{E_3^{(3)}}\right) & \left(\frac{E_2^{(2)}}{E_3^{(2)}} - \frac{E_2^{(3)}}{E_3^{(3)}}\right) \end{bmatrix} \begin{Bmatrix} h_{13} \\ h_{23} \end{Bmatrix} = \begin{Bmatrix} \frac{P_3}{wE_3^{(3)}} \\ \frac{P_3}{wE_3^{(3)}} \end{Bmatrix} \tag{1.30}$$

which can be solved to yield the coupling loss factors. Also:

$$\begin{bmatrix} E_1^{(1)} & E_2^{(1)} & E_3^{(1)} \\ E_1^{(2)} & E_2^{(2)} & E_3^{(2)} \\ E_1^{(3)} & E_2^{(3)} & E_3^{(3)} \end{bmatrix} \begin{Bmatrix} h_1 \\ h_2 \\ h_3 \end{Bmatrix} = \begin{Bmatrix} \frac{P_1}{w} \\ \frac{P_2}{w} \\ \frac{P_1}{w} \end{Bmatrix} \tag{1.31}$$

which can be solved to obtain the damping loss factors. Mathematically, the extension to higher order systems is straightforward.

Even though the problem is recast, exhibiting improved computational speed and diagonal dominance, Lalor shows that errors such as negative coupling can result. Additionally, the situation of moderate to high coupling still remains problematic in this improved PIM. Despite this, favorable results were obtained by Ming et al [45] using the method on an automobile rear section, though; the system was comprised of only eight subsystems.

1.4.3 NORMALIZED ENERGY INVERSION METHOD

As suggested by De Langhe [3], the most uncomplicated way to combine the individual power balance equations, 1.24 and 1.26, into a single matrix equation is via augmentation as follows:

$$w[H]\begin{bmatrix} E_1^{(1)} & E_1^{(2)} & E_1^{(3)} \\ E_2^{(1)} & E_2^{(2)} & E_2^{(3)} \\ E_3^{(1)} & E_3^{(2)} & E_3^{(3)} \end{bmatrix} = \begin{bmatrix} P_1 & 0 & 0 \\ 0 & P_2 & 0 \\ 0 & 0 & P_3 \end{bmatrix} \tag{1.32}$$

As a matter of convenience, both sides of the equation can be normalized by the input powers to yield an equivalent form:

$$[H]\begin{bmatrix} \frac{wE_1^{(1)}}{P_1} & \frac{wE_1^{(2)}}{P_2} & \frac{wE_1^{(3)}}{P_3} \\ \frac{wE_2^{(1)}}{P_1} & \frac{wE_2^{(2)}}{P_2} & \frac{wE_2^{(3)}}{P_3} \\ \frac{wE_3^{(1)}}{P_1} & \frac{wE_3^{(2)}}{P_2} & \frac{wE_3^{(3)}}{P_3} \end{bmatrix} = \begin{bmatrix} 1 & 0 & 0 \\ 0 & 1 & 0 \\ 0 & 0 & 1 \end{bmatrix} \tag{1.33}$$

Denoting the normalized energies as $\hat{E}_i^{(j)}$, where $\hat{E}_i^{(j)} = \omega E_i^{(j)}/P_i$, yields:

$$[H]\begin{bmatrix} \hat{E}_1^{(1)} & \hat{E}_1^{(2)} & \hat{E}_1^{(3)} \\ \hat{E}_2^{(1)} & \hat{E}_2^{(2)} & \hat{E}_2^{(3)} \\ \hat{E}_3^{(1)} & \hat{E}_3^{(2)} & \hat{E}_3^{(3)} \end{bmatrix} = \begin{bmatrix} 1 & 0 & 0 \\ 0 & 1 & 0 \\ 0 & 0 & 1 \end{bmatrix} \tag{1.34}$$

For simplicity this can be written symbolically as:

$$[H][\hat{E}] = [I] \tag{1.35}$$

Finally, the experimentally identified coupling matrix is, then, the inverted normalized energy matrix, $[\hat{E}]^{-1}$ obtained by solving equation 1.35. Obviously, this can readily be extended to systems of higher dimension.

Insight into the guidelines for acquiring a measured energy matrix exists in the literature. Hodges, et al [46] discuss some of the analytical properties possessed by the ideal $[\hat{E}]$ matrix revealed by examining its ideal equivalent, the $[H]^{-1}$ matrix. The following observations can be made:

1) The inverse of $[H]$ is non-negative everywhere. Indeed, this makes sense since all energy components are positive.

2) The inverse of $[H]$ is weakly diagonally dominant. This also makes sense since the driven subsystem will always have the highest response.

3) If a measured $[\hat{E}]$ matrix is strictly positive and sufficiently diagonally dominant (light coupling), its inverse will yield a matrix with positive diagonal elements and negative off-diagonal elements. Note that this is the ideal form of $[H]$.

4) If the inverse of a measured $[\hat{E}]$ matrix yields a matrix with positive diagonal & negative off diagonal elements and $[A]$ is a diagonal matrix with all positive elements, then the inverse of $[\hat{E}]+[A]$ yields, yet, another matrix with positive diagonal & negative off diagonal elements. In other words, increasing the diagonal dominance of the measured energy matrix does not result in a non-ideal form for its inverse.

5) If the inverse of a measured $[\hat{E}]$ matrix yields a matrix with positive diagonal & negative off diagonal elements and $[A]$ is a positive constant matrix, then the inverse of $[\hat{E}]+[A]$ yields a matrix with positive diagonal & negative off diagonal elements. This implies that, changing the relative variation of the off-diagonal elements of the measured energy matrix does not result in a non-ideal form for its inverse.

6) If any of the elements of a measured $[\hat{E}]$ matrix are zero, it is possible to reorder the matrix into a block-diagonal form with no zero elements in the blocks. This indicates that the only way to have subsystems with zero energy is if they are decoupled from the rest of the global system.

Using simulated systems, the authors, specifically, observe numerical difficulty whenever the energy of different subsystems was relatively close. This causes the energy matrix to be nearly singular with narrow quadratic form (evident in the large ratio between the largest and smallest eigenvalues; see figure 1.11) resulting in an identified coupling matrix with significant error. This poses considerable difficulty for experiments on systems with light damping and/or relatively moderate coupling that are likely to exhibit nearly equivalent energy levels across subsystems such that the measured energy matrix is somewhat uniform. Similar conclusions are drawn by Woodhouse [47] and Clarkson and Ranky [48].

1.5 CONCLUSIONS

To date, the normalized energy inversion method is apparently the best option for steady state SEA parameters identification. De Langhe [3] compares simulations of the normalized energy inversion method to the classical power injection method for identical systems of increasing dimension. The normalized energy method exhibits superior numerical conditioning and consumes less computational time, especially as system dimension increases, than classical PIM. Furthermore, the author asserts that since the improved PIM is mathematically analogous to the normalized energy inversion, there is no need to expend the additional effort in reformulating the energy matrix for improved PIM. Nonetheless, a structured approach that works reliably for complex structures and/or moderate coupling does not exist. The primary objective of this dissertation is to contribute toward that goal.

2 DEVELOPMENT OF A POWER FLOW MODEL REALIZATION METHOD

2.1 PROBLEM DEFINITION AND APPROACH

Techniques to identify parameters from tests on low frequency second-order structural dynamic systems have been widely explored by the modal analysis community for over fifty years [49]. Advances were achieved in testing methods as well as system identification techniques. Early experimental efforts relied almost solely on analog testing. Two early modal identification contributions worth mentioning are “circle-fitting”, introduced by Kennedy and Pancu [50], and a systematic approach to normal mode testing developed by Lewis and Wrisley [51]. Prior to 1970, these two techniques (or variations of them) were used in most modal identification applications. After the introduction of computers into the laboratory and the development of the fast Fourier transform in the 1970’s, frequency response function testing and curve fitting gained popularity. Computational improvements beginning in 1980 resulted in the practical ability to conduct multiple input testing and led to enhancements in excitation, signal processing, and data analysis. Multiple input testing allowed multiple input system identification methods to be employed that offered improved results with increased speed; see, for example, Vold et al [52], Leuridan [53], Craig and Blair [54], and Zhang et al [55]. Also, a renewed interest developed in Auto-Regressive Moving Average (ARMA) techniques that were previously considered too computationally demanding; see, for example Prevosto et al [56]. Currently, many identification schemes exist and wide varieties are employed routinely. Most methods work well on simple structures and must be applied with care to deliver meaningful results on systems that are more complex. Research in this area continues. Other efforts include techniques to improve/update Finite Element Analysis (FEA) models using experimentally identified

modal parameters or to quantify structural changes to a system by tracking parameter discrepancies in an accurate FEA model that has been updated using measured data from the modified structure.

System identification methods have also been widely explored by the automatic control community. This is due, at least, in part to the fact that an accurate system model is often required to develop an effective control scheme. Significant accomplishments in system identification in both the time and frequency domain have been made over the last thirty years. No attempt is made here to detail these developments. However, a technique in the field of controls that is related to modal identification is the process of constructing a space representation from measured data. This is usually termed system realization. Minimum order techniques developed by Ho and Kalman [57], which realize a model with the smallest state space dimension, have been successfully used to identify second order structural dynamic systems [58]. In fact, as Juang [59] points out, minimum realization of a state space model in the time domain is computationally similar to the multiple input/multiple output time-domain methods often used by the modal testing community.

It seems that the question of how to identify SEA parameters from measured data is conceptually similar to the question of how to identify structural dynamic FEA parameters from measured data. Historically, the advancement of modal testing was not significantly motivated by seeking to improve FEA models. Not only do properly identified modal parameters serve very well as an input/output map of a system at measurement locations, real physical appreciation is obtained by examining a structure's modes of vibration. However,

some insight into the practicality of the power injection and energy inversion methods for use in SEA can be obtained by considering the similar problem of obtaining FEA parameters from an inversion of measured response data. The first obvious conclusion is that it is, indeed, quite impractical to attempt to measure input/output data on a structure at all locations where there are finite element nodes in its model. Similarly, it is likely that not all SEA degrees of freedom will be measured, especially, in plane extension or shear modes. Second, inversion of this response matrix from modal tests would suffer from poor numerical conditioning for reasons similar to that for a measured energy response matrix. Nonetheless, there exist FEA updating methods that have proven successful. This is done not by directly measuring physical parameters but by focusing instead on modal parameters, which serve as the common ground between structural dynamic modeling and test.

Very often, measured modal parameters are successfully used to improve existing FEA models using, for example, minimum norm updating via Lagrange multipliers (Berman and Nagy, [60]), generalized matrix inversion (O'Callahan et al., [61]), localized updating (O'Callahan and Chou, [62]), or sensitivity methods (Van Karsen,[63]). It seems, therefore, that in the pursuit of a reliable structured approach to the identification of SEA parameters, a reasonable course would be to incorporate the advances and lessons learned by the modal analysis and controls communities regarding their, very similar, problem.

2.2 SELECTION OF SYSTEM IDENTIFICATION METHOD

System identification is the process of constructing models of dynamical systems to serve certain purposes [64], which, in this case, is to obtain experimental values of SEA parameters. The first step is to determine the class of identified model types that will best serve this purpose. The power balance equations described thus far have been restricted to steady state conditions. However, a transient form of the power balance can be formulated. This, together with an examination of the validity of assumed time-invariant parameters, is detailed in a later section. A complete model for a linear time-invariant system is given by:

$$y(t) = \sum_{k=1}^{\infty} h(k)u(t-k) + \sum_{k=0}^{\infty} g(k)e(t-k) \qquad t = 0,1,2,\ldots \tag{2.1}$$

where *y(t)* is the sampled system output, *u(t)* is the sampled system input, and *e(t)* is a sampled additive disturbance such as measurement noise. *h* is the system impulse response function and *g* is the disturbance impulse response function. Usually, equation 2.1 is written in the following form:

$$y(t) = H(q)u(t) + G(q)e(t) \qquad t = 0,1,2,\ldots \tag{2.2}$$

where,

$$H(q) = \sum_{k=1}^{\infty} h(k)q^{-k} \quad , \quad G(q) = 1 + \sum_{k=1}^{\infty} g(k)q^{-k} \tag{2.3}$$

and the backward shift operator is $q^{-k} = u(t - k)$. *H(q)* is the system transfer function and *G(q)* is the disturbance transfer function as shown in Figure 2.1. Furthermore, if:

$$\sum_{k=1}^{\infty} |h(k)| < \infty \tag{2.4}$$

and the input, *u(t)*, is bounded, then the corresponding output will be bounded. This also assures that:

$$H(z) = \sum_{k=1}^{\infty} h(k) z^{-k} \tag{2.5}$$

converges for all $|z| \geq 1$. Hence, *G(z)* is analytic on and outside the unit circle.

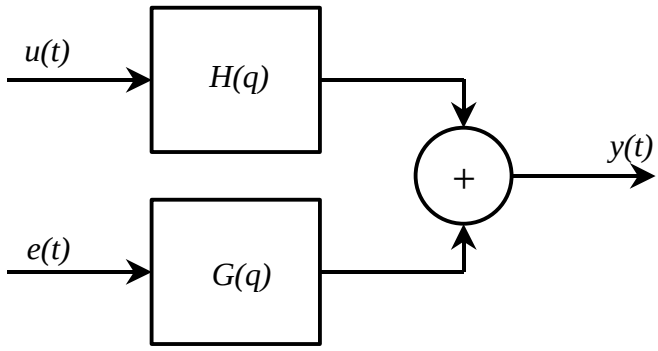

Figure 2.1 Dynamic System with Input and Disturbance

Extension to multiple degrees of freedom is straightforward. The model description is:

$$\{y(t)\} = [H(q,q)]\{u(t)\} + [G(q,q)]\{e(t)\} \qquad t = 0,1,2,\ldots \tag{2.6}$$

where the input, output, and disturbance are vectors. [*H(q,q)*] and [*G(q,q)*] are transfer function matrices. Furthermore, the vector of independent variables, *q*, contains the system parameters, the determination of which is the goal of the system identification.

The manner in which [*H(q,q)*], [*G(q, q)*] and {*e(t)*} are specified define the particular class of models representing the system. Two main classes of models can be defined in terms of their structure:

1) Black Box Models
2) Physical Models

Black box models relate inputs to outputs without regard to physical structure and, often, no a-priori knowledge may exist with regard to the nature or amount of unknown parameters. On the other hand, physical models have a basis on real physical laws allowing restriction to be placed on the variability in the nature and amount of parameters.

Probably the most popular black box model is the transfer function structure. Here, *G* and *H* are represented as rational functions. The parameters, *q*, are coefficients of polynomial terms (*A*,*B*,*C*,*D*,*F*) in the numerator and denominator and, as such, are non physical. The general form is:

$$A(q)y(t) = \frac{B(q)}{F(q)}u(t) + \frac{C(q)}{D(q)}e(t) \tag{2.7}$$

In most circumstances, the general form is not used. Usually, some of the polynomials are set to unity. Several examples are given in Table 2.1.

Table 2.1 Transfer Function Models

Model Structure	**Polynomials Set to Unity**
Finite Impulse Response (FIR)	A,C,D,F
Autoregressive, Extra Input (ARX)	C,D,F
Autoregressive Moving Average (ARMA)	B,D,F
Autoregressive Moving Average, Extra Input (ARMAX)	D,F
Autoregressive, Autoregressive Extra Input (ARARX)	C,F
Autoregressive, Autoregressive Moving Average Extra Input (ARARMAX)	F
Output Error (OE)	A,C,D
Box-Jenkins (BJ)	A

The most popular of the physical class of structures is the state space model. In this form, the relation between the inputs, outputs, and disturbances are written as a set of first order differential equations (continuous time) or difference equations (discrete time). The form is especially useful since the physics of the problem can be readily incorporated into the structure of the model. Usually, after the application of physical laws, the following form is obtained for multiple degrees of freedom:

$$\{\dot{x}(t)\} = [A(q)]\{x(t)\} + [B(q)]\{u(t)\} \tag{2.8}$$

where [*A(q)*] and [*B(q)*] are system matrices that are functions of the physical system parameters, *q*. {*x(t)*} is the state vector containing the physical output quantities such as acceleration, velocity, or displacement. Numerous dynamic systems can be written in this fashion. In fact, with proper layout of the state vector, 2nd order structural dynamic systems can be formulated in state space. In addition, as will be shown, a first order transient SEA power balance can be written in this form as well.

For identifying experimental SEA parameters, a physical model is preferable such that an attempt at obtaining real quantities such as damping and coupling loss factors can be made. However, it is certainly worth mentioning that identification of a non-physical model that provides only a mapping between measured inputs to measured outputs could still be useful in the course of a design or analysis. In fact, for linear time-invariant systems, the identified model could be used to examine how the system would respond to excitation types and levels different from those that were used during the experimentation. Furthermore, it is entirely feasible that an experimentally identified non-physical system could be incorporated into a

larger computational model as a type of “super-element” (or more properly “super-subsystem”) in a hybrid analysis.

2.3 STATE SPACE REALIZATION

Again, the approach used in this dissertation is to apply system realization methods to the state space class of model structures given by:

$$\{\dot{x}(t)\} = [A_c]\{x(t)\} + [B_c]\{u(t)\} \qquad (2.9a \text{ \& } b)$$
$$\{y(t)\} = [C]\{x(t)\}$$

where, $\{x(t)\}$ is the response vector, $\{u(t)\}$ is the input vector, $\{y(t)\}$ is the measurement vector, $[A_c]$ is the state matrix, $[B_c]$ is the input influence matrix, and $[C]$ is the output influence matrix.

2.3.1 QUASI-STEADY STATE SEA

The first step in constructing a state space representation suitable for experimental SEA is to develop a transient form of the power balance equations. The simplest approach is a quasi-steady state SEA obtained from the steady state formulation by adding a term to include a first order change of energy of the subsystem in each of the subsystem power balance equations. The intention is to predict an envelope, or more precisely, an average energy of the response over a short duration compared to the overall transient dynamic response but long enough (at least one or more periods corresponding to system natural frequencies) to effectively filter the second order system behavior. In matrix notation, for *m* subsystems, this is written:

$$\begin{Bmatrix} \frac{dE_1(t)}{dt} \\ \frac{dE_2(t)}{dt} \\ \vdots \\ \frac{dE_m(t)}{dt} \end{Bmatrix} + w \begin{bmatrix} h_1 + \sum_{j \neq 1} h_{1j} & -h_{21} & \cdots & -h_{m1} \\ -h_{12} & h_2 + \sum_{j \neq 2} h_{2j} & \cdots & -h_{m2} \\ \vdots & \vdots & \ddots & \vdots \\ -h_{1m} & -h_{2m} & \cdots & h_m + \sum_{j \neq m} h_{mj} \end{bmatrix} \begin{Bmatrix} E_1(t) \\ E_2(t) \\ \vdots \\ E_m(t) \end{Bmatrix} = \begin{Bmatrix} P_1(t) \\ P_2(t) \\ \vdots \\ P_m(t) \end{Bmatrix} \tag{2.10}$$

where, $E_i(t)$, is the energy of the ith subsystem, P_i, is the input power to the subsystem, h_i, are the damping loss factors, h_{ij} are the coupling loss factors, and w is the center frequency of the analysis band. In compact form, this is:

$$\{\dot{E}(t)\} + w[\text{Ç}]\{E(t)\} = \{P(t)\} \tag{2.11}$$

where, $\{\dot{E}(t)\}$ is a vector of the time rate of change of the subsystem energies, $\{E(t)\}$ is a vector of the subsystem energies, $[H]$ is the loss factor matrix, and $\{P(t)\}$is a vector of the input powers. When $\{\dot{E}(t)\}$ are all zero, this formulation reduces to the steady state SEA power balance:

$$w[\text{Ç}]\{E\} = \{\Pi\} \tag{2.12}$$

The symmetric forms can also be written in quasi-steady state form. In terms of the modal energy, $\{e(t)\}$, this is:

$$[N]\{\dot{e}(t)\} + w[K]\{e(t)\} = \{P(t)\} \tag{2.13}$$

where, $[N]$ is a diagonal matrix of the subsystem mode counts within the frequency band of interest and $[K]$ is the symmetric coupling matrix. Similarly, in terms of the modal power potential, $\{f(t)\}$, this is:

$$[n(w)]\{\dot{f}(t)\}+[b]\{f(t)\}=\{P(t)\} \tag{2.14}$$

where, [*n(w)*] is a diagonal matrix of the subsystem modal densities and [*b*] is the symmetric modal coupling matrix.

The formulation of a transient power balance was considered even in the beginning state of the development of SEA theory [65]. Mercer, Rees, and Fahy [66] showed using a perturbation analysis for weakly coupled oscillators that the instantaneous transmitted energy is inversely proportional to the difference between the blocked natural frequencies of the two oscillators. This is essentially the same as the result for stationary steady state input. Sun et al [67] as well as Powell and Quartararo [68] have reported success, using a quasi-steady state power balance, for transient response predictions of certain structural systems. More recently, Pinnington and Lednik [69,70] compare quasi-steady state SEA as well as wave propagation analysis with exact solutions for impulsively loaded coupled oscillators and coupled beams. They observed that differences between the envelope of the exact transient response and the estimated response occurred with respect to peak levels and the time to rise to peak level. It was also seen that, in the case of the coupled beams, accuracy strongly depended on the modal overlap.

The accuracy of quasi-steady state SEA applied to coupled equal oscillators and coupled multiple degree of freedom systems subject to impulsive inputs is examined by Hall [71]. Results indicate that steady state SEA parameters can be used in a quasi-steady state formulation for transient applications provided standard SEA assumptions are met.

Specifically, coupled subsystems must each maintain a uniform distribution of natural frequencies over the frequency band of interest, an equipartition of energy over the modes of the subsystems, uniform damping, and, most importantly, high modal overlap. For the systems examined, this minimizes the energy prediction error to ± 3 dB. Extension to general excitation can be realized by applying standard convolution techniques and by further requiring the typical SEA assumption that the inputs be uncorrelated.

2.3.2 TRANSFORM THEORY AND STATE SPACE REPRESENTATION

It is a straightforward matter to algebraically manipulate the quasi-steady state SEA power flow equations into a state space form. In fact, all power balance forms, including those with a symmetric coupling matrix, yield identical non-symmetric $[A_c]$ matrices. Rearrangement of equation 2.11 gives:

$$\{\dot{E}(t)\} = -w[H]\{E(t)\} + \{P(t)\} \tag{2.15}$$

This is clearly the state space form where, $[A_c] = -w[H]$, $[B_c] = [I]$, $\{x(t)\} = \{E(t)\}$, and $\{u(t)\} = \{P(t)\}$:

$$\{\dot{x}(t)\} = [A_c]\{x(t)\} + [B_c]\{u(t)\} \tag{2.16}$$

Rearrangement of the symmetric forms, equations 2.13 and 2.14, yield the same state space form. In other words, the state space form of the SEA power balance always reduces to the non-symmetric form.

To best interpret the physical nature of the state space identification it will prove advantageous to use linear transformation theory to obtain diagonal system matrices. This is done by transforming the system equations of choice to "principal" coordinates using the coupling matrix eigenpairs. In this way, the power balance equations are uncoupled. Use of the symmetric form is not strictly necessary; however, transforming the state space or non-symmetric system is slightly more complicated in that the inverse of an eigenvector matrix must be computed for use in the projection instead of its transpose. For the state space (non-symmetric) representation, conservation of modal energy (symmetric), and conservation of modal power potential (symmetric) respectively, the following eigenproblems can be formed:

$$\begin{aligned} ([A_c] + g_i[I])\{u_i\} &= \{0\} \\ (w[K] - g_i[N])\{v_i\} &= \{0\} \\ ([b] - g_i[n(w)])\{w_i\} &= \{0\} \end{aligned} \qquad \text{(2.17a - c)}$$

where, g_i is the i^{th} eigenvalue, u_i, v_i, and w_i are the i^{th} eigenvectors corresponding to each of the three forms. If the system dimension is m x m corresponding to m subsystems, then the eigenproblems can be written in an augmented form for all m eigenpairs each:

$$\begin{aligned} ([A_c] - [\bar{D}][I])[U] &= [0] \\ (w[K] - [\bar{D}][N])[V] &= [0] \\ ([b] - [\bar{D}][n(w)])[W] &= [0] \end{aligned} \qquad \text{(2.18a - c)}$$

where, $[\bar{D}]$ is a diagonal matrix of the eigenvalues, $[U]$, $[V]$, $[W]$ are matrices of the eigenvectors arranged in columns. The choice of the symbol, $[\bar{D}]$, to represent the eigenvalue matrix results from an obvious interpretation that the eigenvalues are damping

bandwidths in principal coordinates or more precisely, damping bandwidths of principal (uncoupled) subsystems.

Note that the eigenvalues for all forms are identical. Furthermore, it will prove useful to properly scale the eigenvectors such that the transformation of any of the power balance equations yields an identical diagonal system. This is done by scaling the eigenvectors such that the following triple products become equal to the identity matrix:

$$\begin{aligned} \left[\tilde{U}\right]^{-1}\left[I\right]\left[\tilde{U}\right] &= \left[I\right] \\ \left[\tilde{V}\right]^{T}\left[N\right]\left[\tilde{V}\right] &= \left[I\right] \\ \left[\tilde{W}\right]^{T}\left[n(w)\right]\left[\tilde{W}\right] &= \left[I\right] \end{aligned} \qquad (2.19a - c)$$

where, $[\tilde{U}]$, $[\tilde{V}]$, and $[\tilde{W}]$ are the scaled eigenvector matrices for each of the three power balance forms. Note that the first linear transformation requires inversion of the eigenvector matrix in view of the fact that the system is non-symmetric. Since the eigenvectors are orthogonal with respect to the system matrices, the scaling is achieved via:

$$\begin{aligned} \left[\tilde{U}\right] &\equiv \left[U\right]\left(\left[U\right]^{-1}\left[I\right]\left[U\right]\right)^{-1/2} \\ \left[\tilde{V}\right] &\equiv \left[V\right]\left(\left[V\right]^{T}\left[N\right]\left[V\right]\right)^{-1/2} \\ \left[\tilde{W}\right] &\equiv \left[W\right]\left(\left[W\right]^{T}\left[N\right]\left[W\right]\right)^{-1/2} \end{aligned} \qquad (2.20a - c)$$

The response can be written as the linear combination of uncoupled (principal) subsystem responses. Akin to mode summation for 2nd order dynamical systems, the response of subsystem *i* is:

$$x_i(t) = \sum_{k=1}^{m} \tilde{u}_i^{(k)} \bar{x}_k(t) \qquad \text{(2.21a - c)}$$

$$e_i(t) = \sum_{k=1}^{m} \tilde{v}_i^{(k)} \bar{e}_k(t)$$

$$f_i(t) = \sum_{k=1}^{m} \tilde{w}_i^{(k)} \bar{f}_k(t)$$

where, $\tilde{u}_i^{(k)}$, $\tilde{v}_i^{(k)}$, and $\tilde{w}_i^{(k)}$ are the components of the k^{th} eigenvector at subsystem i for each of the power balance forms respectively. $\bar{x}_k(t)$ is the energy, $\bar{e}_k(t)$ is the modal energy, and $\bar{f}_k(t)$ is the modal power potential of principal subsystem k. For simplicity, the symbolic matrix representation for the summation can be used:

$$\{x(t)\} = [\tilde{U}]\{\bar{x}(t)\} \qquad \text{(2.22a - c)}$$

$$\{e(t)\} = [\tilde{V}]\{\bar{e}(t)\}$$

$$\{f(t)\} = [\tilde{W}]\{\bar{f}(t)\}$$

Substituting equations 2.22a - c into equations 2.11, 2.13, and 2.14 respectively yields:

$$[I][\tilde{V}]\{\dot{\bar{x}}(t)\} - [A_c]\{\bar{x}(t)\} = \{P(t)\} \qquad \text{(2.23a - c)}$$

$$[N][\tilde{V}]\{\dot{\bar{e}}(t)\} + w[K][\tilde{V}]\{\bar{e}(t)\} = \{P(t)\}$$

$$[n(w)][\tilde{W}]\{\dot{\bar{f}}(t)\} + [b][\tilde{W}]\{\bar{f}(t)\} = \{P(t)\}$$

Pre-multiplying by the appropriate adjoint of the eigenvector matrix gives:

$$[\tilde{U}]^{-1}[I][\tilde{U}]\{\dot{\bar{x}}(t)\} - [\tilde{U}]^{-1}[A_c][\tilde{U}]\{\bar{x}(t)\} = [\tilde{U}]^{-1}\{P(t)\} \qquad \text{(2.24a - c)}$$

$$[\tilde{V}]^T[N][\tilde{V}]\{\dot{\bar{e}}(t)\} + w[\tilde{V}]^T[K][\tilde{V}]\{\bar{e}(t)\} = [\tilde{V}]^T\{P(t)\}$$

$$[\tilde{W}]^T[n(w)][\tilde{W}]\{\dot{\bar{f}}(t)\} + [\tilde{W}]^T[b][\tilde{W}]\{\bar{f}(t)\} = [\tilde{W}]^T\{P(t)\}$$

Making use of orthogonality, this reduces to simply:

$$[I]\{\dot{\bar{x}}(t)\}+[\bar{D}]\{\bar{x}(t)\}=[\tilde{U}]^{-1}\{u(t)\} \qquad \text{(2.25a - c)}$$

$$[I]\{\dot{\bar{e}}(t)\}+[\bar{D}]\{\bar{e}(t)\}=[\tilde{V}]^{T}\{P\ (t)\}$$

$$[I]\{\dot{\bar{f}}\ (t)\}+[\bar{D}]\{\bar{f}\ (t)\}=[\tilde{W}]^{T}\{P\ (t)\}$$

where, [*I*] is an *m* x *m* identity matrix, $[\bar{D}]$ is, again, a diagonal matrix of the system eigenvalues, $\{\bar{x}(t)\}$ is a vector of the energies of the principal subsystems, $\{\bar{e}(t)\}$ is a vector of the modal energies of the principal subsystems, and $\{\bar{f}(t)\}$ is a vector of the modal power potentials of the principal subsystems. Thus, equations 2.25 are the quasi-steady state SEA power balances in principal coordinates. These can also be recast into state space form. The various forms are summarized in Table 2.2.

Table 2.2 State Space Form of the Quasi-steady State Power Balance

$\{\dot{x}(t)\}=[A_c]\{x(t)\}+[B_c]\{u(t)\}$			
Form	$[A_c]$	$[B_c]$	$\{x(t)\}$
Conservation of Energy	$-w[H]$	$[I]$	$\{E(t)\}$
Conservation of Modal Energy	$-w[N]^{-1}[K]=-w[H]^{T}$	$[N]^{-1}$	$\{e(t)\}$
Conservation of Modal Power Potential	$-[n(w)]^{-1}[b]=-w[H]^{T}$	$[n(w)]^{-1}$	$\{f(t)\}$
Conservation of Energy for Principal Subsystems	$-[\bar{D}]=-w[\tilde{U}]^{-1}[H][\tilde{U}]$	$[\tilde{U}]^{-1}$	$\{\bar{E}(t)\}$
Conservation of Modal Energy for Principal Subsystems	$-[\bar{D}]=-w[\tilde{V}]^{T}[K][\tilde{V}]^{T}$	$[\tilde{V}]^{T}$	$\{\bar{e}(t)\}$
Conservation of Modal Power Potential for Principal Subsystems	$-[\bar{D}]=-w[\tilde{W}]^{T}[b][\tilde{W}]^{T}$	$[\tilde{W}]^{T}$	$\{\bar{f}(t)\}$

Since the physical coupling matrices are positive definite as shown previously, then the system eigenvalues are all positive. This characterizes a dynamic system whose free response decays as expected. Components of the eigenvectors, which represent the distribution of energy among the principal subsystems can, however, be negative. This does not imply that a true physical subsystem will have negative energy, which is, in fact, impossible for positive definite systems. Instead, a negative eigenvector component only acts to reduce the total energy of a physical subsystem in the summation process of equation 2.21 in the same way that a positive eigenvector component acts to increase the total energy.

In structural dynamics, the state space matrix equation, which is 1^{st} order, is usually a reformulated or augmented set of 2^{nd} order differential equations of motion representing some linear finite-dimensional dynamic system. The reformulation into state space is performed because it often provides a computational advantage over the original form. Hence, the reformulation of the SEA power balance is not strictly necessary since it is already a 1^{st} order system. However, it is done because existing state space realization methods are to be adapted for use in this study and this may best be achieved without the burden of adjusting nomenclature.

The state space forms shown to this point are in the continuous-time domain. A discrete-time state space model can be constructed such that the system becomes represented by a set of difference as oppose to differential equations. This is necessary because the experimental

data used to perform the system identification is sampled response (at an interval *Dt*) acquired using digital data acquisition. This is:

$$\{x(k+1)\} = [A]\{x(k)\} + [B]\{u(k)\} \qquad (2.26a \text{ \& } b)$$
$$\{y(k)\} = [C]\{x(k)\} \qquad k = 0,1,2,\ldots$$

where, the discrete time state space matrices are given by:

$$[A] = e^{[A_c]Dt} \qquad (2.27)$$

$$[B] = \int_0^{Dt} e^{[A_c]t}\, dt\, [B_c] \qquad (2.28)$$

2.3.3 SYSTEM REALIZATION

The basic concept of a state space realization is to compute the [*A*], [*B*], and [*C*] matrices, which satisfy the discrete-time model equations 2.26, from measurements of the response of the system to some known disturbance. Typically, the measurement is either a directly or indirectly acquired pulse response; see, for example, Juang [72]. To relate the system matrices to the pulse response, a unity pulse is applied to equation 2.26. In the absence of initial energy, the following is obtained for $k = 0$:

$$\begin{Bmatrix} x_1(1) \\ x_2(1) \\ \vdots \\ x_m(1) \end{Bmatrix} = [A]\begin{Bmatrix} 0 \\ 0 \\ \vdots \\ 0 \end{Bmatrix} + [B]\begin{Bmatrix} 1 \\ 0 \\ \vdots \\ 0 \end{Bmatrix} \qquad \begin{Bmatrix} y_1(0) \\ y_2(0) \\ \vdots \\ y_m(0) \end{Bmatrix} = [C]\begin{Bmatrix} 0 \\ 0 \\ \vdots \\ 0 \end{Bmatrix} = \begin{Bmatrix} 0 \\ 0 \\ \vdots \\ 0 \end{Bmatrix} \qquad (2.29a \text{ \& } b)$$

Augmenting to include a pulse singly delivered to each degree of freedom (subsystem) gives for $k = 0$:

(2.30a & b)

$$\begin{Bmatrix} x_{11}(1) & x_{12}(1) & \cdots & x_{1m}(1) \\ x_{21}(1) & x_{22}(1) & \cdots & x_{2m}(1) \\ \vdots & \vdots & \ddots & \vdots \\ x_{m1}(1) & x_{m2}(1) & \cdots & x_{mm}(1) \end{Bmatrix} = [A] \begin{Bmatrix} 0 & 0 & \cdots & 0 \\ 0 & 0 & \cdots & 0 \\ \vdots & \vdots & \ddots & \vdots \\ 0 & 0 & \cdots & 0 \end{Bmatrix} + [B] \begin{Bmatrix} 1 & 0 & \cdots & 0 \\ 0 & 1 & \cdots & 0 \\ \vdots & \vdots & \ddots & \vdots \\ 0 & 0 & \cdots & 1 \end{Bmatrix} = [B]$$

$$\begin{Bmatrix} y_{11}(0) & y_{12}(0) & \cdots & y_{1m}(0) \\ y_{21}(0) & y_{22}(0) & \cdots & y_{2m}(0) \\ \vdots & \vdots & \ddots & \vdots \\ y_{m1}(0) & y_{m2}(0) & \cdots & y_{mm}(0) \end{Bmatrix} = [C] \begin{Bmatrix} 0 & 0 & \cdots & 0 \\ 0 & 0 & \cdots & 0 \\ \vdots & \vdots & \ddots & \vdots \\ 0 & 0 & \cdots & 0 \end{Bmatrix} = [0]$$

For $k = 1$, the following is obtained:

(2.31a & b)

$$\begin{Bmatrix} x_{11}(2) & x_{12}(2) & \cdots & x_{1m}(2) \\ x_{21}(2) & x_{22}(2) & \cdots & x_{2m}(2) \\ \vdots & \vdots & \ddots & \vdots \\ x_{m1}(2) & x_{m2}(2) & \cdots & x_{mm}(2) \end{Bmatrix} = [A][B] + [B][0] = [A][B]$$

$$\begin{Bmatrix} y_{11}(1) & y_{12}(1) & \cdots & y_{1m}(1) \\ y_{21}(1) & y_{22}(1) & \cdots & y_{2m}(1) \\ \vdots & \vdots & \ddots & \vdots \\ y_{m1}(1) & y_{m2}(1) & \cdots & y_{mm}(1) \end{Bmatrix} = [C][B]$$

For $k = 2$, the following results:

(2.32a & b)

$$\begin{Bmatrix} x_{11}(3) & x_{12}(3) & \cdots & x_{1m}(3) \\ x_{21}(3) & x_{22}(3) & \cdots & x_{2m}(3) \\ \vdots & \vdots & \ddots & \vdots \\ x_{m1}(3) & x_{m2}(3) & \cdots & x_{mm}(3) \end{Bmatrix} = [A][A][B] + [B][0] = [A]^2[B]$$

$$\begin{Bmatrix} y_{11}(2) & y_{12}(2) & \cdots & y_{1m}(2) \\ y_{21}(2) & y_{22}(2) & \cdots & y_{2m}(2) \\ \vdots & \vdots & \ddots & \vdots \\ y_{m1}(2) & y_{m2}(2) & \cdots & y_{mm}(2) \end{Bmatrix} = [C][A][B]$$

In general, a recursive relation can be written:

$$\begin{Bmatrix} x_{11}(k+1) & x_{12}(k+1) & \cdots & x_{1m}(k+1) \\ x_{21}(k+1) & x_{22}(k+1) & \cdots & x_{2m}(k+1) \\ \vdots & \vdots & \ddots & \vdots \\ x_{m1}(k+1) & x_{m2}(k+1) & \cdots & x_{mm}(k+1) \end{Bmatrix} = [A]^k [B] \qquad (2.33a \text{ \& } b)$$

$$\begin{Bmatrix} y_{11}(k) & y_{12}(k) & \cdots & y_{1m}(k) \\ y_{21}(k) & y_{22}(k) & \cdots & y_{2m}(k) \\ \vdots & \vdots & \ddots & \vdots \\ y_{m1}(k) & y_{m2}(k) & \cdots & y_{mm}(k) \end{Bmatrix} = [C][A]^{k-1}[B]$$

Clearly, the matrix of pulse responses, $[y_{ij}(k)]$, where $y_{ij}(k)$ is the response of subsystem *i* to a pulse at subsystem *j* at time sample *k* are simply related to the discrete-time state space matrices. Summarizing and denoting the matrix of pulse responses as $[Y(k)]$, the following is obtained:

$$[Y(0)] = [0] \;,\quad [Y(1)] = [C][B] \;,\quad [Y(2)] = [C][A][B] \;,\quad \ldots \;,\quad [Y(k)] = [C][A]^{k-1}[B] \qquad (2.34a - d)$$

Note that the constant matrices, $[Y(k)]$, are known as the system Markov parameters.

Arranging the Markov parameters into rows for the first *b* states leads to definitions for controllability and observability:

$$\begin{bmatrix} [Y(0)] \\ [Y(1)] \\ \vdots \\ [Y(b)] \end{bmatrix} = [C][Q_b] = [P_b][B] \qquad (2.35)$$

where, the controllability matrix, $[Q_b]$, and the observability matrix, $[P_b]$ can be seen to be:

$$[Q_b] = \begin{bmatrix} [B] \\ [A][B] \\ \vdots \\ [A]^{b-1}[B] \end{bmatrix}^T \qquad [P_b] = \begin{bmatrix} [C] \\ [C][A] \\ \vdots \\ [C][A]^{b-1} \end{bmatrix} \qquad \text{(2.36a \& b)}$$

The state or response of a system at *b* is said to be controllable if the state can be reached from any initial state of the system in a finite time interval when subject to some control action. If all states are controllable, the system is said to be completely controllable. It can be shown [72] that the system of order *m* is completely controllable if and only if the *m x bp* controllability matrix, $[Q_b]$, is of rank *m* for all *b* states, where *p* is the number of inputs. In essence, for an input singly delivered, this occurs when all eigenvector components are non-zero at the input location.

The state or response of a system at *b* is said to be observable if knowledge of the input and output over a finite time interval, $0 < k \leq b$, completely determines the response or state at *b*. If all states are observable, the system is said to be completely observable. Similarly, it can be shown [72] that the system of order *m* is completely observable if and only if the *qb x m* observability matrix, $[P_b]$, is of rank *m* for all *b* states, where *q* is the number of outputs. In essence, this occurs at a particular output location when all eigenvector components are non-zero at that location.

The identification procedure is to utilize measured Markov parameters to reconstruct or realize a system, $[\hat{A}]$, $[\hat{B}]$, and $[\hat{C}]$ that will yield outputs that are, ideally, equal to the measured response used to build the Markov parameters. The realization, however, is not

unique. The effort to characterize the system can be simplified by seeking a minimum realization, which is one with the smallest dimension of all the possible realizations. In terms of pure input/output behavior, the system parameters are the eigenpairs of the minimally realized system. Indeed, all minimal realizations have the same eigenpairs. Finally, the realized eigenvalues, $[\overline{D}]_R$, are then converted to the continuous-time domain via:

$$\left[\overline{D}_c\right]_R = \frac{ln\left(\left[\overline{D}\right]_R\right)}{Dt} \tag{2.37}$$

If the eigenvalues are complex such as with 2nd order dynamic systems, the associated continuous time eigenvalues are not unique since their imaginary parts can be scaled by any multiple of $2p$ and still satisfy the equation. Typically, the sample interval, Dt, is adjusted or frequencies beyond Nyquist are filtered to eliminate this aliasing effect. However, the quasi-steady state SEA power balance, which is 1st order, will ideally have purely real discrete-time eigenvalues which transform to purely real continuous-time eigenvalues avoiding this issue altogether. However, this could provide a means for distinguishing true 1st order SEA behavior from extraneous 2nd order response phenomena or measurement noise.

The basic development of minimal state space realization is attributed to Ho and Kalman [57]. This procedure uses what is known as a generalized Hankel matrix in the realization. The Hankel matrix is assembled from the Markov parameters as follows:

$$\left[H(k-1)\right] = \begin{bmatrix} \left[Y(k)\right] & \left[Y(k+1)\right] & \cdots & \left[Y(k+s-1)\right] \\ \left[Y(k+1)\right] & \left[Y(k+2)\right] & \cdots & \left[Y(k+s)\right] \\ \vdots & \vdots & \ddots & \vdots \\ \left[Y(k+a-1)\right] & \left[Y(k+a)\right] & \cdots & \left[Y(k+a+s-2)\right] \end{bmatrix} \tag{2.38}$$

where, a and s are arbitrary integers. Note that in order for the Hankel matrix to be of full rank, *m*, the system must be both controllable and observable, a must be greater than or equal to *m*, and s must be greater that or equal to *m*, where *m* is the number of subsystems. Extension of the Ho-Kalman procedure to realize systems from noisy measurement data resulted in the development of the Eigensystem Realization Algorithm (ERA) by Juang and Pappa [58]. With ERA, rows and columns of the Hankel matrix associated with poorly measured data can be deleted provided that the first block, [*Y(k)*] is kept intact. By maintaining only the strongly measured signals, distortion of realized parameters caused by noise is minimized without losing identification capability. Still denoting the matrix as [*H(k-1)*] since it was formed from the Hankel matrix, the modified form is hereafter referred to as the ERA block data matrix.

The process begins by decomposing the block data matrix at $k = 1$. This is done using singular valued decomposition; see, for example, Keener [30]:

$$[H(0)] = [R][S][S]^T \tag{2.39}$$

where [R] is a matrix whose columns makeup the left singular orthonormal vectors and [S] is a matrix whose columns makeup the right singular orthonormal vectors such that:

$$[R]^T [R] = [S]^T [S] = [I] \tag{2.40}$$

[*S*] is a diagonal matrix of the singular values in decreasing magnitude. For sufficiently low noise data, the matrix of singular values is then partitioned to isolate the *m* non-zero singular values:

$$[S] = \begin{bmatrix} [S]_m & [0] \\ [0] & [0] \end{bmatrix} \tag{2.41}$$

Note that if noise is present in the measured data, the preserved singular values are those that are considered significant. The discarded singular values are non-zero and, hence, the decomposition is approximate. The first m columns of $[R]$ and $[S]$ can be denoted as $[R]_m$ and $[S]_m$. Therefore, the $k = 1$ block data matrix, $[H(0)]$ can be written:

$$[H(0)] = [R]_m [S]_m [S]_m^T \tag{2.42}$$

Furthermore, the pseudo-inverse of the $k = 1$ block data matrix can be written:

$$[H(0)]' = [S]_m [S]_m^{-1} [R]_m^T \tag{2.43}$$

where the prime indicates the pseudo-inverse. It can then be shown [58,72-77] that the following realization is minimal:

$$[\hat{A}] = [S]_m^{-1/2} [R]_m^T [H(1)] [S]_m [S]_m^{-1/2} \tag{2.44a - c}$$

$$[\hat{B}] = [S]_m^{1/2} [S]_m^T \begin{bmatrix} [I]_p \\ [0]_p \\ \vdots \\ [0]_p \end{bmatrix} \qquad [\hat{C}] = \begin{bmatrix} [I]_q \\ [0]_q \\ \vdots \\ [0]_q \end{bmatrix}^T [R]_m [S]_m^{1/2}$$

where, $[\hat{A}]$, $[\hat{B}]$, and $[\hat{C}]$ are the realized system matrices, $[I]_p$ is an identity matrix of order p, where p is the number of experimental inputs, $[0]_p$ is a null matrix of order p, $[I]_q$ is an identity matrix of order q, where q is the number of experimental outputs, and $[0]_q$ is a null

matrix of order q. In essence, ERA is a least squares fit to the pulse response functions. The steps for performing the ERA are shown in Figure 2.2.

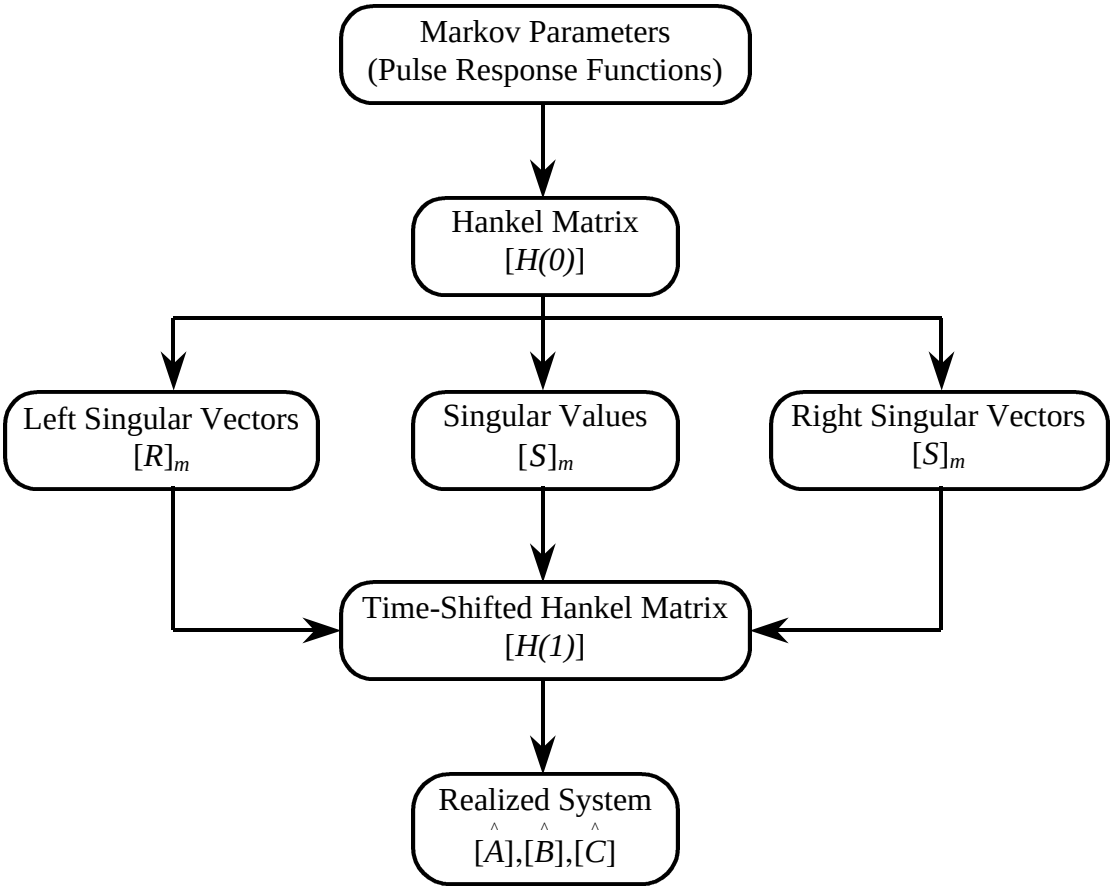

Figure 2.2 Eigensystem Realization Algorithm (ERA)

The realized discrete-time model represented by $[\hat{A}]$, $[\hat{B}]$, and $[\hat{C}]$ is then converted back to the continuous-time domain. Ideally, the realized system eigenpairs are equivalent to those obtained from a computational SEA model that perfectly represents the dynamic system. Examination of equation 2.42 reveals that, ideally:

$$[H(0)] = [R]_m [S]_m [S]_m^T = \left[[R]_m [S]_m^{1/2} \right] \left[[S]_m^{1/2} [S]_m^T \right] = [P][Q] \tag{2.45}$$

where, [P] and [Q] are then generalized observability and controllability matrices respectively. Furthermore, it can be shown [72] that the observability and controllability grammians, $[P]^T[P]$ and $[Q][Q]^T$ are both equal to the diagonal matrix of singular values:

$$[P]^T[P] = [Q][Q]^T = [S_n] \tag{2.46}$$

Since both are equal, the system is as controllable as it is observable. As a result, ERA is said to be an internally balanced realization of the [$\hat{A}$], [$\hat{B}$], and [$\hat{C}$] matrices. In other words, the mappings from input to state and from state to output are similar and balanced.

Utilization of corrupted data resulting from measurement noise can lead to bias error in the system realization. This can be minimized when using ERA by over-specification of the identified model. However, an improved method, using data correlations, can be formulated for minimizing this error without the need for model over-specification. The approach is very similar to that for ERA. Instead of decomposing a block data matrix, [$H(0)$], a decomposition of a data correlation matrix, [$R(0)$], is required. In general, the correlation matrix, [$R(k)$], is defined as follows:

$$[R(k)] = [H(k)][H(0)]^T \tag{2.47}$$

where, [$R(k)$] is a square matrix of order qa. Showing the elements of the matrices, equation 2.47 can be written as:

(2.48)

$$[R(k)] = \begin{bmatrix} [Y(k+1)] & [Y(k+2)] & \cdots & [Y(k+s)] \\ [Y(k+2)] & [Y(k+3)] & \cdots & [Y(k+s+1)] \\ \vdots & \vdots & \ddots & \vdots \\ [Y(k+a)] & [Y(k+a+1)] & \cdots & [Y(k+a+s-1)] \end{bmatrix} \begin{bmatrix} [Y(1)] & [Y(2)] & \cdots & [Y(s)] \\ [Y(2)] & [Y(3)] & \cdots & [Y(s+1)] \\ \vdots & \vdots & \ddots & \vdots \\ [Y(a)] & [Y(a+1)] & \cdots & [Y(a+s-1)] \end{bmatrix}^T$$

Or, after simplifying:

$$[R(k)] = \begin{bmatrix} \sum_{i=1}^{s} [Y(k+i)][Y(i)]^T & \sum_{i=1}^{s} [Y(k+i)][Y(i+1)]^T & \cdots & \sum_{i=1}^{s} [Y(k+i)][Y(a+i-1)]^T \\ \sum_{i=1}^{s} [Y(k+i+1)][Y(i)]^T & \sum_{i=1}^{s} [Y(k+i+1)][Y(i+1)]^T & \cdots & \sum_{i=1}^{s} [Y(k+i+1)][Y(a+i-1)]^T \\ \vdots & \vdots & \ddots & \vdots \\ \sum_{i=1}^{s} [Y(k+a+i-1)][Y(i)]^T & \sum_{i=1}^{s} [Y(k+a+i-1)][Y(i+1)]^T & \cdots & \sum_{i=1}^{s} [Y(k+a+i-1)][Y(a+i-1)]^T \end{bmatrix} \tag{2.49}$$

Note, especially, that the data correlation matrices contain auto-correlations of Markov parameters along the diagonal and cross-correlations of Markov parameters for the off-diagonal terms. As a result, uncorrelated measurement noise present in measured Markov parameters that potentially corrupts the block data matrices, [*H(k)*], is minimized in the data correlation matrices, [*R(k)*].

ERA uses the block data matrices to obtain $[\hat{A}]$, $[\hat{B}]$, and $[\hat{C}]$. Similarly, a block correlation matrix, [*H(k)*], can be built as follows:

$$[H(k)] = \begin{bmatrix} [R(k)] & [R(k+t)] & \cdots & [R(k+zt)] \\ [R(k+t)] & [R(k+2t)] & \cdots & [R(k+(z+1)t)] \\ \vdots & \vdots & \ddots & \vdots \\ [R(k+xt)] & [R(k+(x+1)t)] & \cdots & [R(k+(x+z)t)] \end{bmatrix} \tag{2.50}$$

The integer, *k*, is chosen to avoid correlation terms which give rise to bias when noise exists. The integer, *t*, is chosen to avoid excessive overlap in adjacent data correlation matrices.

Finally, the integers, *z* and *x*, define how many correlation lags exist in the block correlation matrix.

At this point, the realization of the state space matrices proceeds in the same manner as for ERA. Keeping the same notation, singular value decomposition of the block correlation matrix gives:

$$[H(0)] = [R][S][S]^T \tag{2.51}$$

The matrix of singular values is then partitioned to preserve only the *m* non-zero singular values:

$$[S] = \begin{bmatrix} [S]_m & [0] \\ [0] & [0] \end{bmatrix} \tag{2.52}$$

Again, if measurement noise is present, the decomposition is approximate. The realization can then be shown to be:

$$[\hat{A}] = [S]_m^{-1/2} [R]_m^T [H(1)] [S]_m [S]_m^{-1/2} \tag{2.53a - c}$$

$$[\hat{B}] = \left(\begin{bmatrix} [I]_{qa} \\ [0]_{qa} \\ \vdots \\ [0]_{qa} \end{bmatrix}^T [R]_m [S]_m^{1/2} \right)' [H(0)] \begin{bmatrix} [I]_p \\ [0]_p \\ \vdots \\ [0]_p \end{bmatrix} \qquad [\hat{C}] = \begin{bmatrix} [I]_q \\ [0]_q \\ \vdots \\ [0]_q \end{bmatrix}^T [R]_m [S]_m^{1/2}$$

where the prime, again, denotes the pseudo-inverse. In essence, this is a least squares fit to the pulse response auto-correlations and cross-correlations. As a result, uncorrelated measurement noise can be minimized, or even omitted, by properly choosing the integer, *k*.

Furthermore, to reduce overlap in the adjacent data correlation matrices, the integer, t, must be greater than or equal to a. Again, the realized discrete-time model represented by $[\hat{A}]$, $[\hat{B}]$, and $[\hat{C}]$ is then converted back to the continuous-time domain. Ideally, the realized system eigenpairs are equivalent to those obtained from a perfect computational SEA model. In this dissertation, the method is referred to as the power flow model realization method or simply PRM. The steps of PRM are shown in Figure 2.3.

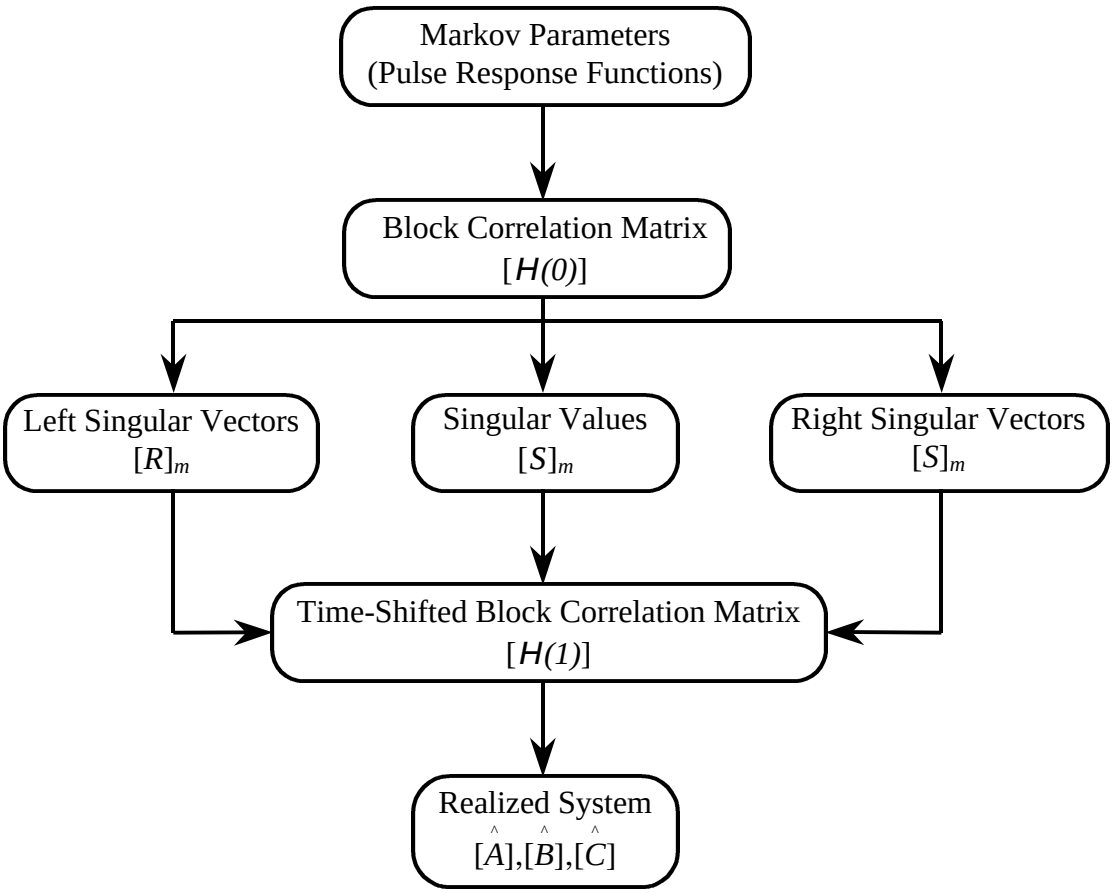

Figure 2.3 Power Flow Realization Method (PRM)

Other techniques for realizing minimal state space systems exist. Many can be shown to be similar [59]. For example, a method based on covariance equivalent realizations, which resembles PRM is the Q-Markov Cover algorithm [79-81]. However, as Juang et al [82] observe, the realization becomes accurate only asymptotically as the amount of data approaches infinity. Additionally, a bias was seen that reduces, again, only as the length of the data becomes large.

2.3.4 RESPONSE SYNTHESIS AND TEST/ANALYSIS CORRELATION

To synthesize response predicted by the realized system, the state space equations are simply used:

$$\{x_s(k+1)\} = [\hat{A}]\{x_s(k)\} + [\hat{B}]\{u_s(k)\} \qquad \text{(2.54a \& b)}$$
$$\{y_s(k)\} = [\hat{C}]\{x_s(k)\} \qquad k = 0,1,2,\ldots$$

where, the subscript, *s*, denotes synthesized response. This can be used to assess the accuracy of the realization by comparing response (synthesized from measured inputs) with actual measured response. Similarly, the realized system can be used to synthesize input/output type quantities such as pulse response or steady state frequency response. These can then be compared to the same measured quantities to further assess realization accuracy.

If a computational SEA model is available, test/analysis accuracy can be similarly examined by comparing synthesized response with response predicted by the SEA model. Furthermore, comparisons can be made between eigenpairs computed from eigensolution of the computational model with eigenpairs obtained from the realized system. Conversion of the realized discrete-time matrices given by $[\hat{A}]$ and $[\hat{B}]$ yields the realized continuous-time

representation, $[\hat{A}_c]$ and $[\hat{B}_c]$. Eigensolution of the $[\hat{A}_c]$ matrix gives the realized eigenvalue matrix, $[\overline{D}_R]$, and the realized eigenvector matrix, $[Y]$. The eigenvalues can be directly compared. The eigenvectors can be compared by computing their statistical correlation. Similar to a least squares correlation coefficient, an eigenvector correlation coefficient, r_a, for pair a can be computed:

$$r_a = \frac{\left(\{U_a\}^T \{Y_a\}\right)^2}{\{U_a\}^T \{U_a\} \{Y_a\}^T \{Y_a\}} \tag{2.55}$$

where, $\{U_a\}$ is eigenvector a from the computational SEA model and $\{Y_a\}$ is eigenvector a of the realized system. The value of r_a can vary from zero to unity. As r_a approaches unity the pair of eigenvectors approach complete correlation; whereas, when r_a goes to zero, the pair are completely uncorrelated. Furthermore, by summing over all eigenvectors at a particular degree of freedom, a subsystem eigenvector correlation coefficient can be computed:

$$r_s = \frac{\left(\sum_a U_{sa} Y_{sa}\right)^2}{\left(\sum_a U_{sa}^2\right)\left(\sum_a Y_{sa}^2\right)} \tag{2.56}$$

where, r_s, is the correlation coefficient for subsystem s, U_{sa} is the component of eigenvector a at subsystem s from the eigensolution of the computational SEA model, and Y_{sa} is the component of eigenvector a at subsystem s from the realized system.

Another method of assessing test/analysis accuracy via eigenvector correlation is to compute the cross-orthogonality. Properly identified eigenvectors are orthogonal to the eigenvectors of a perfect model with respect to its system matrices. This can be assessed by computing the triple product orthogonality relation between the measured and the model eigenvectors, which ideally produces the identity matrix. Provided modal energies are used in the system realization, the cross-orthogonality is computed as follows:

$$[\tilde{V}]^T [N][Y] \stackrel{?}{=} [I] \tag{2.57}$$

For realization based upon modal power potential measurements, cross-orthogonality is given by:

$$[\tilde{W}]^T [n(w)][Y] \stackrel{?}{=} [I] \tag{2.58}$$

2.4 CONCLUSIONS

Again, direct inversion of a matrix of measured energies can suffer from poor numerical conditioning and is likely to produce a measured coupling matrix that lacks physical sense. Furthermore, it is impractical to attempt to measure input/output data on a structure at all locations where there are subsystems in its model. This problem, however, is similar to that encountered in the structural dynamic analysis of low frequency 2^{nd} order systems. Instead of directly measuring physical parameters, focus is given to acquiring modal parameters, which serve as the common ground between structural dynamic modeling and test. State space realization, which is a popular system identification method seems similarly well suited for identifying experimental SEA parameters, since a transformation can be readily formed between physical quantities and parameters obtained from a minimal realization.

The incorporation of theoretical examination, simulation studies, and large scale testing on appreciably complex structures has led to a significant database of experience and lessons learned on the application of state space realization methods. At the forefront of this advance, ERA has earned substantial credibility for reliably identifying structural dynamic parameters [83-93]. Hence, the eigensystem realization algorithms have been adapted, in this investigation, for use in the identification of a minimum order power flow model (PRM) suitable for obtaining SEA parameters.

3 DEVELOPMENT OF A SEA MODEL IMPROVEMENT PROCEDURE

3.1 APPROACH

One of the most common approaches to updating computational structural dynamic models is outlined in Figure 3.1.

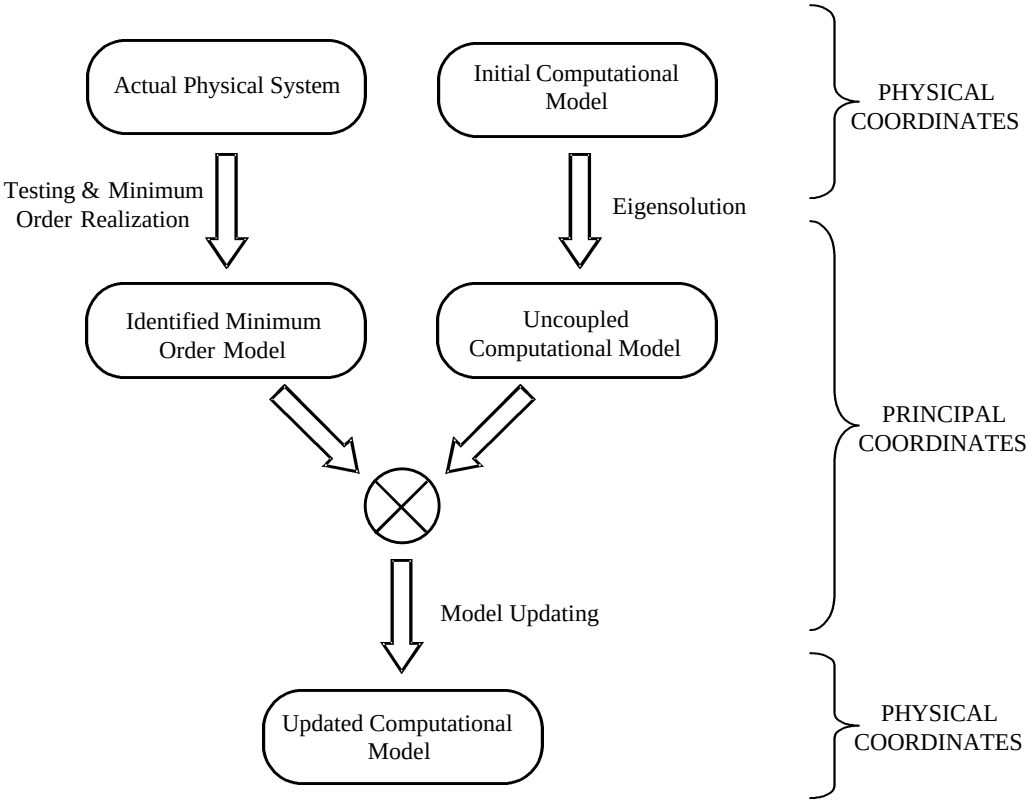

Figure 3.1 Structural Dynamic Model Updating

Basically, the eigenpairs of a realized model obtained from testing are used to update an initial computational model such that the input/output behavior of the updated model is a best fit to the measured data used in the realization. The approach is often successfully used with respect to updating structural dynamic FEA models using data obtained from modal testing.

In this investigation, the same approach is introduced to update an initial computational SEA model using a minimum order model obtained from energy and input power measurements.

3.2 EIGENVECTOR INVERSION

Probably the simplest way to update the initial computational SEA model is to project the realized eigenpairs back to physical coordinates. This transformation, however, is not unique. In fact, there exist an infinite number of physical systems that will produce the realized eigenpairs. The challenge is to obtain an updated model that, ideally, produces the measured input/output relations and maintains physical sense to its structure.

3.2.1 NON-SYMMETRIC SYSTEM

The most straightforward approach is to directly invert the realized eigenvectors. To illustrate, the non-symmetric form of the SEA power balance is written in terms of an initial coupling matrix, [H_0], and a perturbation, [DH], required such that eigensolution of the new system yields the realized eigenpairs:

$$\{\dot{E}(t)\}+w([H_0]+[DH])\{E(t)\}=\{P(t)\} \tag{3.1}$$

where, the subscript, *0*, refers to the initial system. Denoting the new system as improved, gives:

$$\{\dot{E}(t)\}+w[H_I]\{E(t)\}=\{P(t)\} \tag{3.2}$$

where, $[H_I] = [H_0]+[DH]$ is the improved coupling matrix. Solving for the perturbation yields:

$$[DH]=[H_I]-[H_0] \tag{3.3}$$

Projecting this equation into principal coordinates using the realized eigenvectors, [Y], gives:

$$[Y]^{-1}[DH][Y] = [Y]^{-1}[H_I][Y] - [Y]^{-1}[H_0][Y] \tag{3.4}$$

where, the inverse is used as the adjoint operator since the coupling matrix is non-symmetric. Provided that the eigenvectors are scaled for unity magnitude, $[Y]^{-1}[Y] = [I]$, equation 3.4 simplifies to:

$$[Y]^{-1}[DH][Y] = [\bar{D}_R] - [Y]^{-1}[H_0][Y] \tag{3.5}$$

where, $[\bar{D}_R]$ are the realized eigenvalues. Solving for perturbation matrix yields:

$$[DH] = [Y][\bar{D}_R][Y]^{-1} - [H_0] \tag{3.6}$$

where, it can also be seen that the improved coupling matrix is given by:

$$[H_I] = [Y][\bar{D}_R][Y]^{-1} \tag{3.7}$$

It can be seen that the improved coupling matrix in is nothing more than the realized eigenvalue matrix projected back to physical coordinates using the properly scaled realized eigenvectors.

Assuming reciprocity holds, the realized non-symmetric coupling matrix can be used to determine the subsystem mode counts (or modal densities). Recall that the ratio of mode counts is equal to the ratio of coupling loss factors. For subsystems *i* and *j*, this is:

$$\frac{N_i}{N_j} = \frac{h_{ji}}{h_{ij}} \tag{3.8}$$

where, the now known coupling loss factors are simply the off diagonal elements of the realized coupling matrix. However, this system of equations is rank deficient. Therefore, only a least-squares determination can be made or at least one subsystem mode count must be known prior to solving for the others.

3.2.2 SYMMETRIC SYSTEM

There is no guarantee that the updated non-symmetric coupling matrix will maintain any physical sense other than the number of degrees of freedom which is set by the initial computational SEA model. On the other hand, a generalized inverse of the realized eigenvectors weighted by the initial model can be utilized in the updating such that a degree of physical sense is preserved. It can be seen in the development of this method that a symmetric form of the coupling matrix is required.

The symmetric form of conservation of modal energy is written in terms of an initial mode count matrix, $[N_0]$, initial coupling matrix, $[K_0]$, and perturbations, $[DN]$ and $[DH]$, required such that eigensolution of the new system yields the realized eigenpairs:

$$([N_0]+[DN])\{\dot{e}(t)\}+w([H_0]+[DH])\{e(t)\}=\{P(t)\} \tag{3.9}$$

where, the subscript, *0*, refers to the initial system. Denoting the new system as improved, gives:

$$[N_I]\{\dot{e}(t)\}+w[H_I]\{e(t)\}=\{P(t)\} \tag{3.10}$$

where, $[N_I] = [N_0]+[DN]$ is the improved mode count matrix and $[K_I] = [K_0]+[DK]$ is the improved coupling matrix. Solving for the mode count perturbation yields:

$$[DN] = [N_I] - [N_0] \tag{3.11}$$

Projecting this equation into principal coordinates using the realized eigenvectors, $[Y]$, gives:

$$[Y]^T [DN][Y] = [Y]^T [N_I][Y] - [Y]^T [N_0][Y] \tag{3.12}$$

where, in this case, the transpose is used as the adjoint operator since the coupling matrix is symmetric. Provided the eigenvectors are scaled for unity mode count, $[Y]^T[N_I][Y] = [I]$. Equation 3.12 simplifies to:

$$[Y]^T [DN][Y] = [I] - [Y]^T [N_0][Y] \tag{3.13}$$

Defining the projection of the initial mode count matrix to principal coordinates as $[\overline{N}_0] \equiv [Y]^T[N_0][Y]$, equation 3.13 can be written as:

$$[Y]^T [DN][Y] = [I] - [\overline{N}_0] \tag{3.14}$$

Pre and post-multiplying equation 3.14 with the inverse of the original mode count projection yields the following:

$$\left([Y]^T [N_0][Y]\right)^{-1}[Y]^T [DN][Y]\left([Y]^T [N_0][Y]\right)^{-1} = \left([Y]^T [N_0][Y]\right)^{-1}\left([I] - [\overline{N}_0]\right)\left([Y]^T [N_0][Y]\right)^{-1} \tag{3.15}$$

Equation 3.15 can be somewhat simplified by substituting $[\overline{N}_0]$ into the right hand side as follows:

$$\left([Y]^T [N_0][Y]\right)^{-1}[Y]^T [DN][Y]\left([Y]^T [N_0][Y]\right)^{-1} = [\overline{N}_0]^{-1}\left([I] - [\overline{N}_0]\right)[\overline{N}_0]^{-1} \tag{3.16}$$

Solving for the mode count perturbation gives:

$$[DN] = \left([Y]^T\right)^{-1}[Y]^T[N_0][Y][\bar{N}_0]^{-1}\left([I]-[\bar{N}_0]\right)[\bar{N}_0]^{-1}[Y]^T[N_0][Y][Y]^{-1} \tag{3.17}$$

Further simplifying yields:

$$[DN] = [N_0][Y][\bar{N}_0]^{-1}\left([I]-[\bar{N}_0]\right)[\bar{N}_0]^{-1}[Y]^T[N_0] \tag{3.18}$$

Inspection of equation 3.18 reveals that:

$$[DN] = \left([Y]^g\right)^T\left([I]-[\bar{N}_0]\right)[Y]^g \tag{3.19}$$

where, $[Y]^g$, is the generalized inverse weighted by the mode count matrix of the initial computational SEA model:

$$[Y]^g = [\bar{N}_0]^{-1}[Y]^T[N_0] \tag{3.20}$$

Up to this point it is assumed only that the measured eigenpairs are correct and they are orthogonal with respect to the improved mode count matrix. Finally, the resulting improved mode count matrix is:

$$[N_I] = [N_0] + \left([Y]^g\right)^T\left([I]-[\bar{N}_0]\right)[Y]^g \tag{3.21}$$

To determine the improved coupling matrix, satisfaction of the power balance and coupling matrix symmetry become additional constraints. The eigenproblem for the improved system can be written:

$$\left([K_I]-[\bar{D}_R][N_I]\right)[Y] = [0] \tag{3.22}$$

substituting $[K_I] = [K_0]+[DK]$ yields:

$$([K_0]+[DK])[Y] = [\bar{D}_R][N_I][Y] \tag{3.23}$$

Projecting equation 7.11 to principal coordinates gives:

$$[Y]^T([K_0]+[DK])[Y] = [Y]^T[\bar{D}_R][N_I][Y] \tag{3.24}$$

Denoting the projection of the original coupling matrix to principal coordinates by $[E_R]^T[K_0][E_R] = [\bar{K}_0]$, equation 7.12 simplifies to:

$$[\bar{K}_0]+[Y]^T[DK][Y] = [Y]^T[N_I][Y][\bar{D}_R] \tag{3.25}$$

Solving for the coupling perturbation using the generalized inverse defined previously, the following is obtained:

$$[DK] = \left([Y]^g\right)^T([\bar{D}_R]+[\bar{K}_0])[Y]^g - \left([K_0][Y][Y]^g\right) - \left([K_0][Y][Y]^g\right)^T \tag{3.26}$$

Finally, the improved coupling matrix is:

$$[K_I] = [K_0] + \left([Y]^g\right)^T([\bar{D}_R]+[\bar{K}_0])[Y]^g - \left([K_0][Y][Y]^g\right) - \left([K_0][Y][Y]^g\right)^T \tag{3.27}$$

A similar result can be obtained using conservation of modal power potential, where the mode count matrix is replaced by the modal density matrix and the coupling matrix is replaced by the modal coupling matrix. In this investigation, the model updating procedures described are collectively referred to as SEA model improvement or simply SMI.

Although the procedure for updating a symmetric system offers more physical realizability than the non-symmetric update, gross global modeling errors can lead to a breakdown of system connectivity in the structure of the coupling matrix. The intention, here, is to possess a somewhat reasonable initial model and then update it to correct a number of localized modeling errors. The extent of initial model accuracy necessary for reasonable updates is further examined in later sections.

3.3 EXPANSION OF UNMEASURED DEGREES OF FREEDOM

As previously discussed, not all degrees of freedom need be excited to employ a minimum order realization provided that the number of inputs allow for complete controllability. In many situations, a single input may suffice if no eigenvector component is zero at that degree of freedom. However, in most real situations it is unlikely that response measurements on a physical structure will be gathered at all degrees of freedom that exist in a computational model of the system. Not only might this prove to be time consuming, the response of certain SEA subsystems (such as in-plane mode groups) would, in fact, prove difficult, if not impossible, to measure. Therefore, a means of expanding measured eigenvectors back to the full number of degrees of freedom is needed in order to perform the model updating.

For the steady state SEA power balance, an expansion based upon a transformation that is mathematically identical to that used in a static reduction of an FEA model would suffice for expanding the coupling matrix without approximation. However, for the quasi-steady state power balance this method would not be an exact mapping even for a perfect coupling matrix.

An exact mapping can be constructed using the eigenpairs from eigensolution of the symmetric power balance equations. To develop this method, recall that the modal energy, for example, can be written as the linear superposition of modal energies of the principal subsystems. At the full number of degrees of freedom, *m* subsystems, this is:

$$\{e_m(t)\} = [V_{ma}]\{\bar{e}_a(t)\} \tag{3.28}$$

where, $\{e_m(t)\}$ is the vector of modal energies of all *m* physical subsystems, $[V_{ma}]$ is the eigenvector matrix at all *m* degrees of freedom of the computational model for *a* eigenvectors, and $\{\bar{e}_a(t)\}$ is a vector of the modal energies of *a* principal subsystems. At the reduced, test degrees of freedom, *t*, the superposition is:

$$\{e_t(t)\} = [V_{ta}]\{\bar{e}_a(t)\} \tag{3.29}$$

multiplying equation 3.29 by $[V_{ta}]^T$ gives:

$$[V_{ta}]^T \{e_t(t)\} = [V_{ta}]^T [V_{ta}]\{\bar{e}_a(t)\} \tag{3.30}$$

solving equation 3.30 for $\{\bar{e}_a(t)\}$ yields:

$$\{\bar{e}_a(t)\} = \left([V_{ta}]^T [V_{ta}]\right)^{-1} [V_{ta}]^T \{e_t(t)\} \tag{3.31}$$

Substituting equation 3.31 into 3.28 gives:

$$\{e_m(t)\} = [V_{ma}]\left([V_{ta}]^T [V_{ta}]\right)^{-1} [V_{ta}]^T \{e_t(t)\} \tag{3.32}$$

The embedded transformation from test degrees of freedom to full degrees of freedom can be seen:

$$\{e_m(t)\} = [T_{mt}]\{e_t(t)\} \tag{3.33}$$

where, the transformation is given by,

$$[T_{mt}] = [V_{ma}]\left([V_{ta}]^T [V_{ta}]\right)^{-1} [V_{ta}]^T \tag{3.34}$$

Finally, the expansion of the realized eigenvectors, $[Y]$ at the test degrees of freedom back to the full number of degrees of freedom in the computational model can be written:

$$[Y_m] = [T_{mt}][Y_t] \tag{3.35}$$

Provided that the eigenvectors of the computational model are from a full eigensolution and the number of test degrees of freedom used in the transformation exceeds the number of eigenvectors chosen for the update, then this is a least squares mapping that exactly expands a reduced set of eigenvectors back to the full set. The transformation does not introduce further approximation on its own. Error manifested here results only from discrepancy between the initial computational model and the true physical system. A transformation can also be constructed when the number of eigenvectors exceeds the number of test degrees of freedom. However, this represents an average, not least squares, solution and, as such, would introduce approximation into the mapping process. Furthermore, it should be obvious that the eigenvectors from the computational model chosen for use in the least squares transformation should be observable at the test input/output locations.

3.4 SUMMARY

The procedure for performing the realized model expansion and SEA model updating is shown in Figure 3.2.

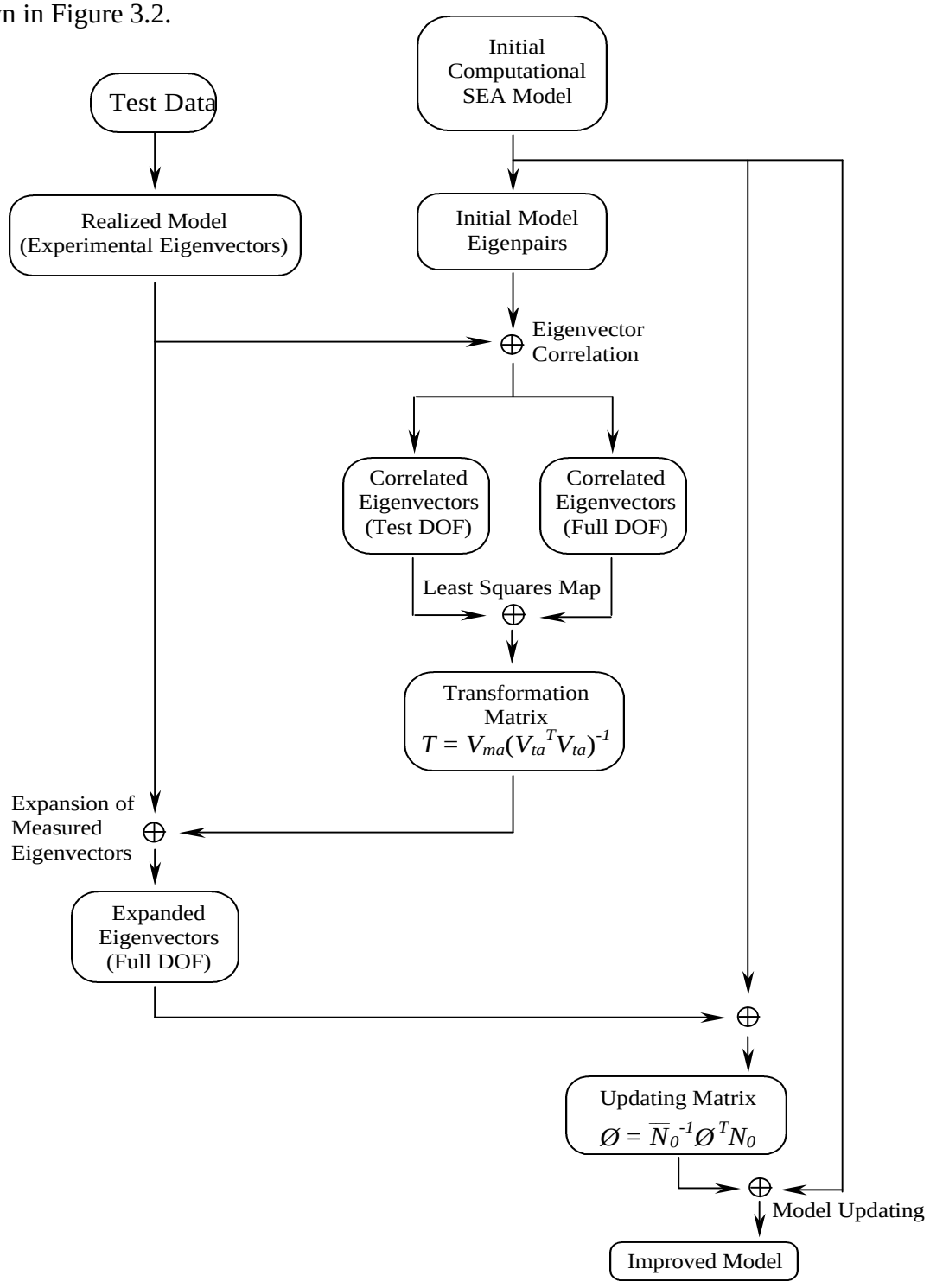

Figure 3.2 Power Flow Realization Method (PRM) and SEA Model Improvement (SMI)

4 SIMULATIONS

Prior to using experimentation to assess the accuracy of the system identification and model updating procedures presented in this dissertation, it makes sense to attempt the same using simulated experimental data. In this way, a means of quantifying identification and update accuracy is readily available since the true parameters used to generate the simulated data are known. In other words, the results of the experimental SEA can be directly compared to the true parameters used to construct the simulated response. Laboratory investigations on both simple and complex structures are presented in later sections.

4.1 TWO-SUBSYSTEM MODEL

The first simulation examined here is the two-subsystem model, which, in essence, represents the simplest of SEA systems. The two-subsystem SEA model is shown in Figure 4.1.

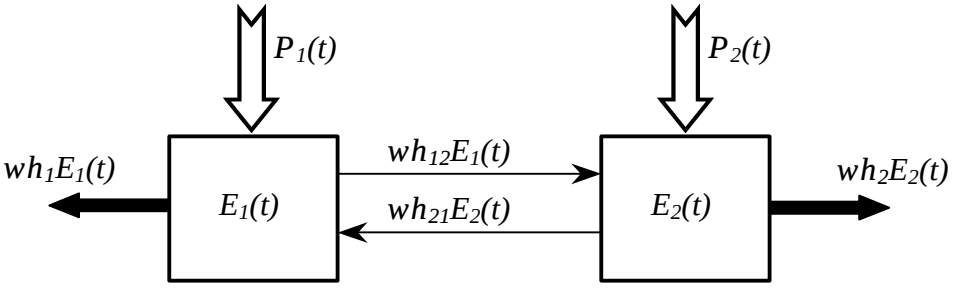

Figure 4.1 Two-Subsystem SEA Model

The approach taken is to maintain two predictive computational SEA models. The first model is the initial computational SEA model. The second SEA model represents the simulation of a true physical system. In this case, it contains, what are usually unknown parameter differences from the initial model intended to represent modeling inaccuracy. This

second model is used only to generate simulated transient experimental data and to provide the reference for assessing system identification and updating accuracy. This imitates a typical situation where one is seeking to improve a “first cut” model that contains potential modeling error. The system identification procedure developed in this study is then applied to the simulated experimental data. The realized minimum order model or “fit” is compared to the simulated data to validate the identification process. Next, the model updating schemes, also developed in this study, are then applied. Finally, since in this case they are available, the updated model parameters can be compared to their true values to assess the accuracy of the update. For excitation, a pulse input is used. Additionally, varying levels of normally distributed random noise are added to both the input and the response to imitate measurement noise. A typical pulse response with a 40 dB signal to noise ratio (SNR) is shown in Figure 4.2.

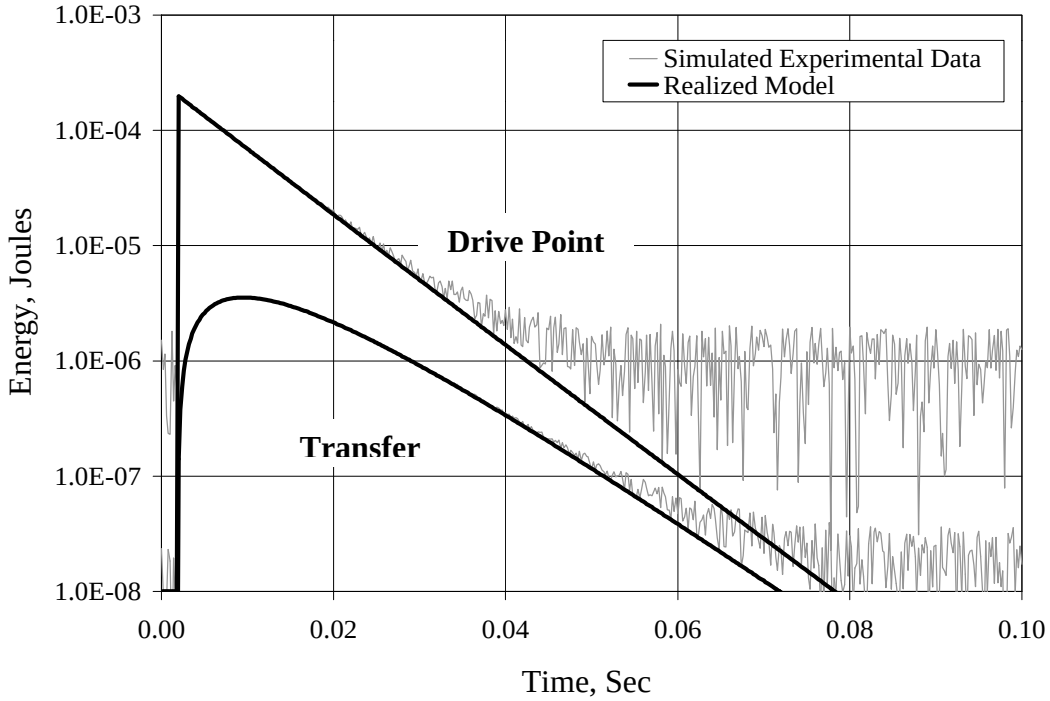

Figure 4.2 Two-Subsystem SEA Simulation

It can be clearly seen that the realization provides a minimum order power flow model that is a best "fit" to the simulated experimental data. The singular values obtained from decomposition of the block correlation matrix for this example are shown in Figure 4.3.

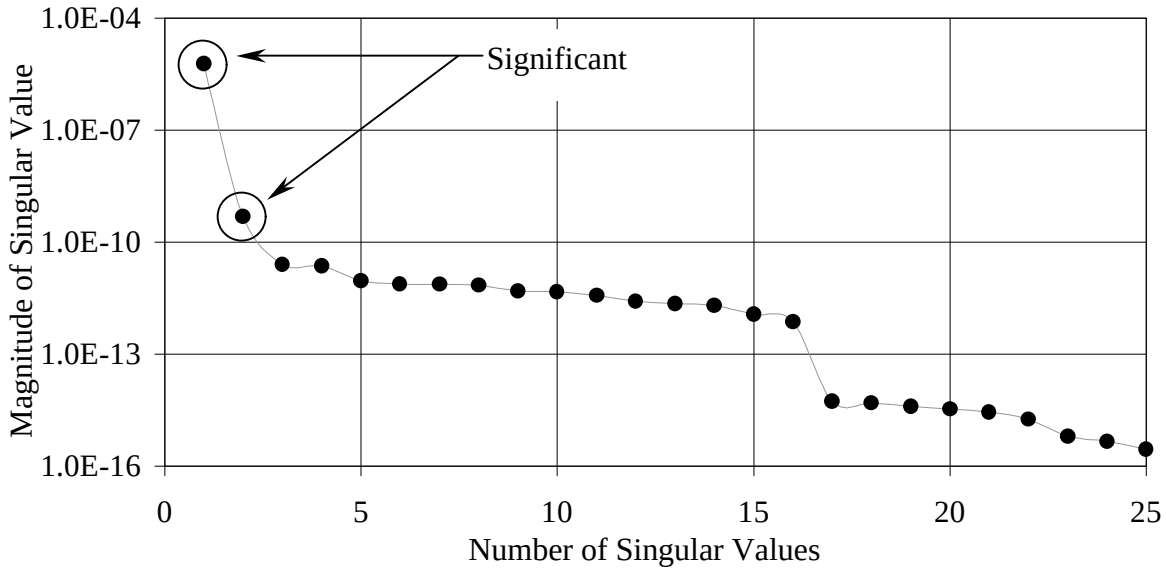

Figure 4.3 Decomposition of Two-Subsystem Block Correlation Matrix

By comparing the relative magnitudes of all of the singular values, it can be seen that only the first two are significant. Indeed, this makes sense since a two-subsystem SEA model was used to generate the simulated response. Furthermore, it can be seen that only the first two associated eigenvalues are real as shown in Table 4.1. In the table, when the real part of a unit vector in the direction of the complex eigenvalue equals unity, the value is completely real. Preserving eigenpairs associated

Table 4.1 Eigenvalues of Two-Subsystem Simulation

Index	Principal Loss Factor	Real Part of Unit Vector	
1	0.018	1.00	Significant
2	0.025	1.00	
3	0.303	0.01	
4	0.492	0.56	
5	0.659	0.14	
6	0.814	0.00	
7	1.056	0.02	
8	1.262	0.01	
9	1.281	0.02	
10	1.623	0.02	
11	1.667	0.02	
12	1.964	0.02	
13	2.184	0.02	
14	2.370	0.02	

with complex eigenvalues in the realized model cause it to generate oscillations when reconstructing the response. This would not represent a best fit. Instead, the complex eigenvalues are discarded since they are associated with the noise added to the simulated measured response. Clearly, this is a means for identifying true system behavior from extraneous 2nd order phenomenon such as measurement or sensor noise.

First, the dependence of realization accuracy on the level of noise in the response is studied. The analysis frequency bandwidth is a full octave centered at 1000 Hz. For case 1, the initial SEA model has mode counts of 110 and 200 for subsystems one and two respectively. The coupling loss factor is h_{12} = 0.001. The damping loss factors are h_1 = 0.01 and h_2 = 0.02. The resulting system matrices for the initial SEA model are:

$$[N_0] = \begin{bmatrix} 110 & 0 \\ 0 & 200 \end{bmatrix} \qquad [H_0] = \begin{bmatrix} 0.01100 & -0.00055 \\ -0.00100 & 0.02055 \end{bmatrix} \qquad \text{(4.1a \& b)}$$

The simulated test data is generated using the same parameters except that the damping loss factor is doubled, h_1 = 0.02. Therefore, a perfect model update should produce a 100% subsystem one damping loss factor increase. The system matrices used to generate the simulation, which are, typically, not known are:

$$[N_E] = \begin{bmatrix} 110 & 0 \\ 0 & 200 \end{bmatrix} \qquad [H_E] = \begin{bmatrix} 0.02100 & -0.00055 \\ -0.00100 & 0.02055 \end{bmatrix} \qquad \text{(4.2a \& b)}$$

The highlighted element represents the simulated SEA inaccuracy. System realization and model updating are performed repeatedly for simulations maintaining a SNR that varies from 0 dB to 80 dB.

The realized eigenvalue errors are shown in Figure 4.4. It can be seen that, obviously, the error decreases as the SNR increases. For reference, the potential maximum error in any of

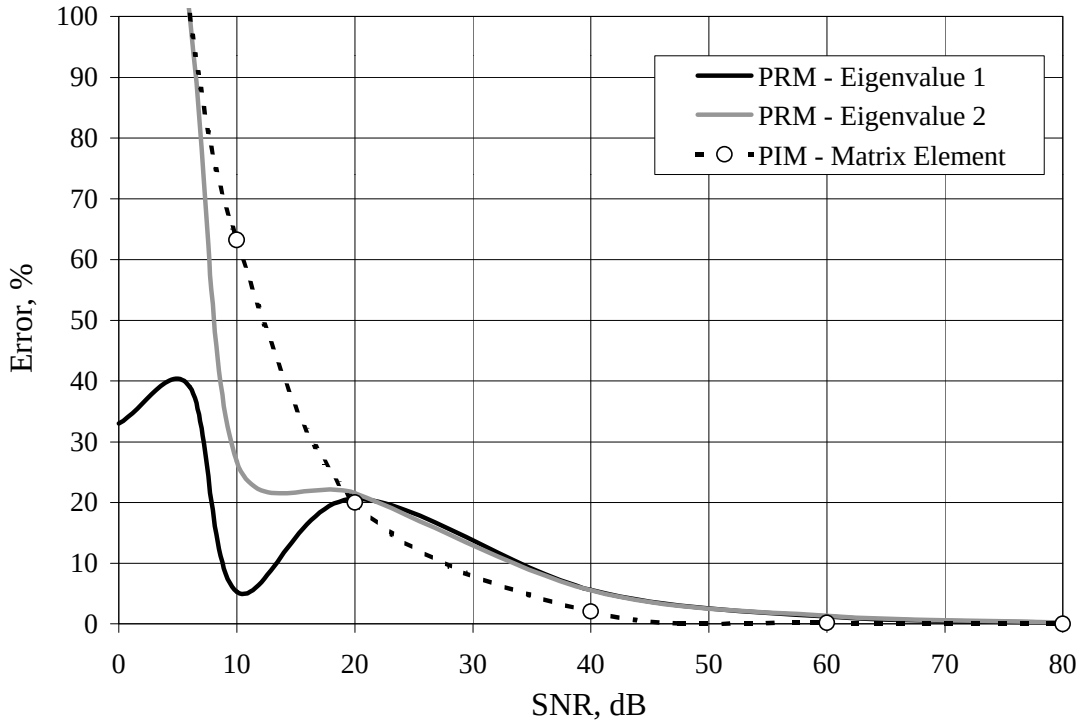

Figure 4.4 Eigenvalue Error (Case 1)

the elements of a coupling matrix computed using PIM subject to the same noise level is plotted as well. For the most part, PRM is comparable to PIM in this respect.

The damping loss factors of the improved model after using the symmetric model update procedure are shown in Figure 4.5. Recalling that the true damping loss factor should be

h_1 = 0.02, it can be seen that accuracy, again, increases with increasing SNR. For the most part, PRM performs comparably to PIM.

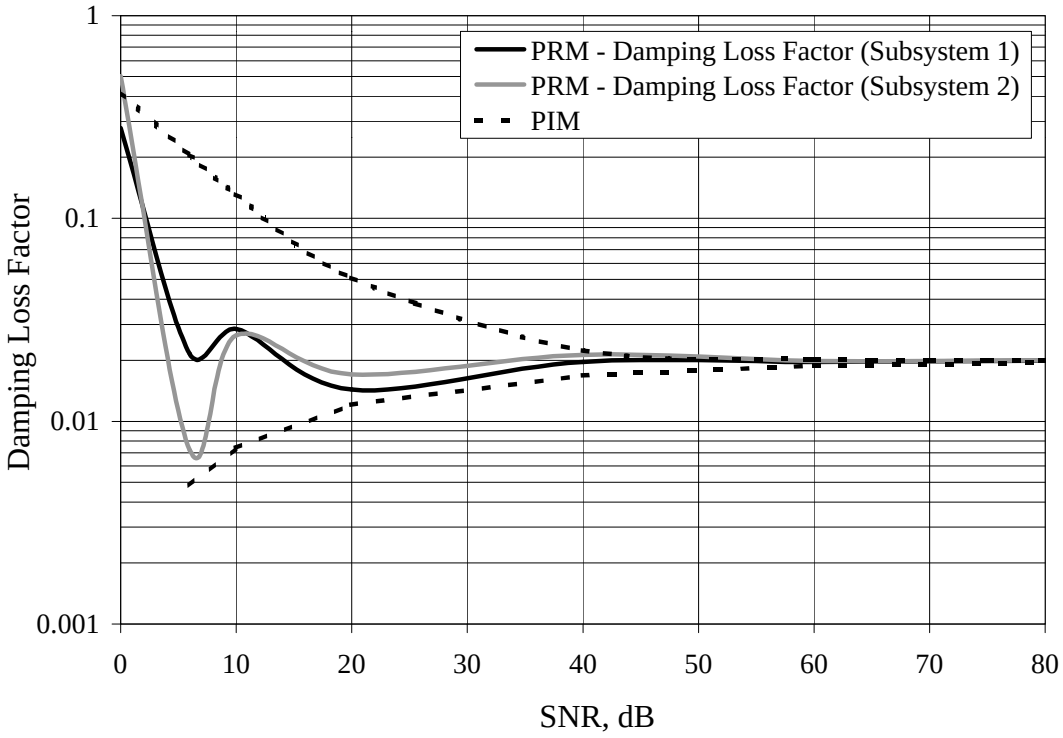

Figure 4.5 Damping Loss Factor (Case 1)

Ideally, the model updating procedure should produce a change to only the (1,1) entry of the coupling matrix since only the damping of subsystem one truly changed. If other elements in the matrix are modified, the improved system looses physical sense. The degree to which this "smearing" depends on response SNR is shown in plots of the normalized coupling matrix update in Figure 4.6, where the elements of the coupling change matrix have been normalized by the maximum change. It can be seen that, as expected, the smearing becomes worst as the SNR decreases. From the fourth subplot, it can be observed that the updated coupling matrix looses physical structure at noise levels below 20 dB SNR.

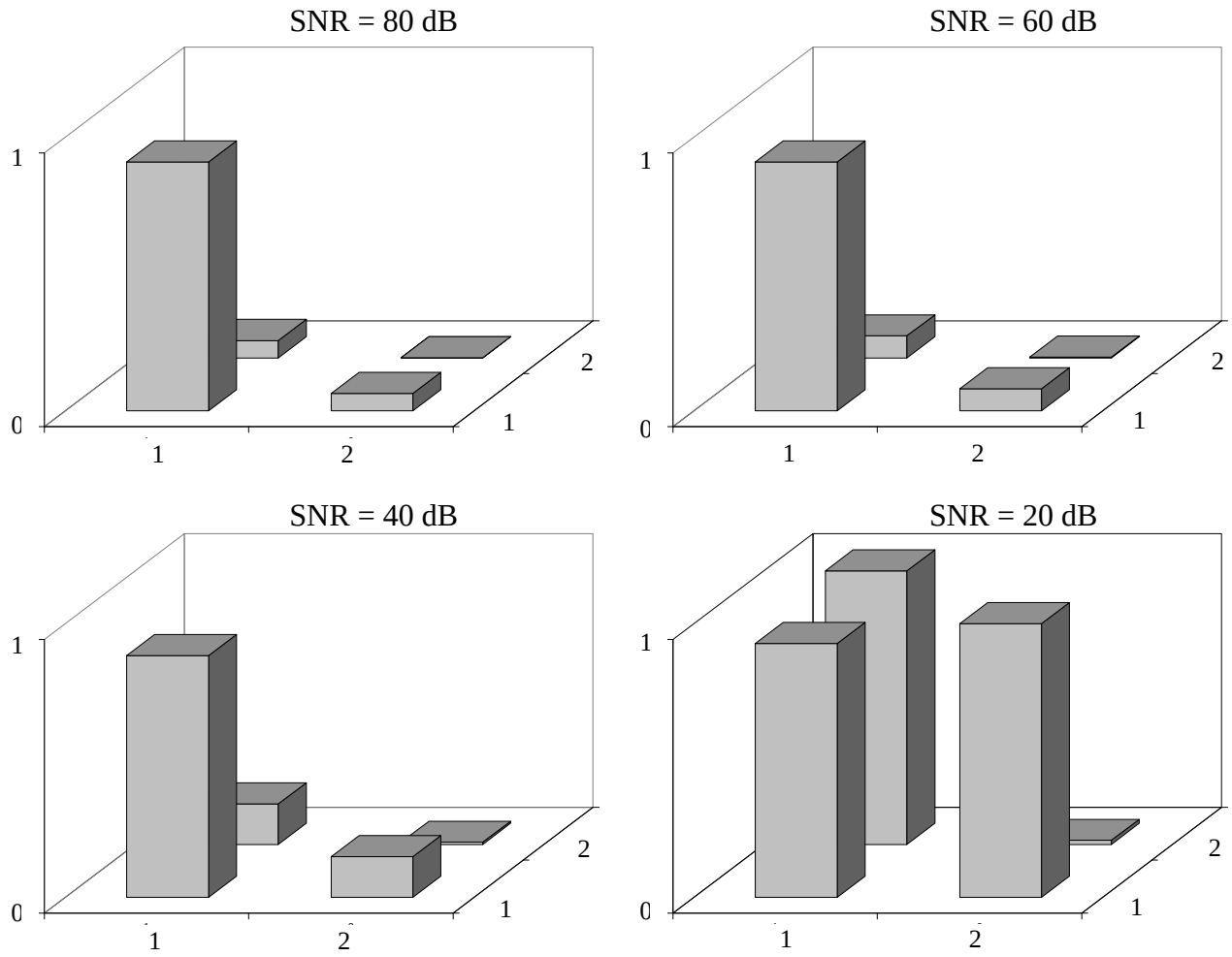

Figure 4.6 Normalized Coupling Matrix Update (Case 1)

For case 2, this procedure is repeated to examine updating of more than a single parameter. The initial SEA model is identical to the previous initial model as shown:

$$[N_0] = \begin{bmatrix} 110 & 0 \\ 0 & 200 \end{bmatrix} \qquad [H_0] = \begin{bmatrix} 0.01100 & -0.00055 \\ -0.00100 & 0.02055 \end{bmatrix} \qquad \text{(4.3a \& b)}$$

The simulated test data is generated using the same parameters except that, in this case, the mode count of subsystem one is increased to 200. This result of this discrepancy forces error

into the coupling matrices. In essence, this simulates a scenario that is inferior to the first case examined since more than a single SEA parameter is inaccurate. The experimental system matrices are:

$$[N_E] = \begin{bmatrix} 200 & 0 \\ 0 & 200 \end{bmatrix} \qquad [H_E] = \begin{bmatrix} 0.01100 & -0.00100 \\ -0.00100 & 0.02100 \end{bmatrix} \qquad \text{(4.4a \& b)}$$

where the highlighted elements represent SEA inaccuracy. System realization and model updating is once again performed repeatedly for simulations maintaining a SNR that varies from 0 dB to 80 dB. The realized eigenvalues errors are shown in Figure 4.7.

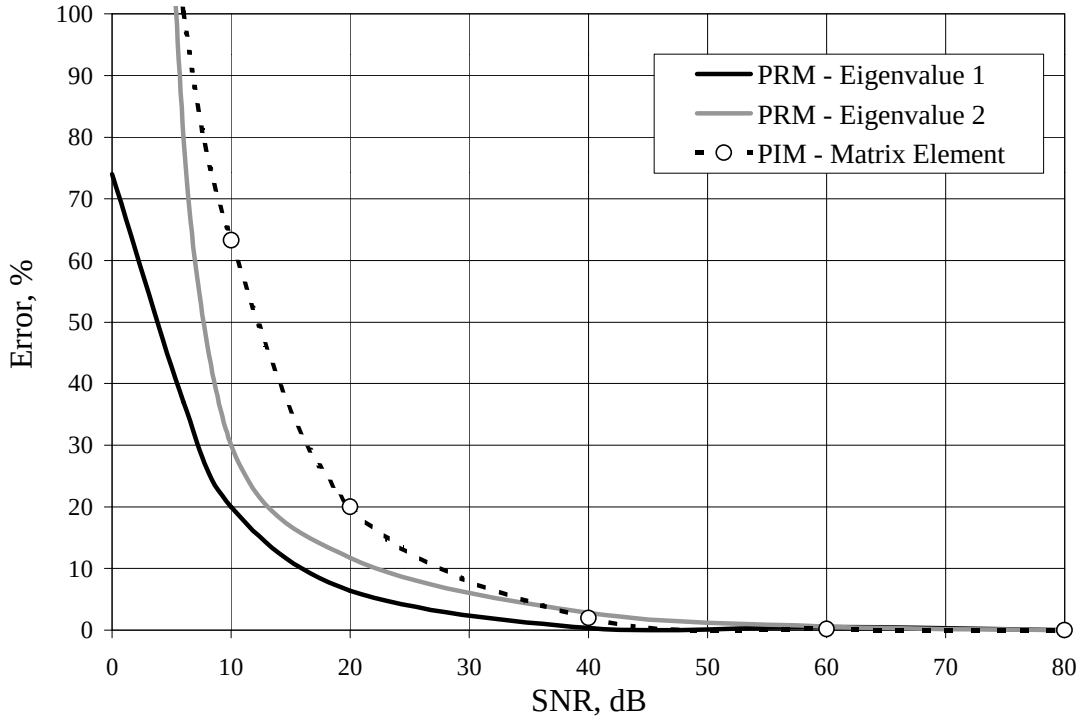

Figure 4.7 Eigenvalue Error (Case 2)

It can be again seen that the error decreases as the SNR increases. For reference, the potential maximum error in any of the elements of a coupling matrix computed using PIM

subject to the same noise level is plotted as well. Once again, the two are somewhat comparable in this respect.

The damping loss factors of the improved model after using the symmetric model update procedure are shown in Figure 4.8.

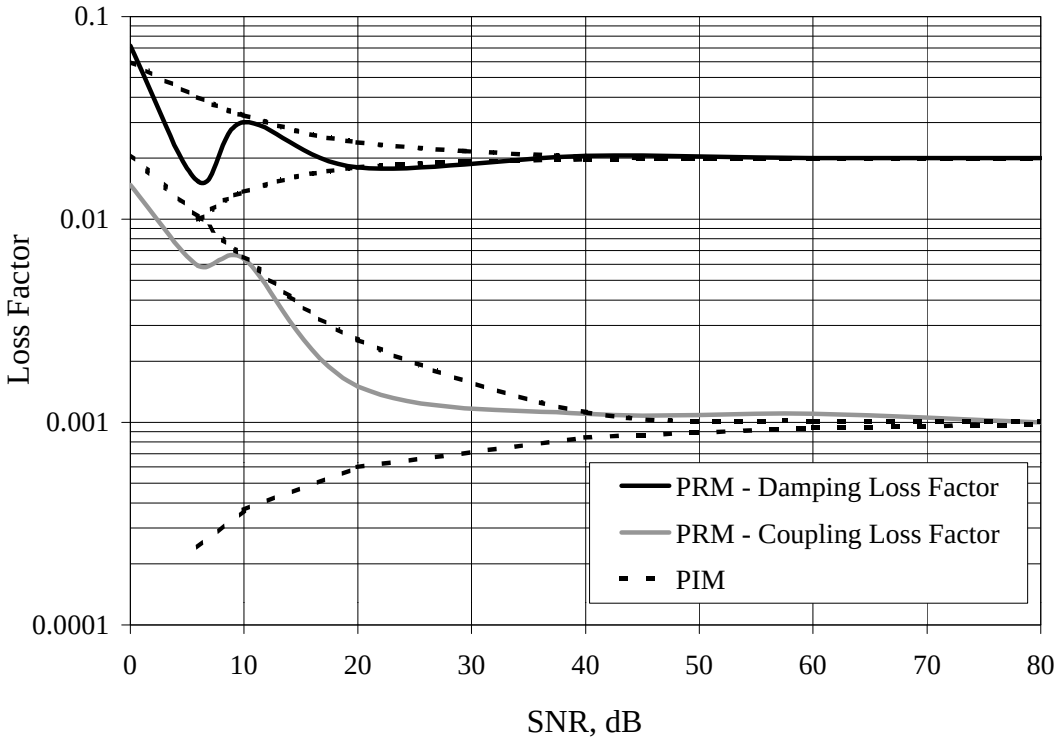

Figure 4.8 Damping and Coupling Loss Factor (Case 2)

Once more PRM and PIM perform similarly in this regard.

In this simulation, the model updating procedure, ideally, should produce a change to three of the four entries of the coupling matrix as shown in equation 4.4. As a result, it is simplest to

observe the degree of smearing by plotting the damping loss factor of subsystem one, which is the only parameter that should not change. This is shown in shown in Figure 4.9.

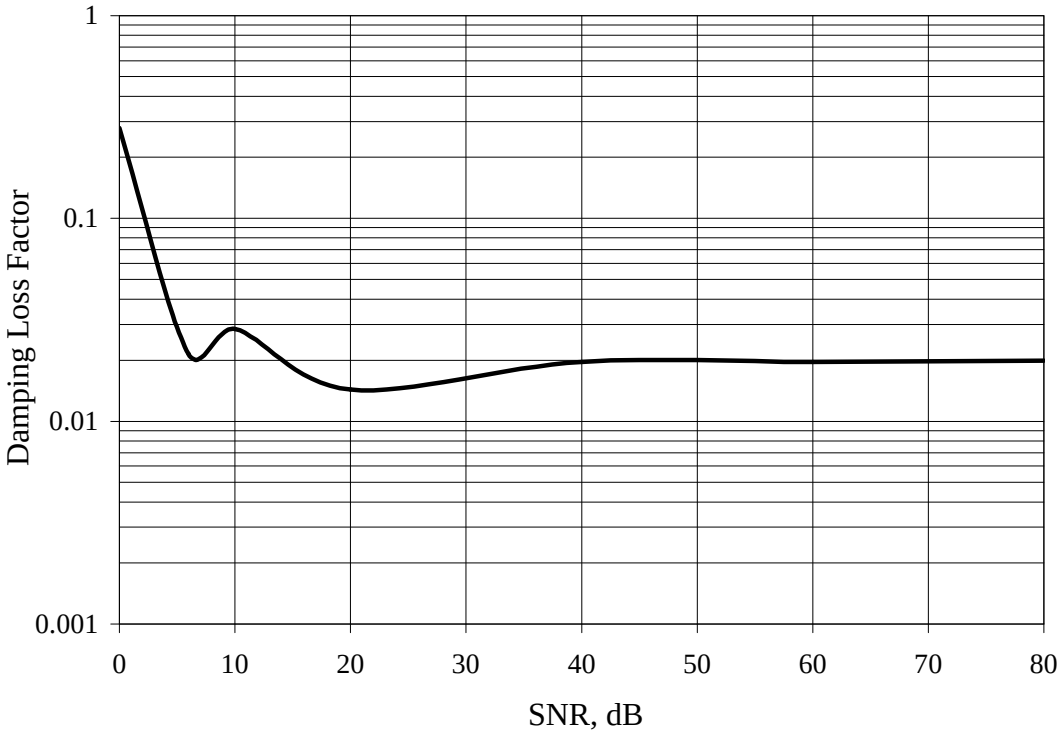

Figure 4.9 Subsystem 1 Damping Loss Factor (Case 2)

Once more, it can be seen that, as expected, the smearing becomes worst as the SNR decreases. However, it appears that the updated coupling matrix maintains physical structure at noise levels above 20 dB SNR.

In conclusion, for the two-subsystem SEA simulation, it seems that both PRM and PIM perform comparably. Although the computational procedure of PIM is considerably more straightforward (especially for only two degrees of freedom), PRM is implemented with only a single input for the realization, whereas, PIM requires two inputs and, hence, twice as much

data. This suggests that PRM may prove more advantageous for complex systems by simplifying experimental procedures.

4.2 MULTI-SUBSYSTEM MODEL

The next simulation examined is a multiple subsystem model. Specifically, the true system is comprised of ten SEA subsystems. The maximum ratio of off-diagonal to diagonal elements is 0.8 and the ratio of the highest to lowest singular values is 35. This indicates that the system maintains light to moderate coupling. The PRM method is used to identify a minimum order power flow model using a single pulse input at subsystem six with response locations on six of the ten subsystems. It is found that only two identified eigenpairs need be used to accurately update an initial model that has a factor of 10 discrepancy in the damping of subsystem one.

It is found that care must be taken to properly chose the eigenpairs of the initial computational SEA model that are used in the expansion of the realized model at the test degrees of freedom up to the full number of degrees of freedom. The 1st eight eigenvectors of the initial computational model are plotted in Figure 4.10.

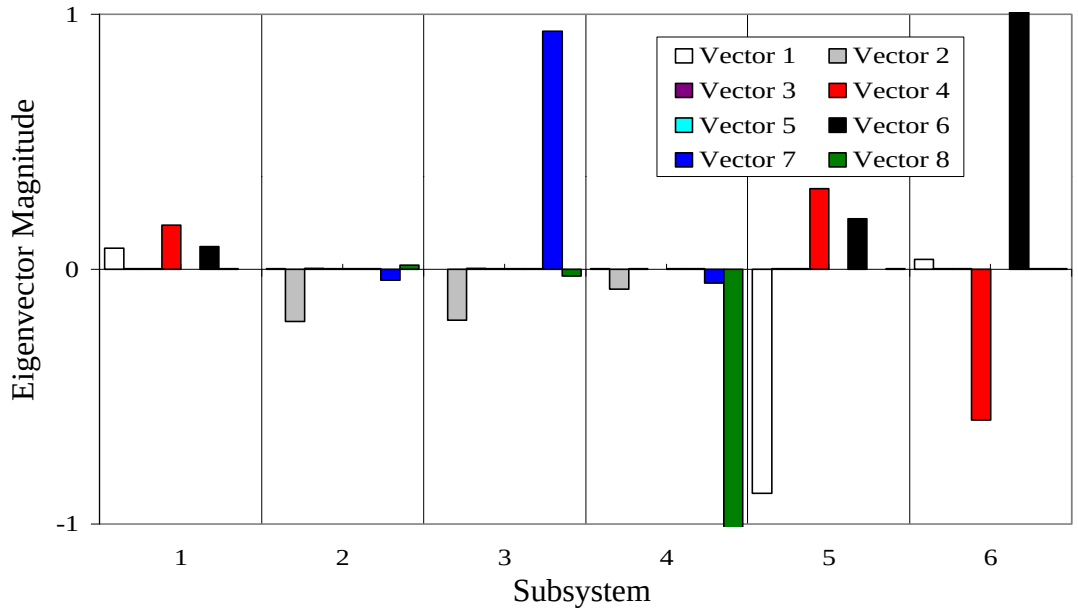

Figure 4.10 Eigenvectors of Initial Multi-subsystem Computational SEA Model

Probably, the most judicious choice would be to use eigenvectors one, four, and six since only those three are controllable at the input location – subsystem six; the other eigenvector components are zero at this subsystem. It is eventually seen that, in this case, only two eigenvectors need be used to successfully update the initial SEA model. In the absence of noise, utilization of eigenvectors one and four lead to a successful SMI with a minimum degree of smearing as shown in Figure 4.11.

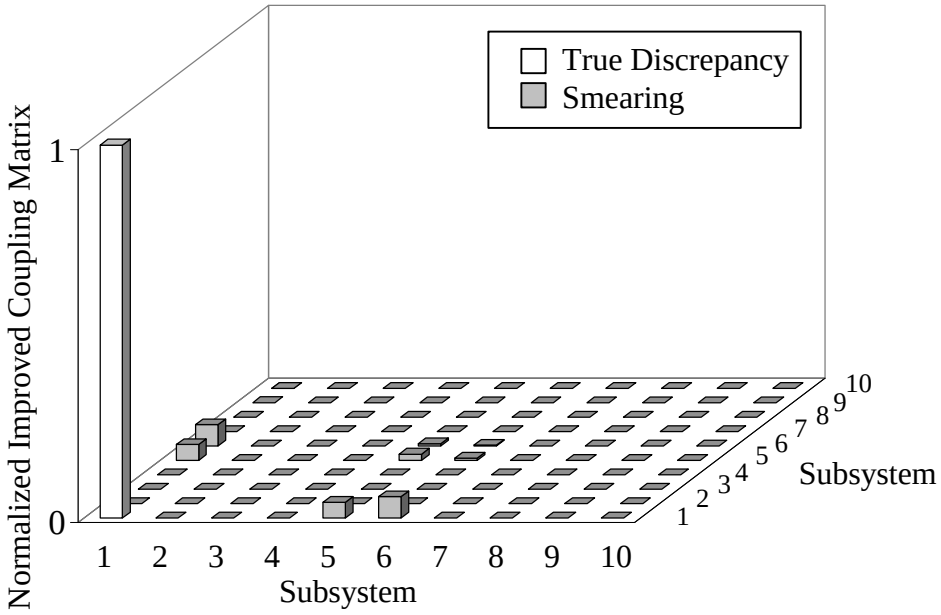

Figure 4.11 SMI With Good Choice of Eigenvectors

Elements of the normalized improved coupling matrix are simply elements of the improved coupling matrix divided by true value of the coupling matrix at the location of the discrepancy $K_E(1,1)$. Furthermore, it can be seen that an improper choice of eigenvectors (three and eight) of the initial computational model leads to a poor expansion of realized eigenvectors which results in a SMI that looses physical sense as shown in Figure 4.12.

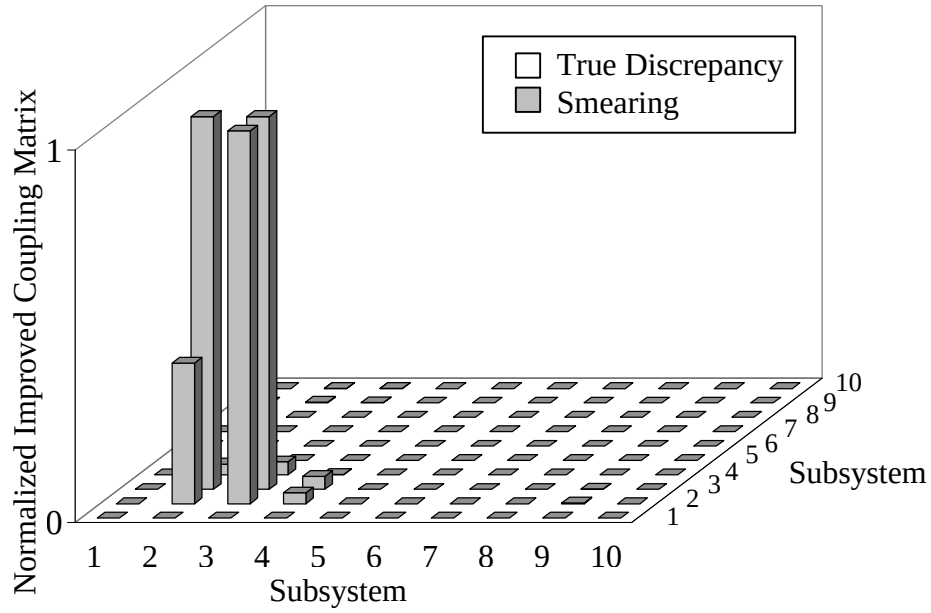

Figure 4.12 SMI With Poor Choice of Eigenvectors

The same study is repeated using a SNR of 20 dB. Again, with a good choice of eigenvectors (one and four) maintaining a non-zero eigenvector component at the input subsystem leads to an SMI with slightly more smearing than is present with no noise yet can still be seen to be successful as shown in Figure 4.13.

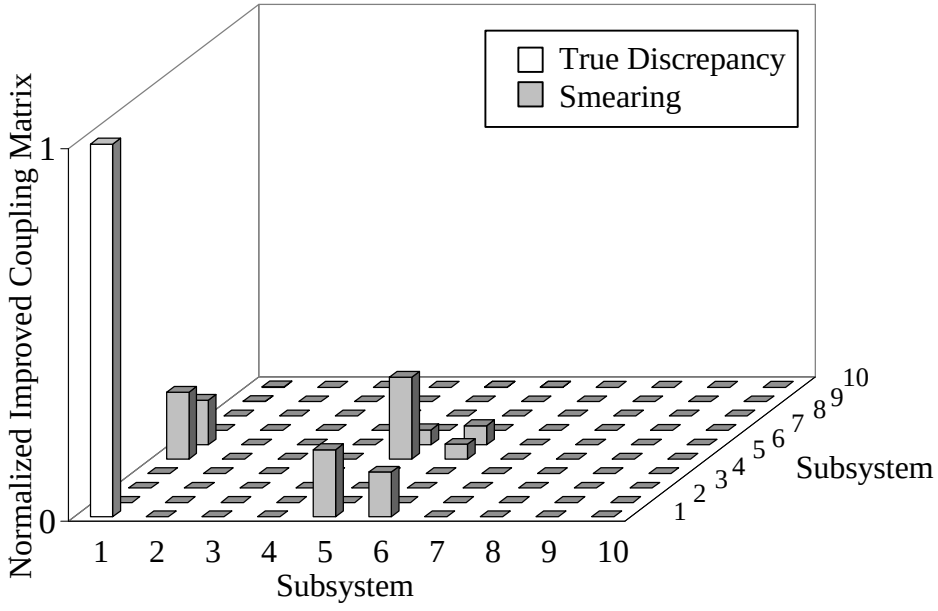

Figure 4.13 SMI With Noise and Good Choice of Eigenvectors

For the situation with poorly chosen eigenvectors realized in the presence of noise, SMI leads, again, to an updated coupling matrix that lacks even less physical sense than the noise free case as shown in Figure 4.14.

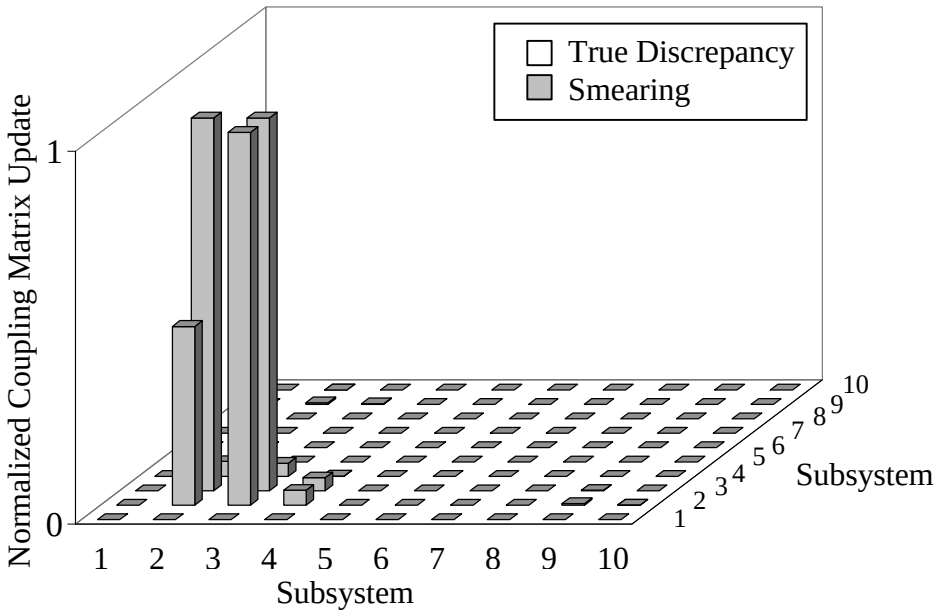

Figure 4.14 SMI With Noise and Poor Choice of Eigenvectors

To examine the extent of initial model accuracy necessary for successful model improvement, simulations were performed for an increasing number of discrepancies in the coupling matrix. Specifically, errors in a range from two to ten of the eleven non-zero coupling loss factors were progressively introduced. The normalized coupling matrix update for each PRM/SMI is shown in Figure 4.15.

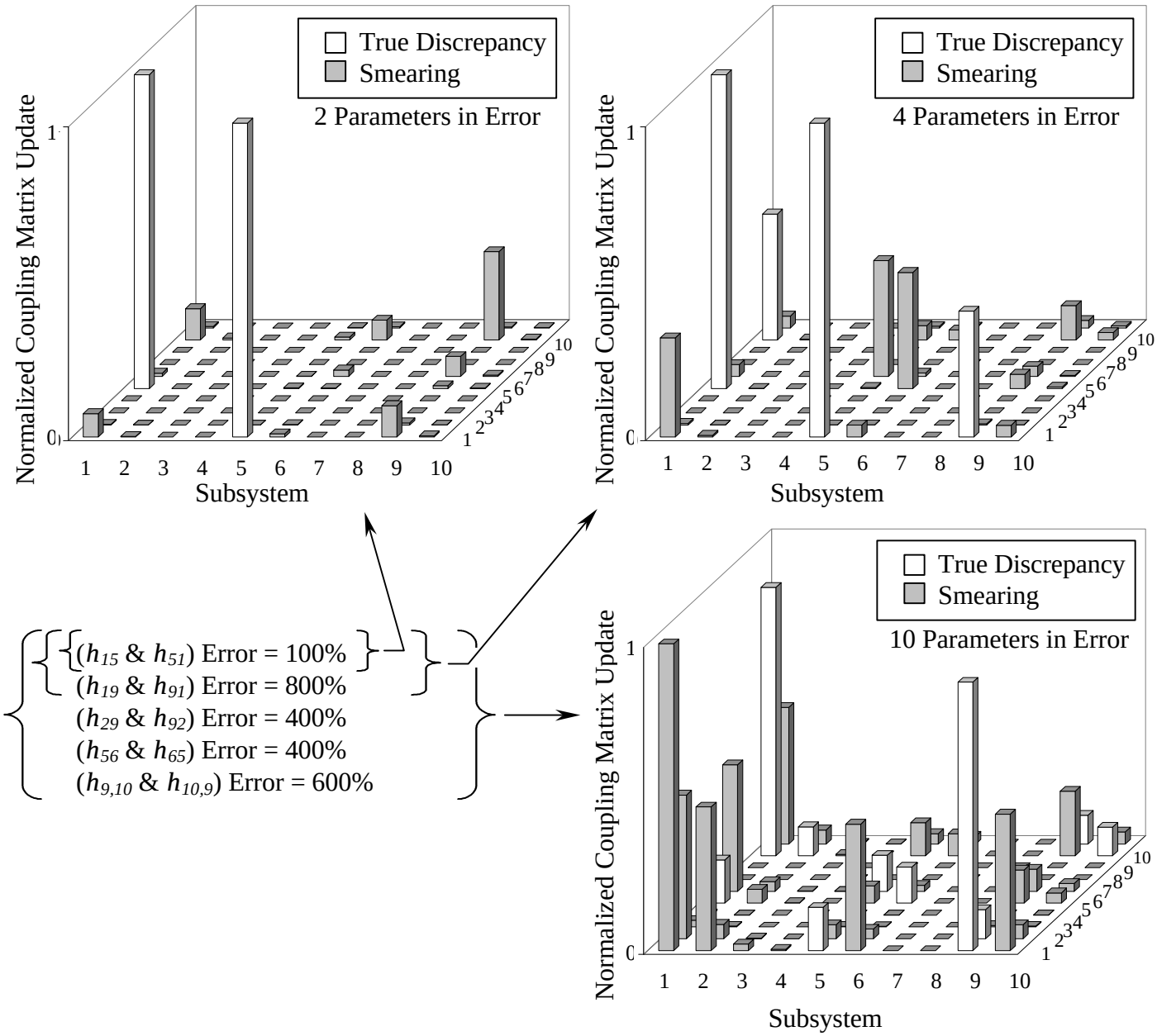

Figure 4.15 Effect of Initial Model Inaccuracy

Note that, in these cases, only eigenvectors that are obviously controllable from the input location are utilized in the expansion. Clearly, as the number of parameters in error becomes greater, the physical sense to the structure of the model updating procedure becomes lost as

evidenced by the smearing. All updates are seen to equally maintain the proper input/output relationships that correlate with the simulated experimental data. However, a reasonably accurate initial model is required to obtain proper physical SEA parameters from the updating process.

4.3 CONCLUSIONS

As a result of simulation studies, it seems that the power flow model realization method (PRM) and the SEA model improvement (SMI) scheme developed in this dissertation show promise for enhancing experimental SEA practices. The realization accuracy of PRM appears to be comparable to PIM without the inherent need to gather a full set of input/output data. Furthermore, the SMI proved to successfully update an initial SEA model and required only a minimal amount of response data and computational effort.

In all cases, accuracy depended on the signal to noise ratio. However, even in the presence of moderately noisy data (20 dB SNR) reasonable success could be achieved. Finally, it was observed that error in the identification of physical SEA parameters manifested in direct relation to initial model inaccuracy.

5 EXPERIMENTAL STUDIES

5.1 SIMPLE STRUCTURE

Experiments conducted on an actual structure allow for true assessment of realization and model updating accuracy. Since the structural dynamics of a simple structure are understood, it serves as a useful test-bed such that experimental techniques appropriate for the methods developed in this dissertation may be refined prior to advancing to a more complex system.

5.1.1 EXPERIMENTAL SETUP

The structure under consideration consists of two 16 gauge steel plates connected at a 90º angle. The plates are 4 ft. by 5 ft. and 3 ft. by 4 ft. respectively and are welded together along the common 4 ft. sides. The entire structure is suspended as shown in Figure 5.1.

Figure 5.1 Test Setup

Simple decay rate measurements showed that the bare plates had a relatively low damping loss factor ($h < 0.001$), see Figure 5.2. As a result, it was necessary to apply damping tile, as shown in the photograph, increasing the damping loss factor above the theoretical coupling loss factors such that weak coupling conditions (favorable for SEA) could be achieved. The damping loss factor for both plates was increased to approximately $h = 0.01$.

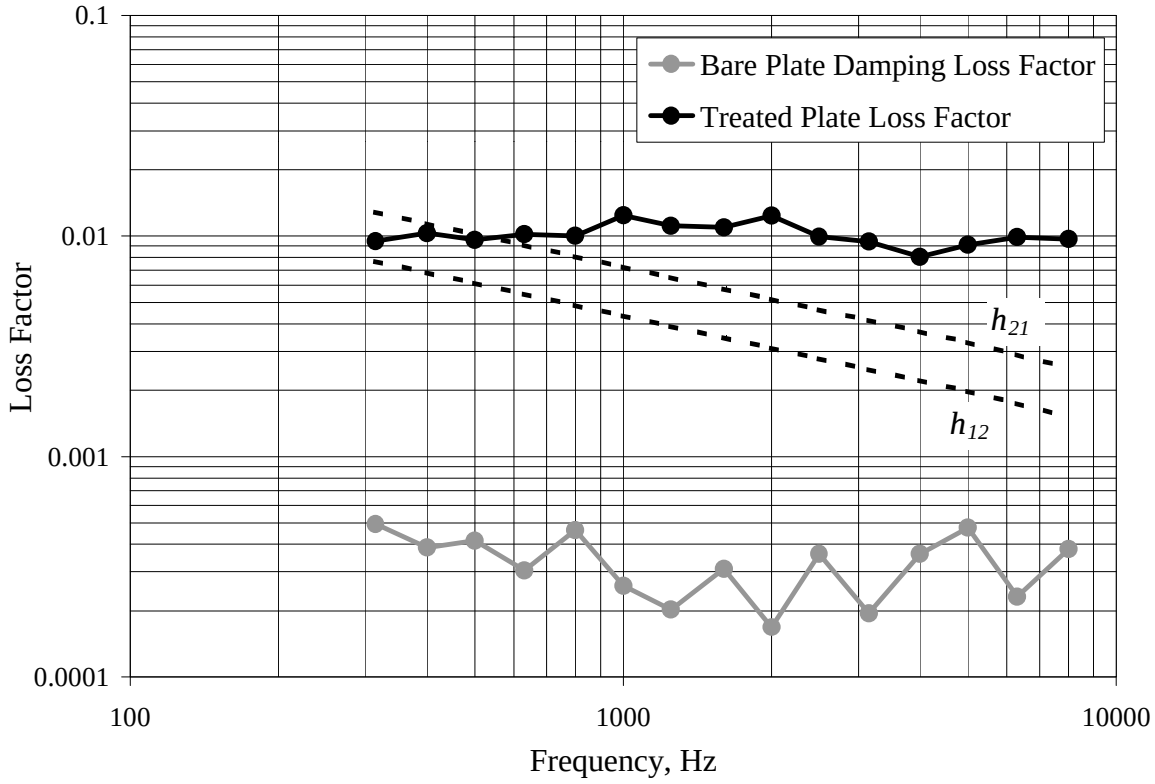

Figure 5.2 Damping Tile Treatment

Test equipment was setup as shown in Figure 5.3. Response acceleration was measured using accelerometers and force inputs were measured using force gauges. Both sensor types were standard piezoelectric transducers with flat response over the entire analysis bandwidth of interest (315 Hz – 8000 Hz).

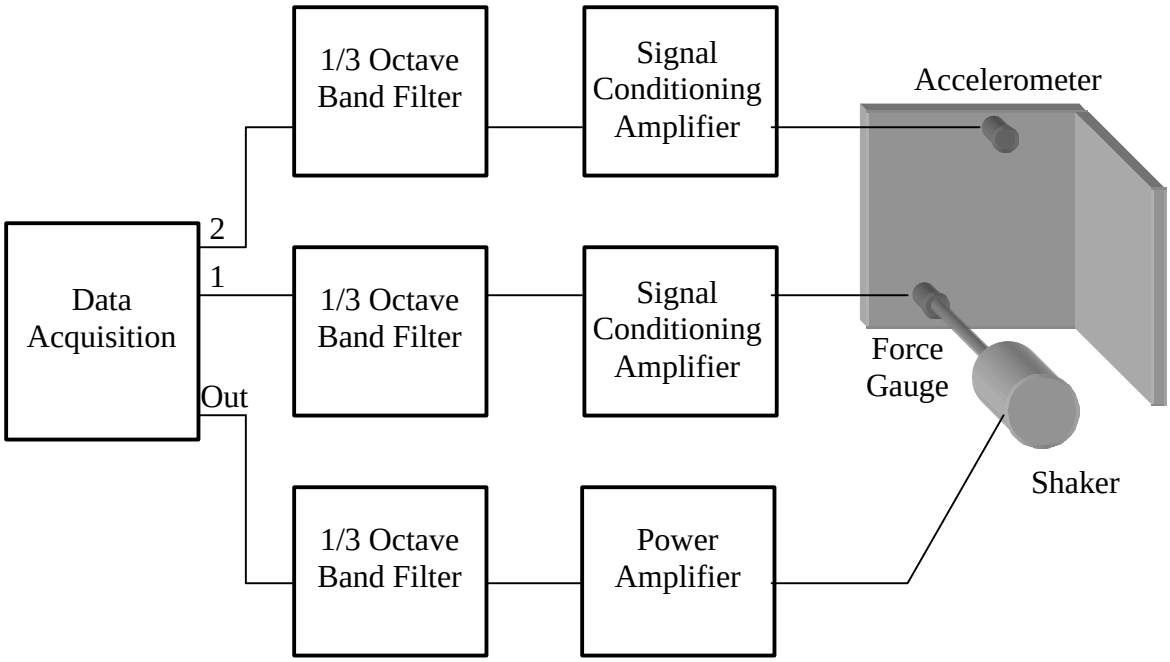

Figure 5.3 Instrument Setup

Broadband frequency response function (FRF) measurements were initially collected to serve as a baseline in the test/analysis comparisons. For use in the power flow model realization, a burst random excitation filtered in successive 1/3 octave bands over the analysis bandwidth was employed. Additionally, during the transient tests, both force gauge and accelerometer outputs were filtered in the same successive 1/3 octave bands. Response data were gathered at ten randomly chosen locations (five on each plate) for each of six different shaker input locations (three on each plate) to obtain reasonable spatial averaging.

Average FRF's were stored digitally and acquired using standard fast Fourier transform (FFT) processing. Chirp excitation that was periodic over each time ensemble was used such that windowing functions were not required, hence, minimizing leakage in the FFT process.

During transient testing, average drive point force, drive point acceleration, and transfer acceleration were acquired and stored digitally in the time domain using five ensembles per average at each input/output location for each of the 1/3 octave bands in the overall analysis bandwidth. Eight samples per period were acquired throughout. A noise burst, as opposed to a pulse, was used. The duration of the burst was sufficiently longer than the computed rise time based on the expected damping level such that steady state conditions would be reached prior to turning off the excitation. In this way, the response measurement would achieve maximum SNR during the event for the given input power.

5.1.2 TRANSIENT DATA PRE-PROCESSING

Since the actual measurements were input force and response acceleration at a point, the data was processed to yield spatially and temporally averaged input power and response energy. Specifically, multiplication of the instantaneous input force by the instantaneous response velocity (obtained by integrating the acceleration) at the drive point gave the instantaneous input power. It was found that proper phase calibration of the collocated force/accelerometer pair was necessary to accurately obtain the instantaneous power measurement. A typical input power measurement for the 1000 Hz 1/3 octave band on the coupled plate structure is shown in Figure 5.4.

Since the measured quantity was 2^{nd} order, it was necessary to compute a short time average input power to yield the 1^{st} order behavior or, loosely, the envelope of the input. To accomplish this, all data within a window consisting of a 5 period duration (or 40 samples) were averaged.

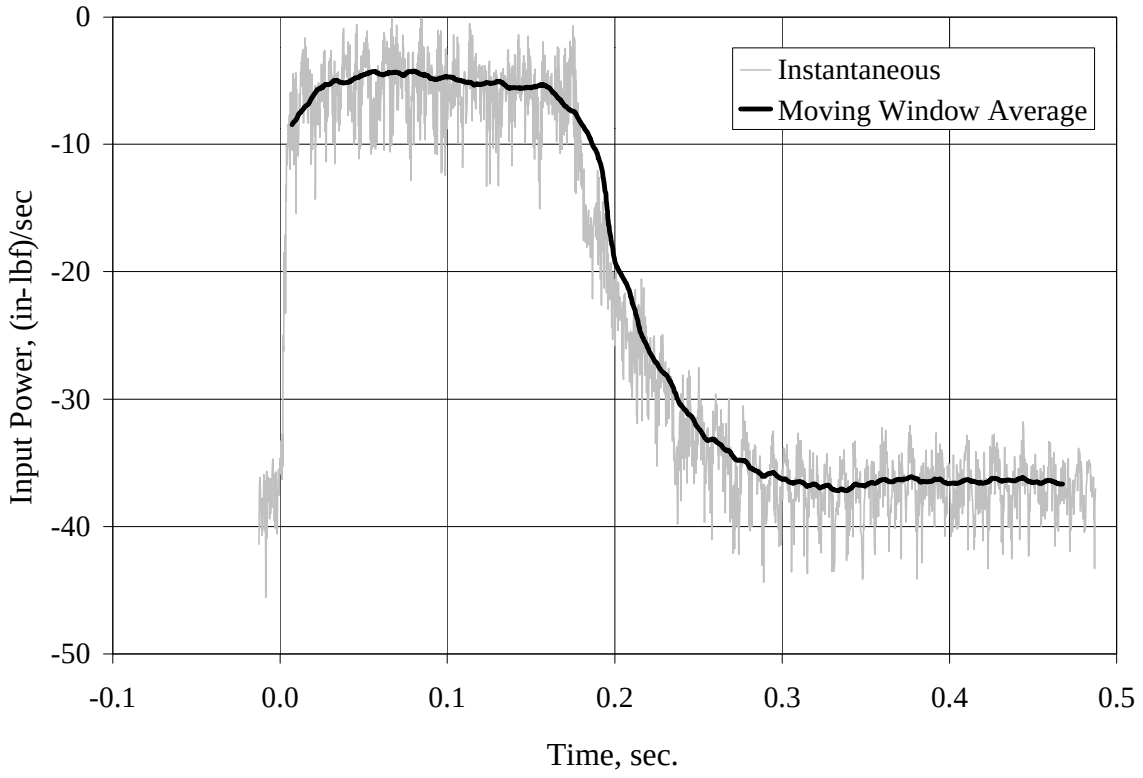

Figure 5.4 Input Power, 1000 Hz

This was repeated for all data points after stepping one sample per repetition. The result is a moving window average of the input power as shown in figure 5.4. It can be seen that the 2nd order behavior has been, effectively, filtered. A similar approach was used on the instantaneous squared velocity to obtain the moving window average or mean square velocity. This is shown in Figure 5.5.

The mean square velocity was then multiplied by the appropriate system mass to obtain the total energy of that particular subsystem.

Even though care was taken to deliver the same voltage to the shaker at each different input location, local differences in plate impedance did not guarantee that power input levels were

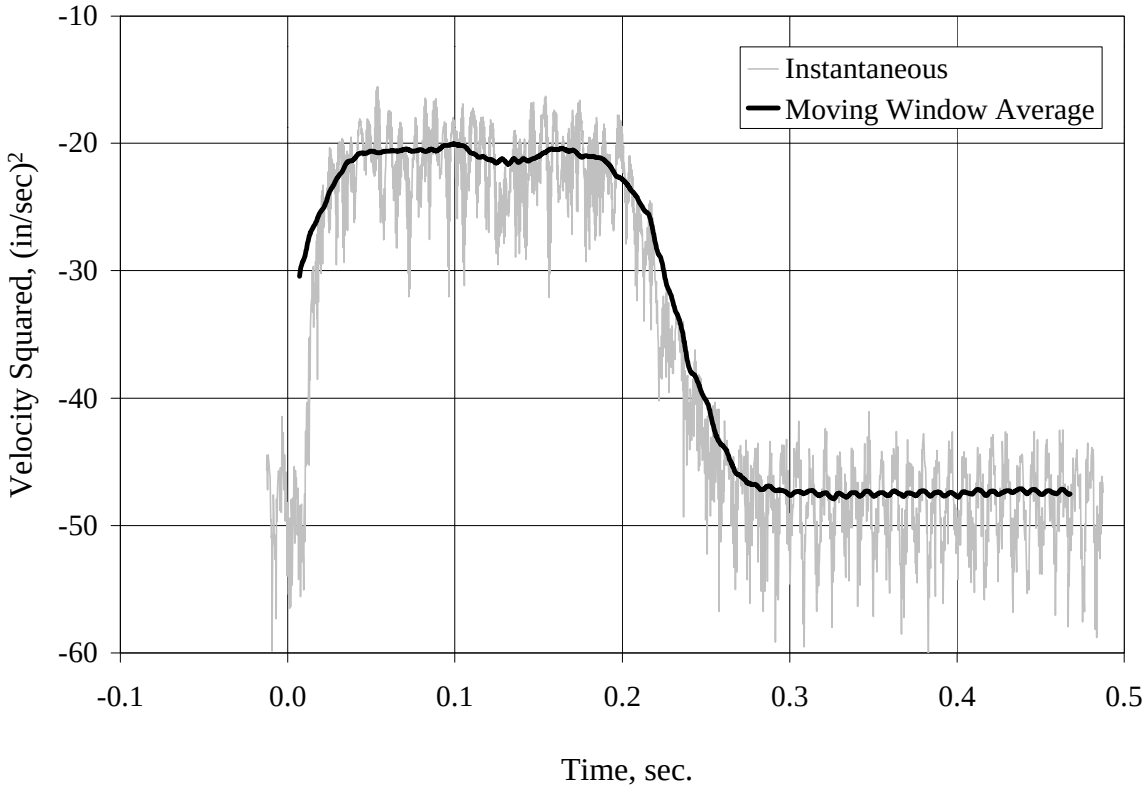

Figure 5.5 Response Velocity, 1000 Hz

consistent. As a result, in order to compute a spatial average of the response, it was necessary to normalize each set of energy measurements by the average power input. Specifically, the energy measurements were divided by the average value of the input power over the steady state portion of the excitation. A typical result, at 1000 Hz, showing the individual measurements, the spatial average, and the +/- 2 s bounds is shown in Figure 5.6.

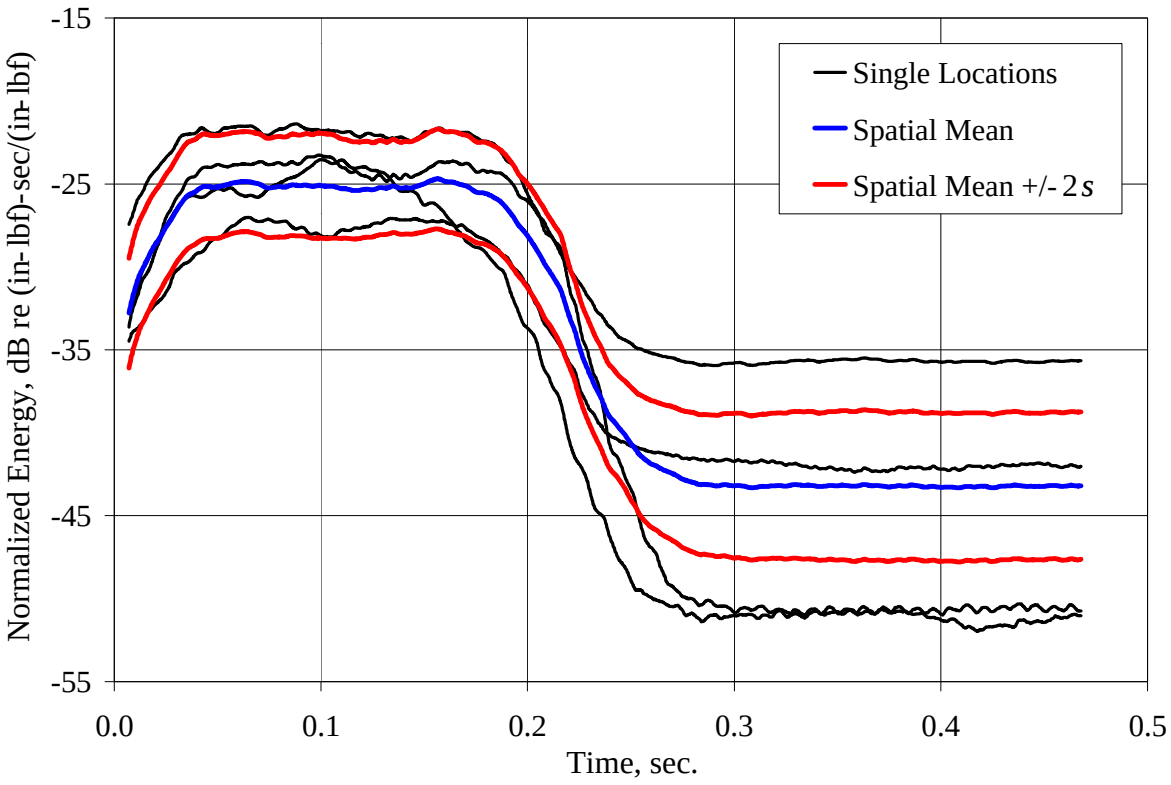

Figure 5.6 Spatial Average of Response, 1000 Hz

5.1.3 REALIZATION OF A MINIMUM ORDER POWER FLOW MODEL

The post-processed measured transient data was used to realize a minimum order power flow model using PRM. This was performed for every 1/3 octave band from 315 Hz to 8000 Hz. A typical comparison between measured energy and that synthesized from the realized model at 1000 Hz is shown in Figure 5.7.

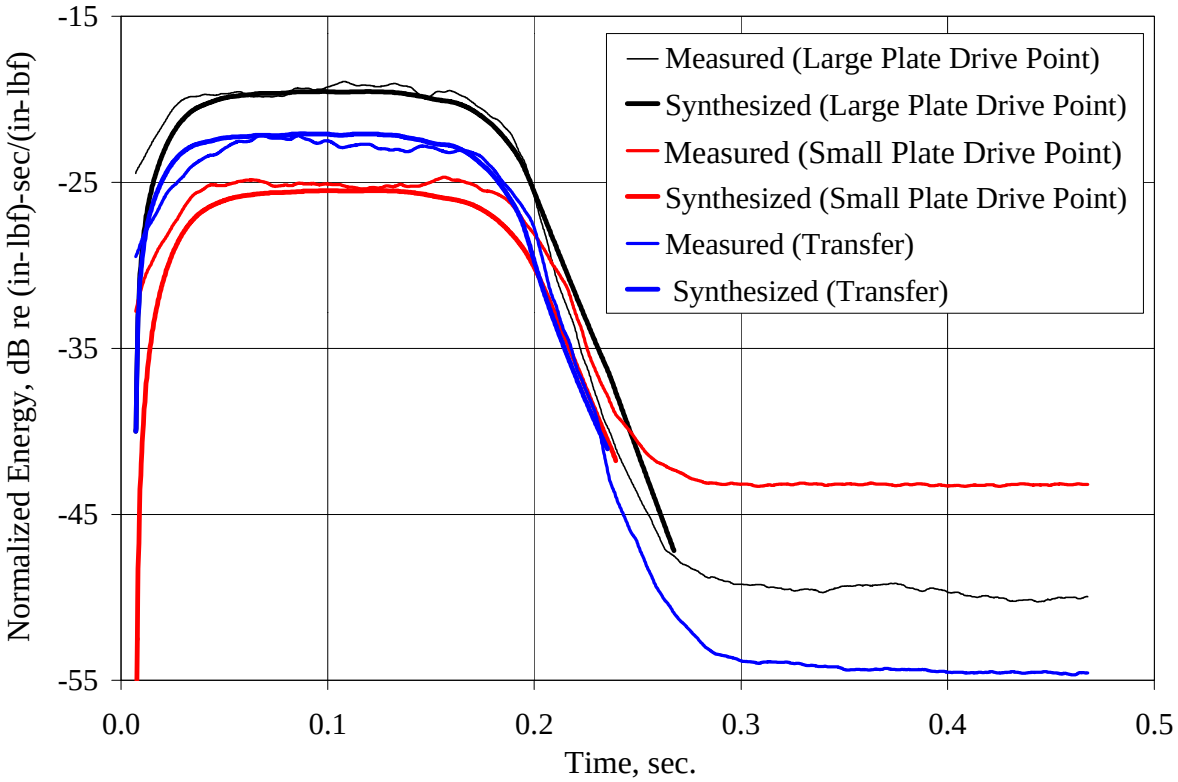

Figure 5.7 Measured and PRM Results, 1000 Hz

It was found that even though data was acquired for excitation on both the large and the small plates, only the response due to a single average input on the large plate was necessary to obtain close correlation between the measured data and the realized model.

5.1.4 SEA MODEL IMPROVEMENT

The initial computational SEA model was generated using AutoSEA™ software. The values of the coupling loss factors were made artificially low and, hence, represented modeling inaccuracy. Model updating using SMI was performed for data gathered in each 1/3 octave band from 315 Hz to 8000 Hz. The SMI (updated) coupling loss factor is shown in Figure

5.8. The coupling loss factor obtained using PIM on the broadband FRF measurements as well as the theoretical values are, additionally, plotted.

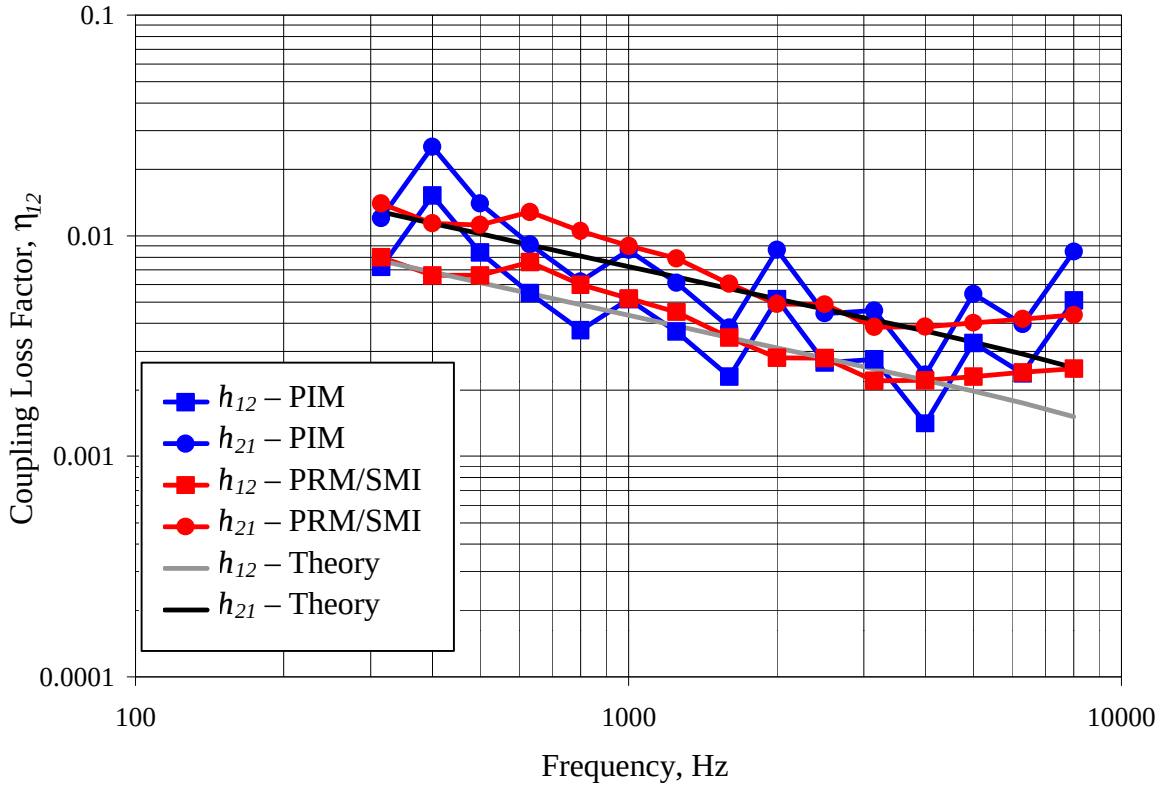

Figure 5.8 Coupling Loss Factors

It can be seen that the identified loss factors using both methods correlate closely with the theoretical values and decrease with increasing frequency. Specifically, the difference, in dB, between identified and theoretical values of the coupling loss factors are shown in Figure 5.9. Both methods lead to relatively accurate coupling identification. PIM results are higher than theoretical by an average of 1.5 dB. The PRM/SMI results are higher than theoretical by an average of 1 dB over the entire analysis range. The PIM can be seen to maintain slightly more variability than PRM/SMI evidenced by their respective standard deviations of 1.5 dB and 4 dB.

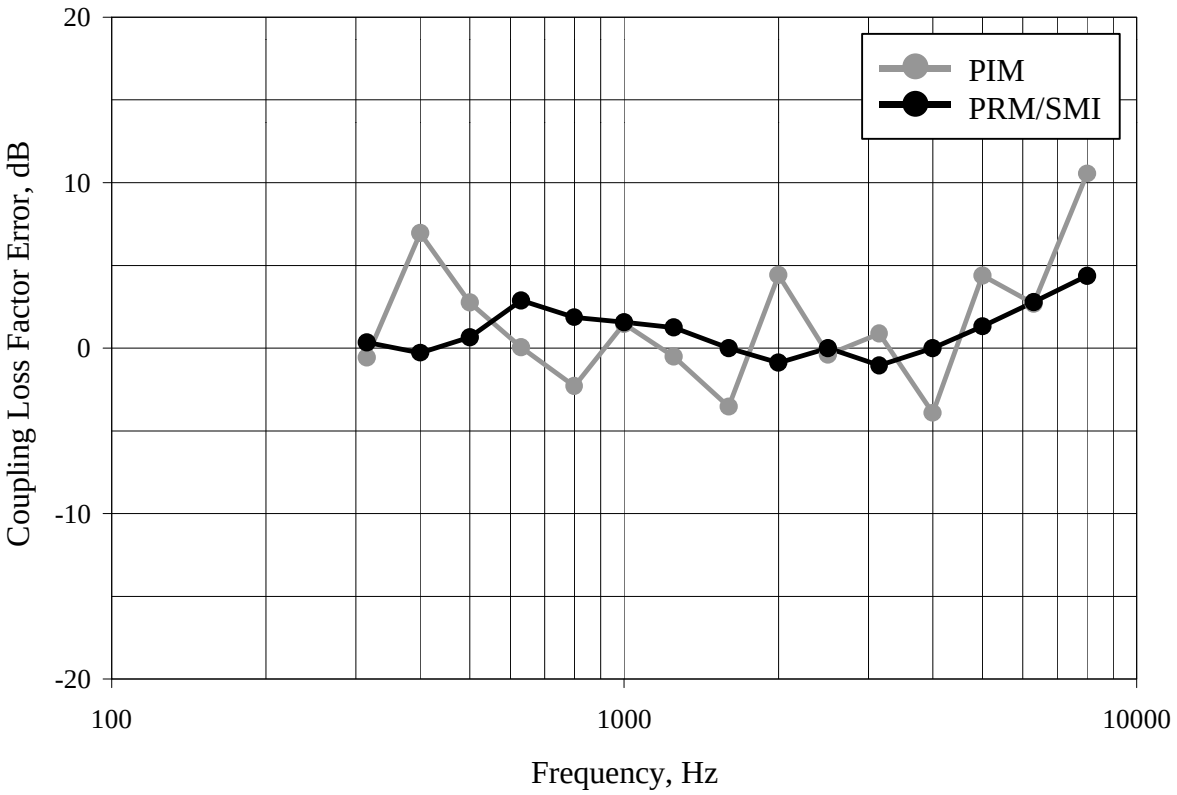

Figure 5.9 Coupling Loss Factor Error

The identified damping loss factors are shown in Figure 5.10.

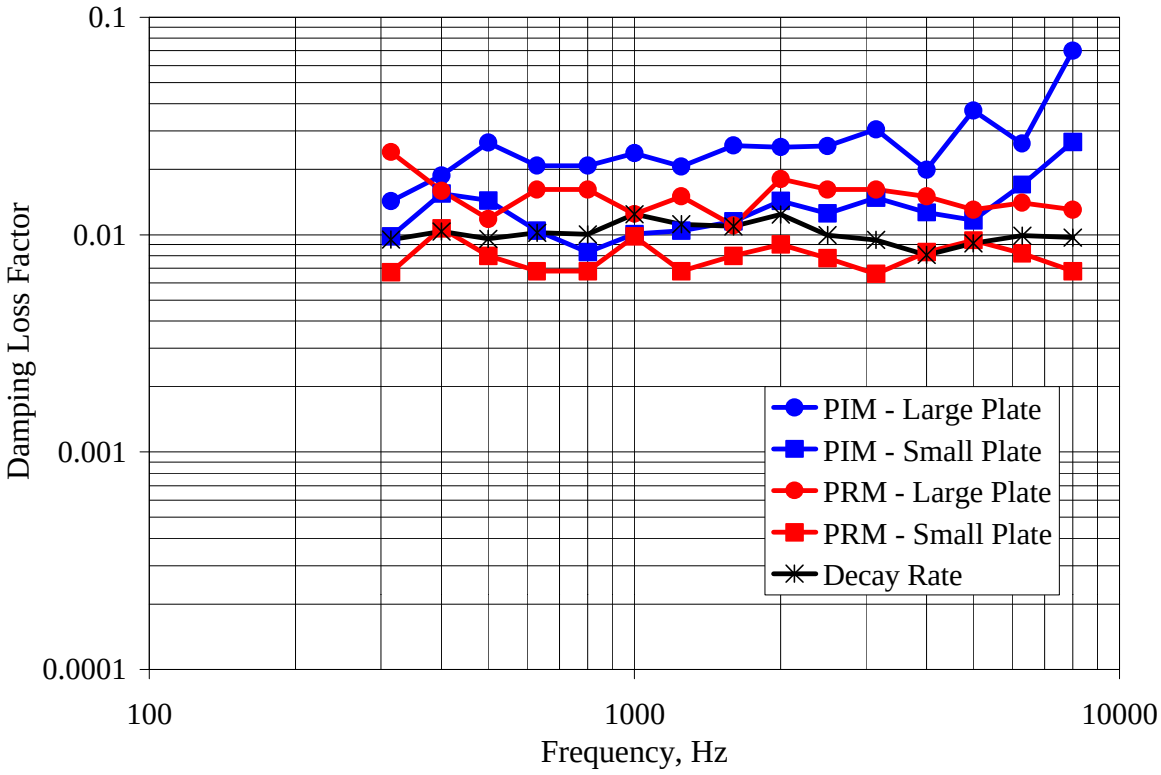

Figure 5.10 Damping Loss Factors

It can be seen that there is reasonably close correlation between identified damping and the values obtained from decay rate tests. The difference, in dB, between identified and theoretical values of the damping loss factors are shown in Figure 5.11.

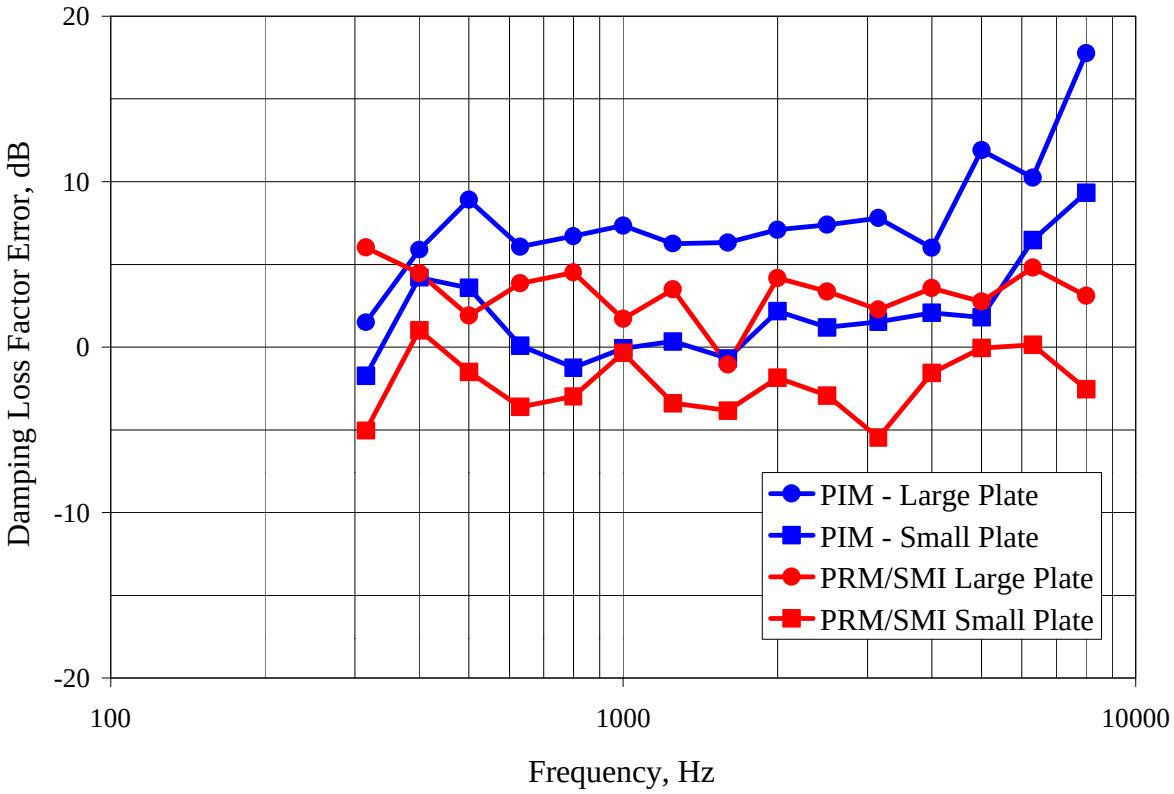

Figure 5.11 Damping Loss Factor Error

Here, the damping loss factor using PRM/SMI is, on average, higher than that from decay rate tests by 0.5 dB. The PIM value has slightly more discrepancy, as it is higher than the decay rate value, on average, by 5 dB. With respect to all parameters, PIM accuracy suffered at relatively high frequencies.

5.1.5 DISCUSSION OF RESULTS

To assess the system realization (PRM) and model updating (SMI) accuracy, the improved computational SEA model was used to synthesize the drive and transfer mobility FRF's. The spatially averaged large plate drive point mobility is shown in Figure 5.12.

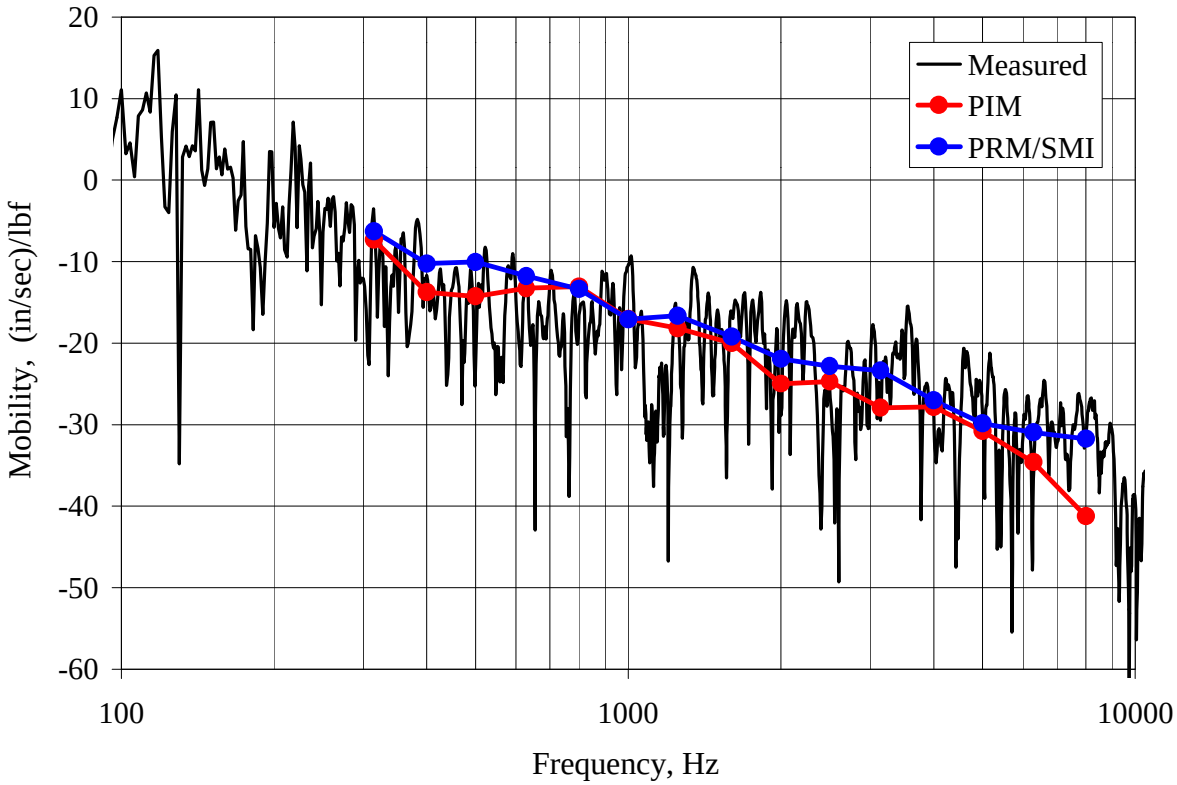

Figure 5.12 Drive Point Mobility of Large Plate

Here, it can be clearly seen that both the PRM and PIM results correlate closely with the measured broadband FRF. Indeed, for PIM, this makes sense since the identified coupling matrix is obtained directly from the band averaged FRF. Similar conclusions can be drawn from the small plate drive point mobility and the transfer mobility shown in Figure 5.13 and Figure 5.14 respectively.

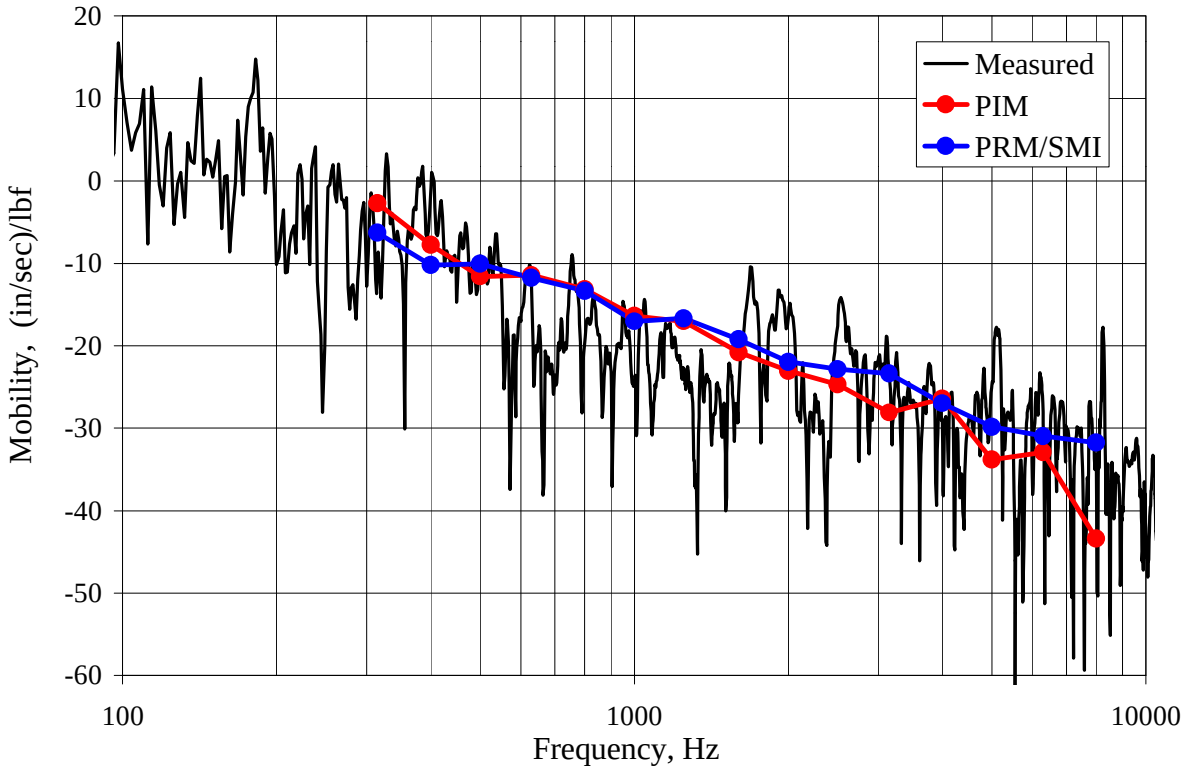

Figure 5.13 Drive Point Mobility of Small Plate

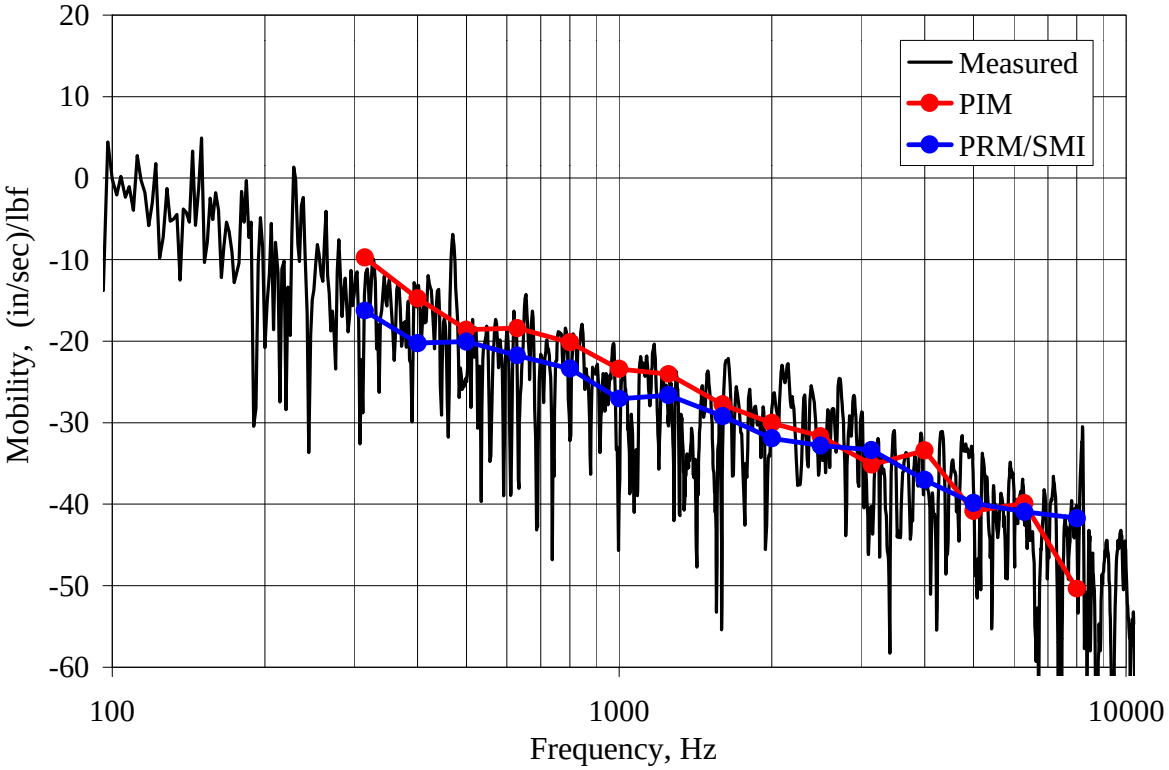

Figure 5.14 Transfer Mobility

5.1.6 CONCLUSIONS

For the simple structure tested, both methods of SEA parameters identification, PIM and PRM/SMI, perform comparably. It was found that the coupling loss factor error was less than 1.5 dB and the damping loss factor deviated from that obtained via decay rate tests by less than 5 dB. Comparisons of measured frequency response functions and those reconstructed from the identified SEA parameters showed close correlation. It was, furthermore, discovered that only a single input was required to successfully implement PRM/SMI on this structure, whereas, a full matrix of measurement inputs and outputs was required for PIM. This, once again, provides some evidence that PRM may prove to be advantageous for obtaining experimental SEA parameters for complex systems by simplifying the testing process.

5.2 COMPLEX STRUCTURE

Often, the structural dynamic or acoustic engineer is faced with the challenge of having to provide input early in a design of a complex system. At this point, there is usually a very limited amount of available analysis and test data. This type of scenario, therefore, is used to subject the methods developed in this dissertation to a worst-case trial, and, hence, complete the range of examined applicability. Specifically, the approach involves gathering a minimum amount of measured data, typical in many real situations, and assuming a relatively rough initial computational SEA model is available prior to testing.

5.2.1 EXPERIMENTAL SETUP

The complex structure used to examine the power flow realization and SEA model improvement methods is a 1995 Mercury Sable automobile donated by the Ford Motor Company. The experimental setup is shown in Figure 5.15.

Figure 5.15 Mercury Sable Test Setup

The vehicle is a “body in trim” meaning that only the chassis, body, and trim are present for the experiments carried out here. Additionally, the hood, trunk, and doors are removed to reduce the extent of testing required without overly sacrificing system complexity. The vehicle is supported from the bottom of the body using a distributed layer of resilient padding. A single 100 lbf rms exciter is attached to the chassis at the left front wheel well as shown in the photograph.

Instrumentation is setup as shown in Figure 5.16.

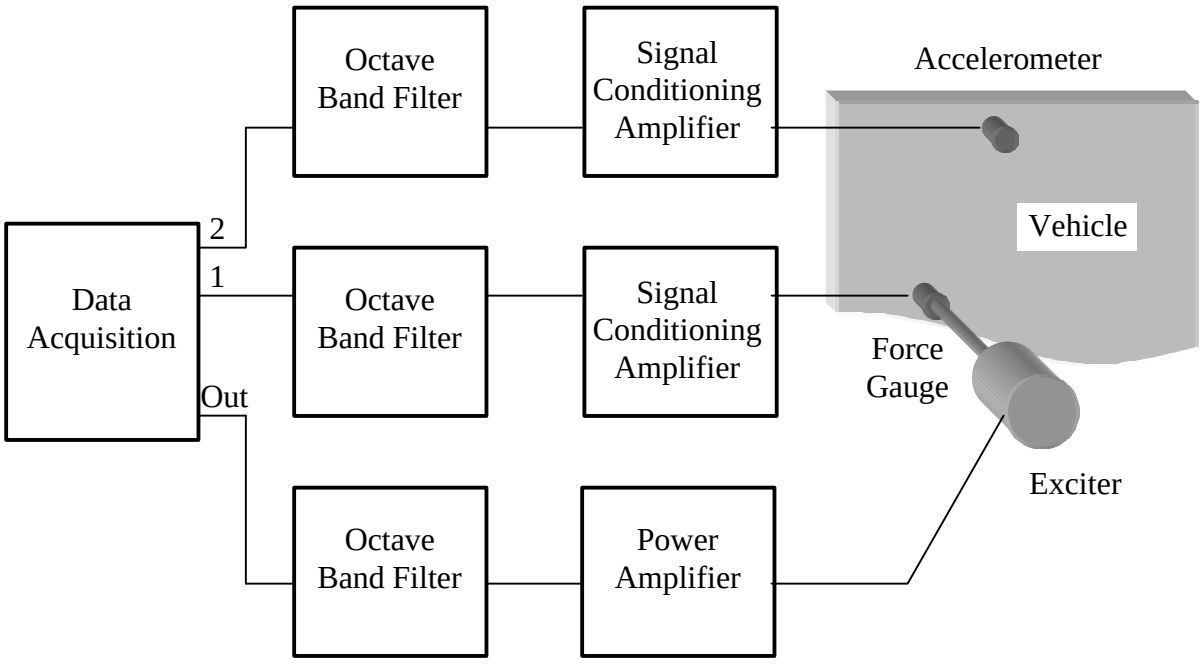

Figure 5.16 Instrument Setup

Response acceleration was measured using accelerometers and force inputs were measured using force gauges. The same approach used during the testing of the coupled plate structure was employed here. Broadband frequency response function (FRF) measurements were collected to serve as a baseline in the test/analysis comparisons. Burst random excitation

filtered in successive full octave bands was used to generate the transient data necessary for the PRM. Again, during the transient tests, both force gauge and accelerometer outputs were filtered in the same successive octave bands. The entire frequency band of interest was from 125 Hz to 8000 Hz.

5.2.2 PRE-TEST ANALYSIS

A SEA model was created using AutoSEA™ software to serve as the initial model for the model improvement phase. The model is shown in Figure 5.17.

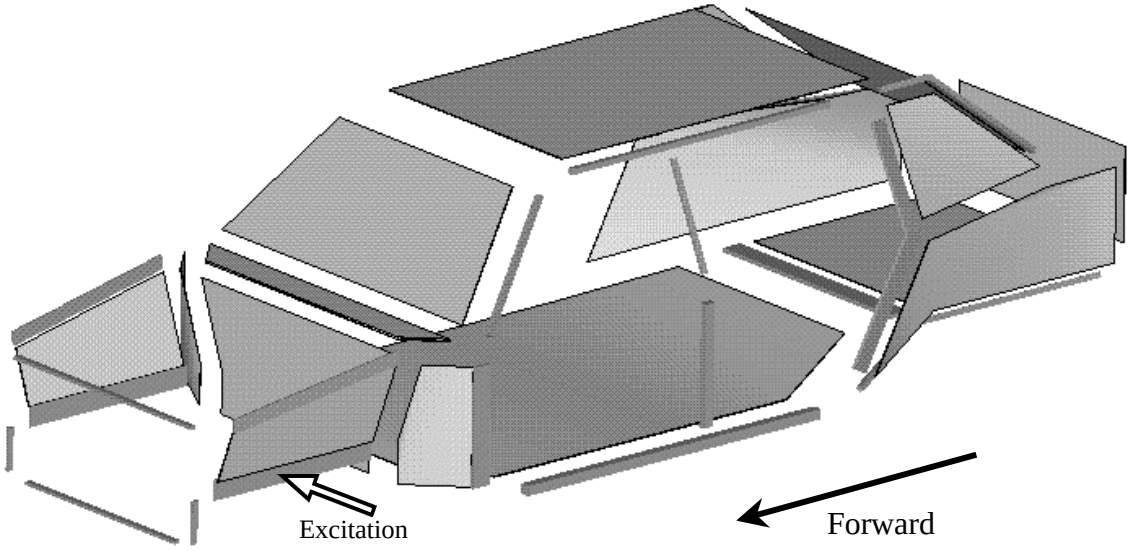

Figure 5.17 SEA Model of Mercury Sable Test Structure

The model is comprised of 16 plate subsystems and 54 beam subsystems totaling 70 subsystems. Only the flexural dynamics of both types of subsystems are represented.

By examining the eigenvectors of the SEA model, it is possible to determine the best choice for input locations at a particular frequency. Specifically, if the eigenvector component is high at a particular input location, the associated principal subsystem can obtain relatively high energy levels from a small amount of power input at that position. On the other hand, if

the component is low, a great deal of input power is required to reach the same energy level. Furthermore, if the eigenvector component is zero at a particular input location, the associated state is not controllable from that point or, in other words, the associated principal subsystem cannot be activated from that particular input position. An activation coefficient can be computed for each eigenvector based on a particular input location. To do this, recall that the power balance in principal coordinates (using the modal energy form) is:

$$[\tilde{V}]^T [N][\tilde{V}]\{\dot{\bar{e}}(t)\} + w[\tilde{V}]^T [K][\tilde{V}]\{\bar{e}(t)\} = [\tilde{V}]^T \{P(t)\} \tag{5.1}$$

where $[\tilde{V}]$ is a matrix of the system eigenvectors, $[N]$ is the matrix of mode counts in the analysis band centered at w, $[K]$ is the symmetric coupling matrix, $\{\bar{e}(t)\}$ is a vector of the modal energies in principal coordinates, and $\{P(t)\}$ is the vector of input powers. If a single input of unity magnitude is considered at some particular subsystem, the right hand side of the equation, being the projection of the input power into principal coordinates, yields a vector of the relative activation of the eigenpairs due to the location of this excitation.

$$[\tilde{V}]^T \{P(t)\} = [\tilde{V}]^T \begin{Bmatrix} 0 \\ \vdots \\ 1 \\ 0 \\ \vdots \\ 0 \end{Bmatrix} \tag{5.2}$$

By separately considering a single input at each subsystem, 70 such activation vectors can be computed (one for an input at each subsystem). This is merely the transpose of the eigenvector matrix. An example, for the 1000 Hz octave band, is plotted in Figure 5.18.

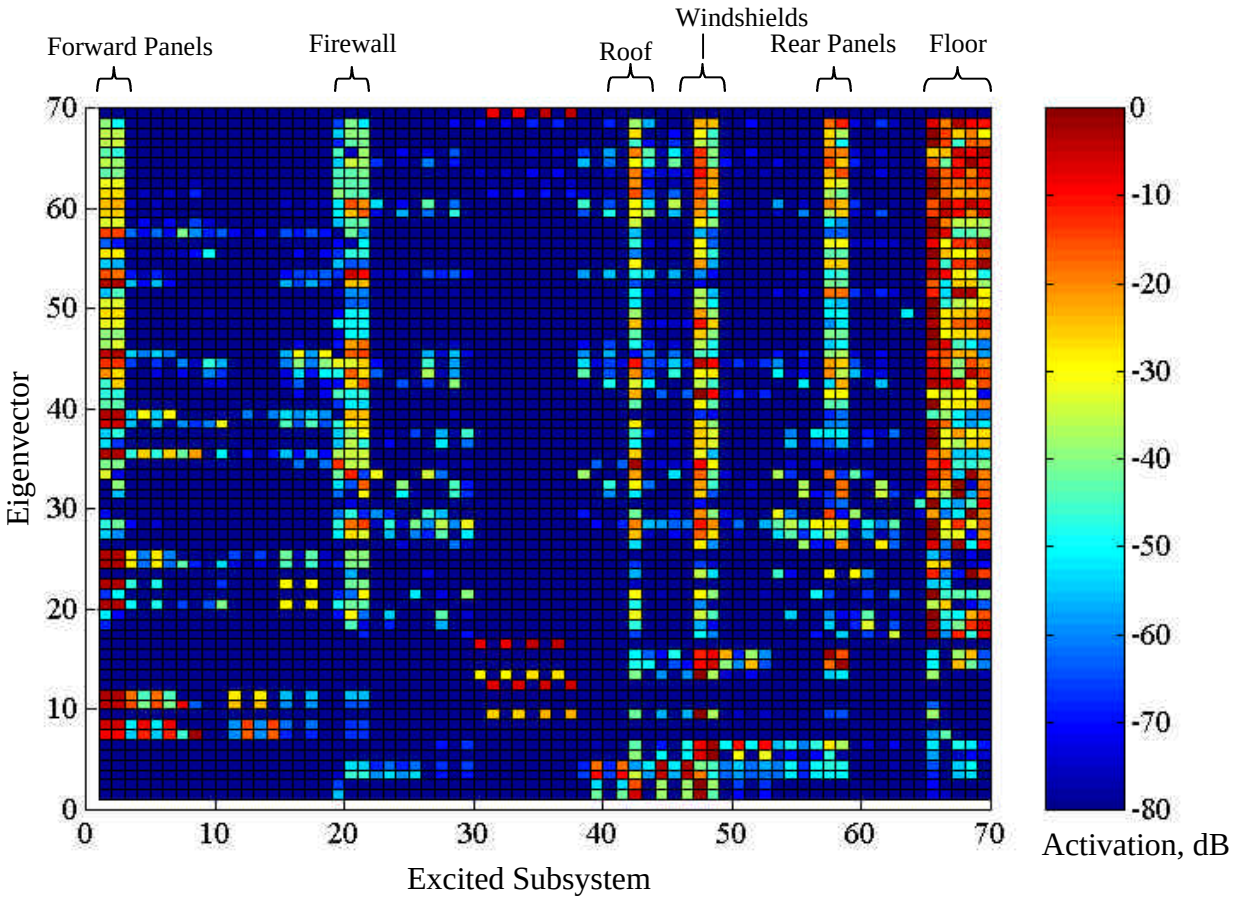

Figure 5.18 Relative Activation of Eigenpairs, 1000 Hz

Note that, for this purpose, all eigenvectors have been scaled for unity magnitude. It can be seen that, in general, inputs at subsystems 1, 2, 19-21, 42, 47, 48, 57, 58, and 66-70 have the highest relative activation and seem, furthermore, to excite most of the system eigenpairs. These subsystems represent the plate flexural dynamics of the regions indicated in the figure and maintain the highest activation because they are somewhat centrally located and couple to most of the remaining subsystems. By summing over the eigenvectors, a total activation can be computed as shown in figure 5.19. This figure is somewhat simpler to interpret and yields the same conclusion regarding the high relative activation of the system eigenvectors when exciting the subsystems previously listed.

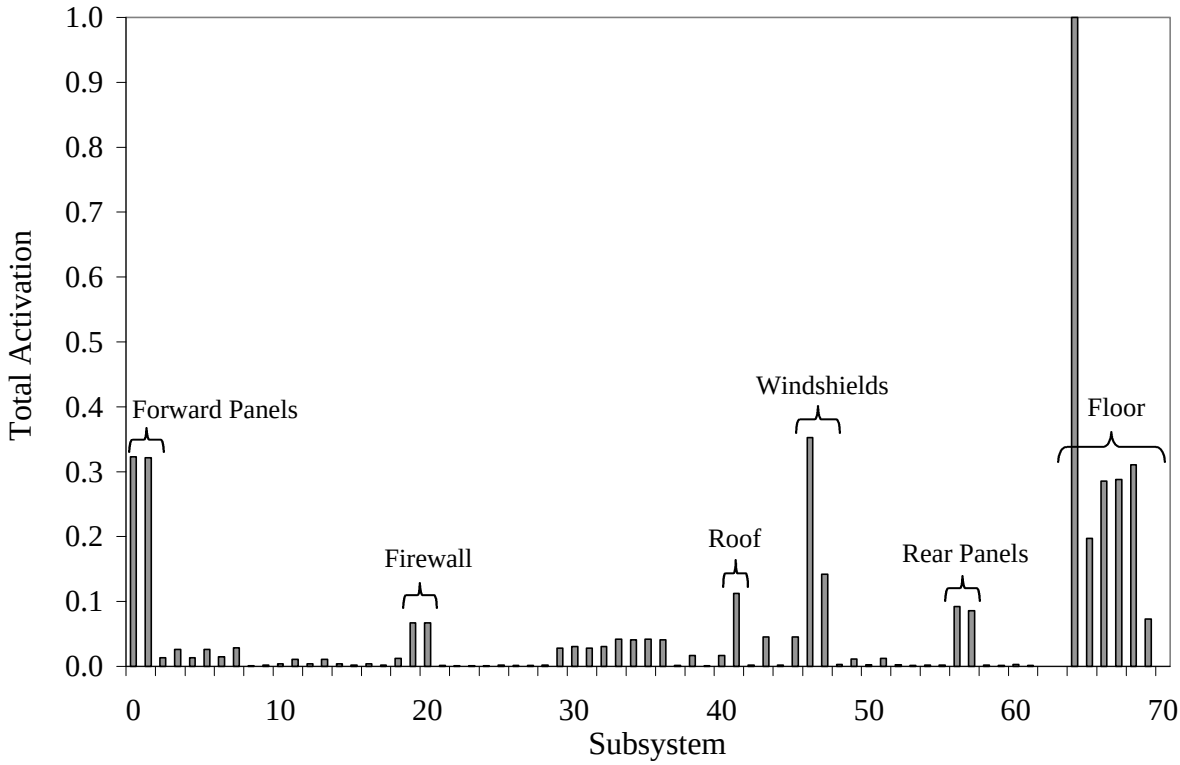

Figure 5.19 Total System Activation, 1000 Hz

The total activation can be computed for each center frequency in the analysis bandwidth as shown in Figure 5.20.

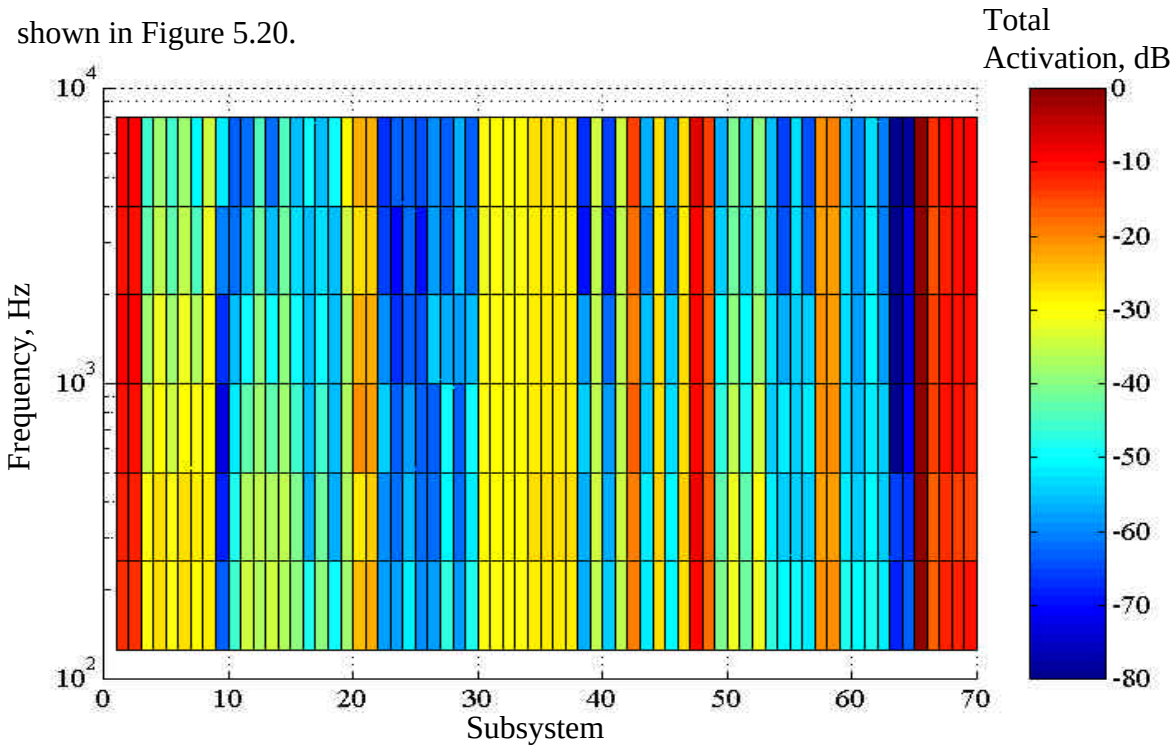

Figure 5.20 Total System Activation

It can be seen that, for this model, the average activation is more or less independent of the octave bandwidth of interest. As a result, the optimal location for exciting the structure, the floor subsystem, is at the same place for all bands over the entire analysis range.

Perhaps, the best way to interpret the result is to superimpose the values of the activation onto a graphic of the vehicle in the form of a thermogram. The frequency average activation for the plate subsystems is shown in Figure 5.21.

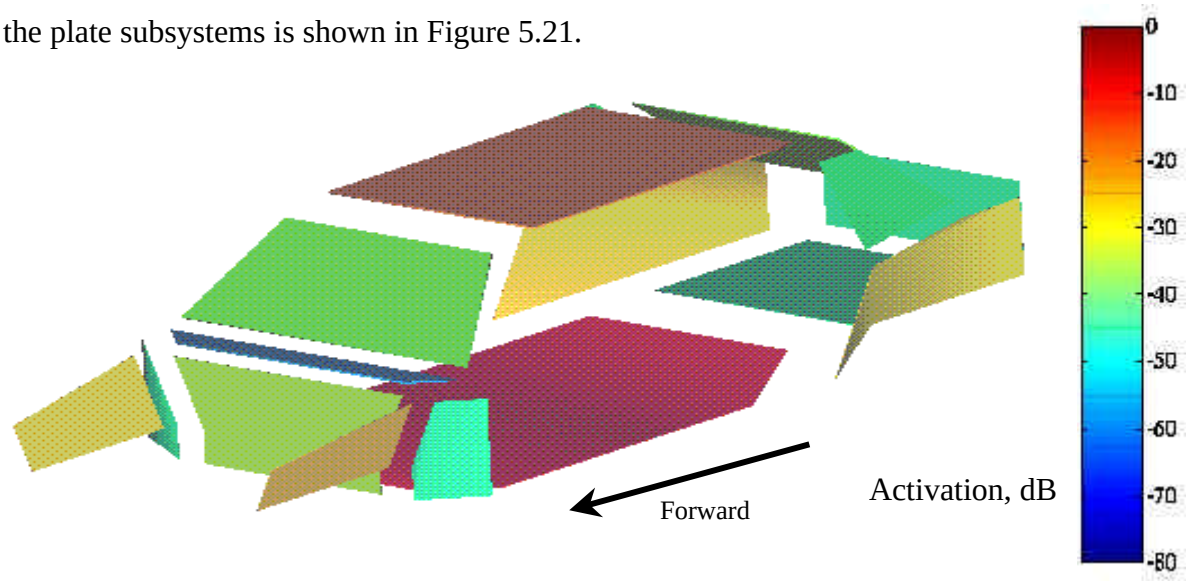

Figure 5.21 Thermogram of Frequency Average Activation (Plates)

Similarly, the thermogram for the beam subsystems is shown in Figure 5.22. The results are clearly consistent with the results of Figures 5.18 – Figures 5.20.

Based upon the activation results, the best choice of input location would seem to be the roof, floor, or roof beam subsystems. However, a relatively low horizontal driving location was needed due to practical limitations regarding shaker attachment and orientation.

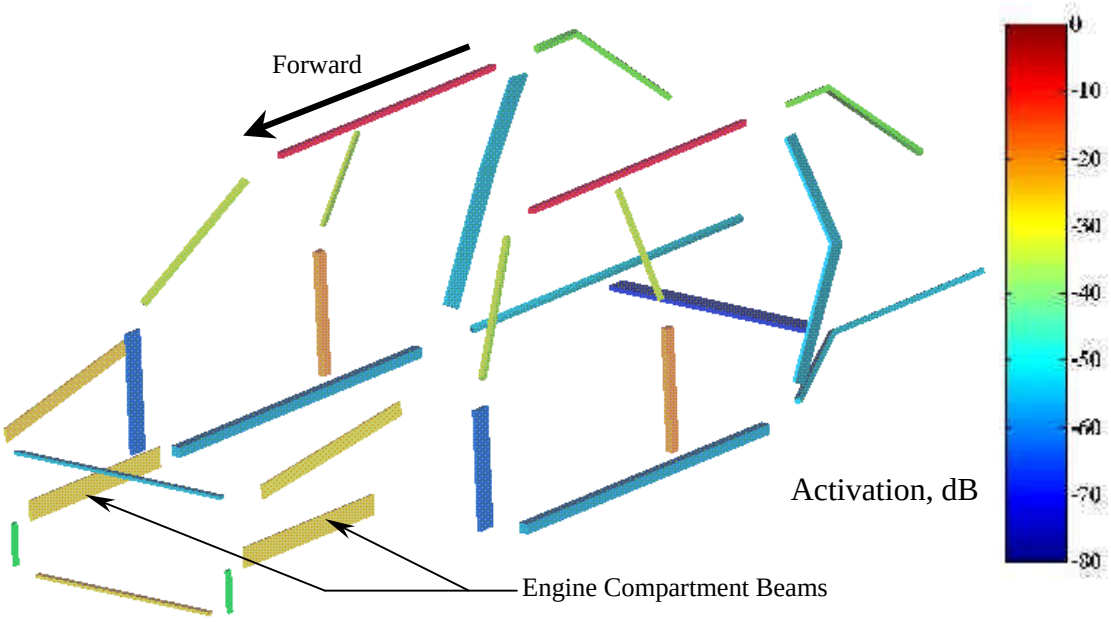

Figure 5.22 Thermogram of Frequency Average Activation (Beams)

Of the lower subsystems, only the beams provided a means of delivering a horizontal force input. Therefore, it was concluded that the best location for the exciter was one of the lower beams (as shown) in the engine compartment as these subsystems had the highest activation of all the lower beams. The location is shown in Figure 5.23

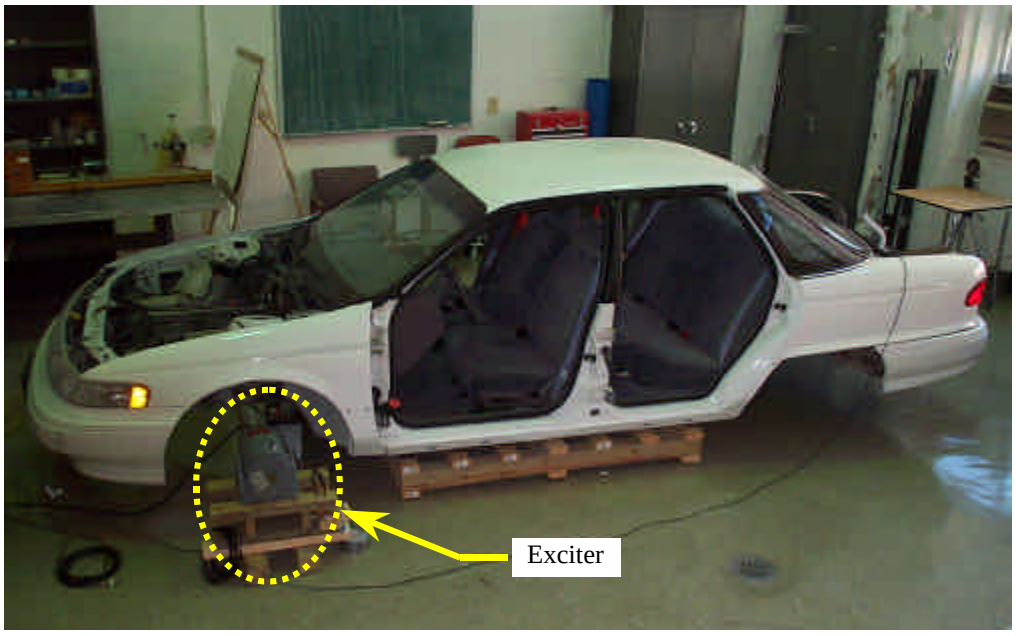

Figure 5.23 Location of Drive Point Excitation

5.2.3 SYSTEM IDENTIFICATION AND MODEL IMPROVEMENT

It has been previously emphasized that when conducting typical dynamic testing on complex systems, it is unlikely that response would be measured at all locations where there are subsystems in a predictive SEA model of the system. For the tests conducted on the Mercury Sable, response was gathered at 20 of the 70 subsystems present in the initial SEA model. These include all 16 plate subsystems and 4 beam subsystems as shown in red in Figure 5.24.

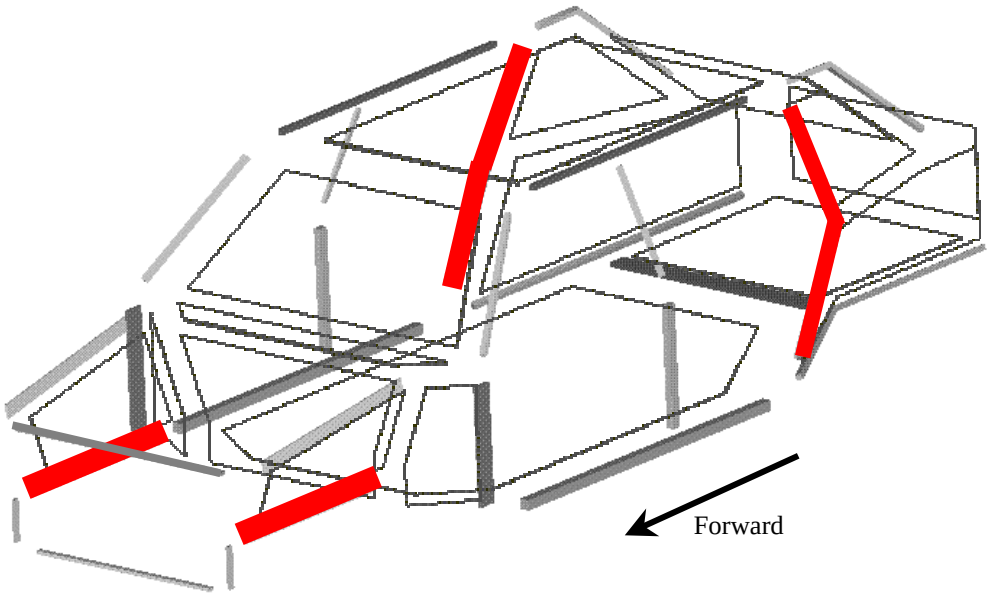

Figure 5.24 Measured Beam Response Locations

The same approach previously used for the coupled plate structure, was re-employed here for the transient testing. Specifically, average drive point force, drive point acceleration, and transfer acceleration were acquired and stored digitally in the time domain using five ensembles per average at each response location for each of the octave bands in the overall analysis bandwidth. Eight samples per period were acquired throughout. A noise burst was utilized, again, to achieve sufficient SNR and long enough duration to attain steady state

conditions prior to deactivating the excitation. The data was processed to averaged input power and response energy using a 5 period moving window average.

Power flow model realization (PRM) was used for the system identification. Ten singular values were obtained from the acquired transient response measurements for each center frequency. Prior to performing the model updating, the experimental eigenvectors were expanded to the full number of degrees of freedom present in the initial SEA model. To properly choose the analytical eigenvectors to use in the transformation, the components of the eigenvectors were summed over the test degrees of freedom for each frequency band and then normalized by the maximum value. High values of this index corresponded to eigenvectors with the greatest participation as observed from the test locations. This is plotted in Figure 5.25.

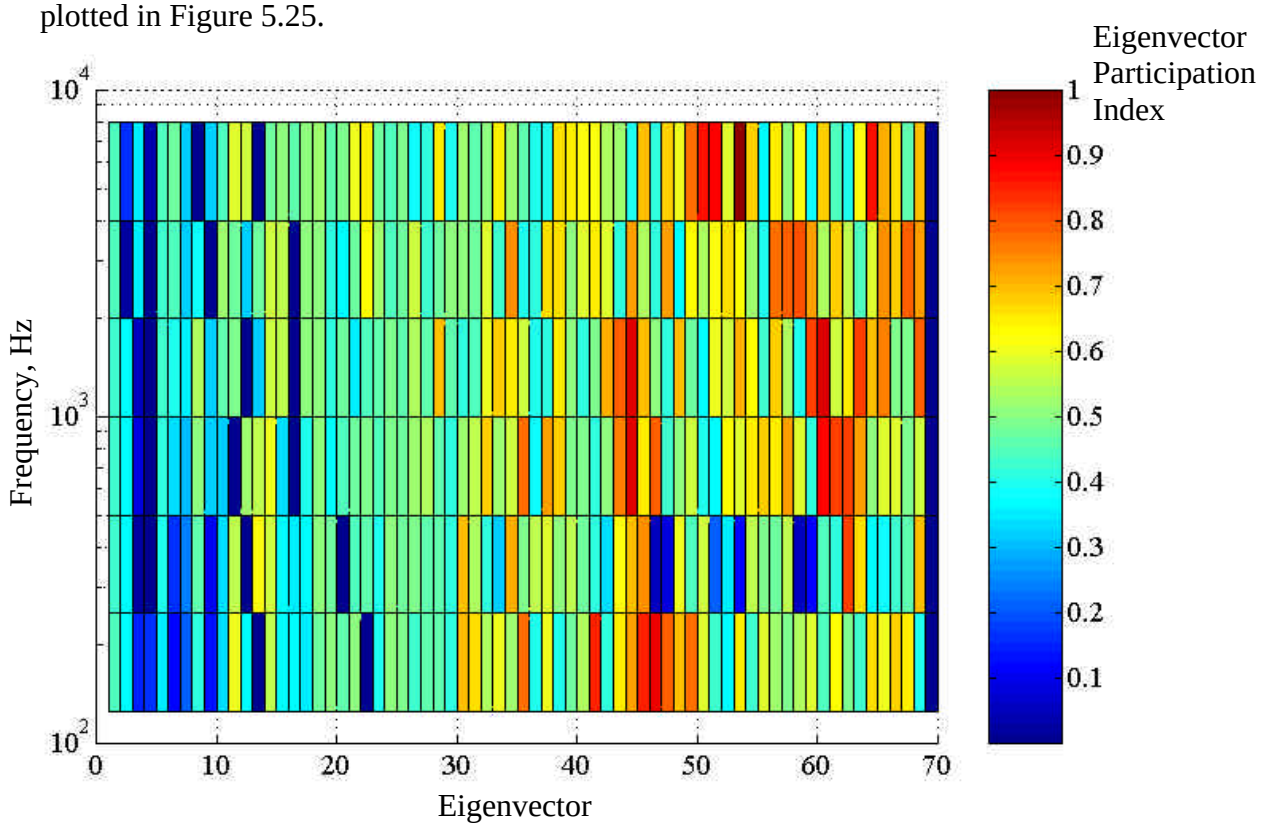

Figure 5.25 Eigenvector Participation at Test Locations

The eigenvectors with the highest indices for each frequency band are summarized in Table 5.1.

Table 5.1 Eigenvectors used in Test Data Expansion

Center Freq. (Hz)	Eigenvectors with Highest Participation				
125	35	41	45	46	47
250	30	34	44	45	62
500	44	46	60	61	62
1000	43	44	59	60	63
2000	34	56	57	58	67
4000	49	50	51	53	64
8000	48	51	66	67	68

After applying the symmetric form of the SEA model improvement (SMI), a coupling change matrix was found for each analysis band. The percent change at 1000 Hz is shown in Figure 5.26.

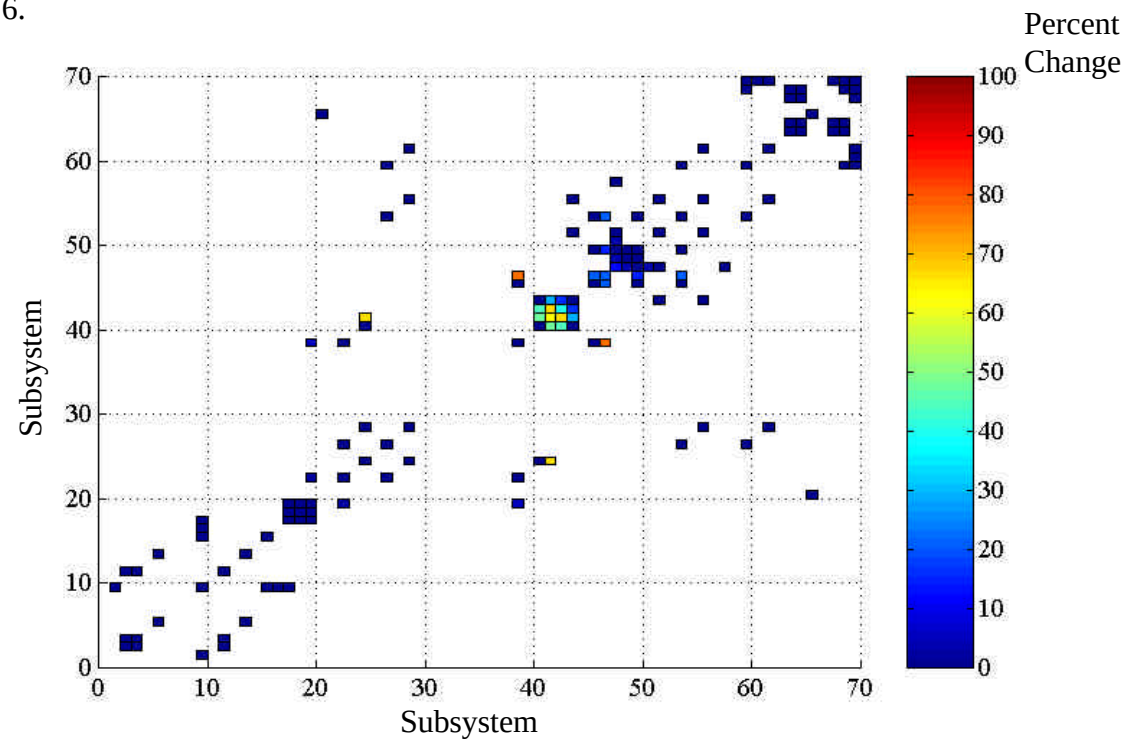

Figure 5.26 Change in Coupling Matrix, 1000 Hz

From the figure, it can be seen that the coupling matrix elements with the highest change are: $DK_{39\text{-}47}$, $DK_{41\text{-}47}$, $DK_{42\text{-}46}$, $DK_{42\text{-}44}$, and $DK_{25\text{-}42}$ together with their corresponding reciprocal elements. This indicates that the highest modeling error occurs with respect to the coupling between the roof (subsystem 47) and the roof beams (subsystems 39 and 41) and also with respect to the windshield (subsystem 42) and the neighboring beams (subsystems 44 and 46). These junctions are highlighted in red in Figure 5.27. The diagonal elements of the matrix, for the most part, are unaffected.

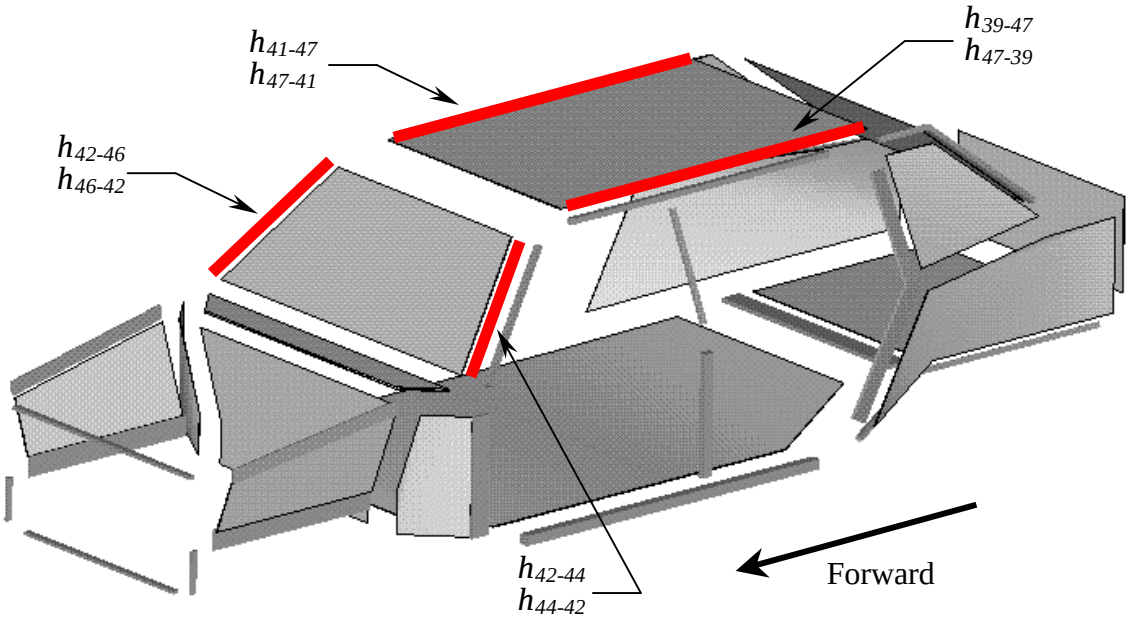

Figure 5.27 Locations of Initial Model Coupling Loss Factor Errors, 1000 Hz

Furthermore, it was observed that error in these modeled junctions was an under prediction of the coupling loss factor that occurred somewhat consistently across all frequency bands in the analysis range as shown in Figure 5.28.

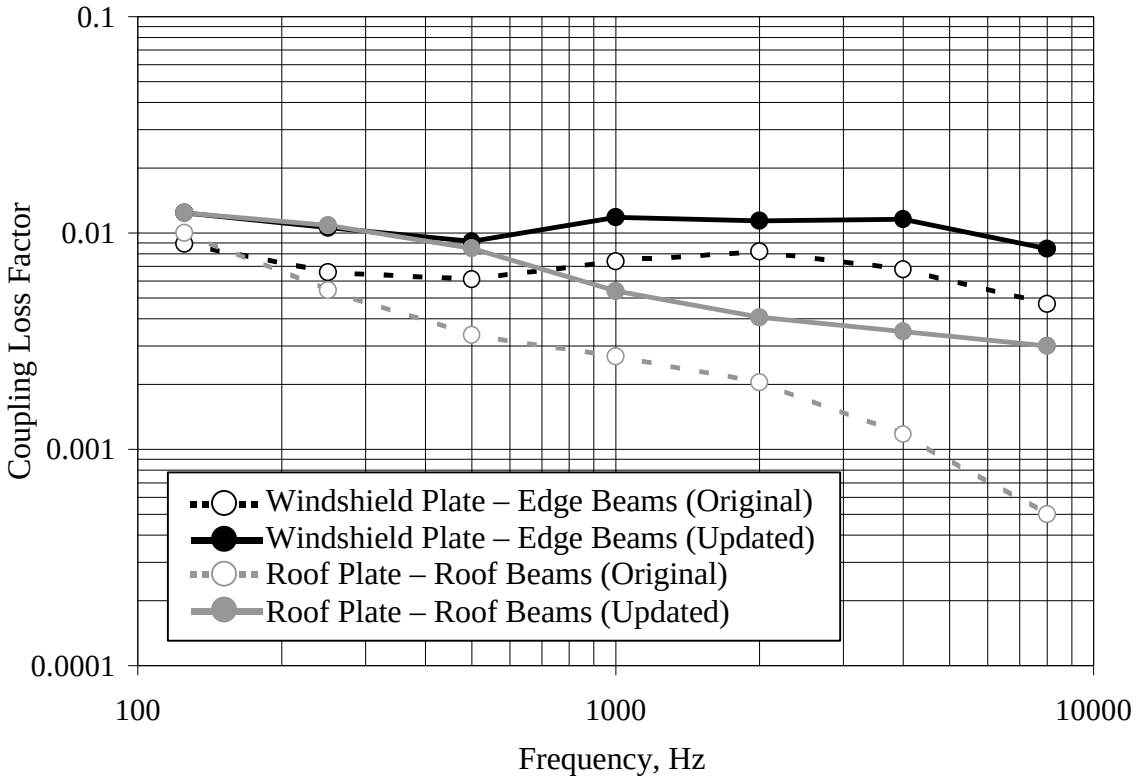

Figure 5.28 Result of SEA Model Improvement

To assess the accuracy of the model improvement, measured frequency response functions were compared to those synthesized using both the original and the improved SEA models. As expected, it was found that the updated SEA prediction correlated more closely to the measured data than did the original SEA prediction. The drive point mobility prediction, shown in Figure 5.29, remained, for the most part, unchanged after the model updating. Indeed, this makes sense since the change in the coupling matrix for the input subsystem was small. Transfer mobility predictions to subsystems coupled through the windshield and the roof subsystems mentioned earlier, however, were improved. The transfer mobility to the roof is shown in Figure 5.30.

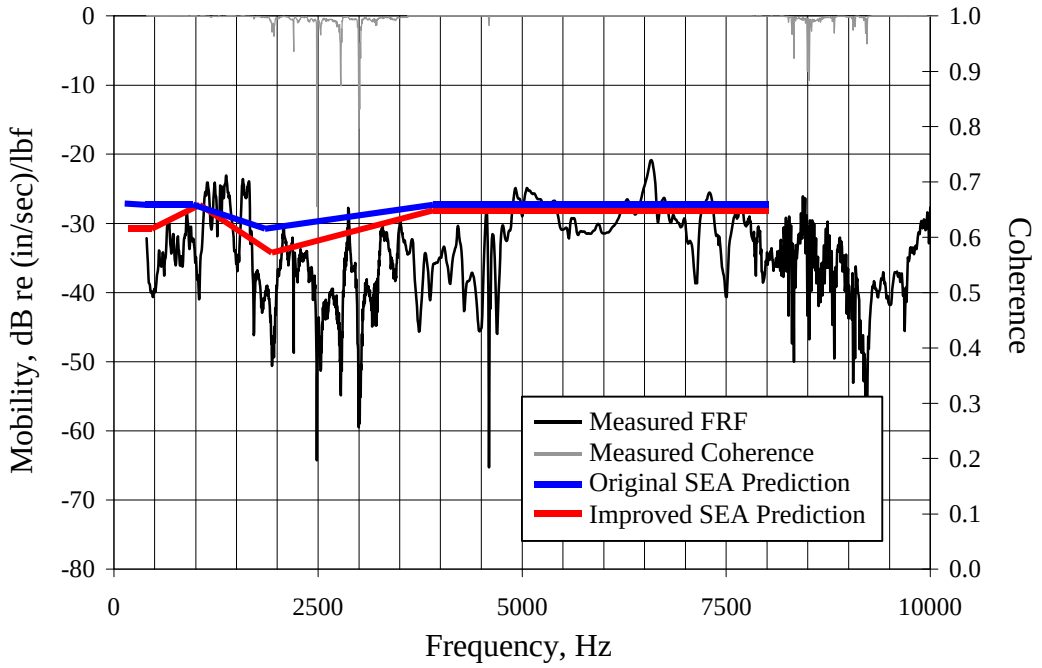

Figure 5.29 Drive Point Mobility

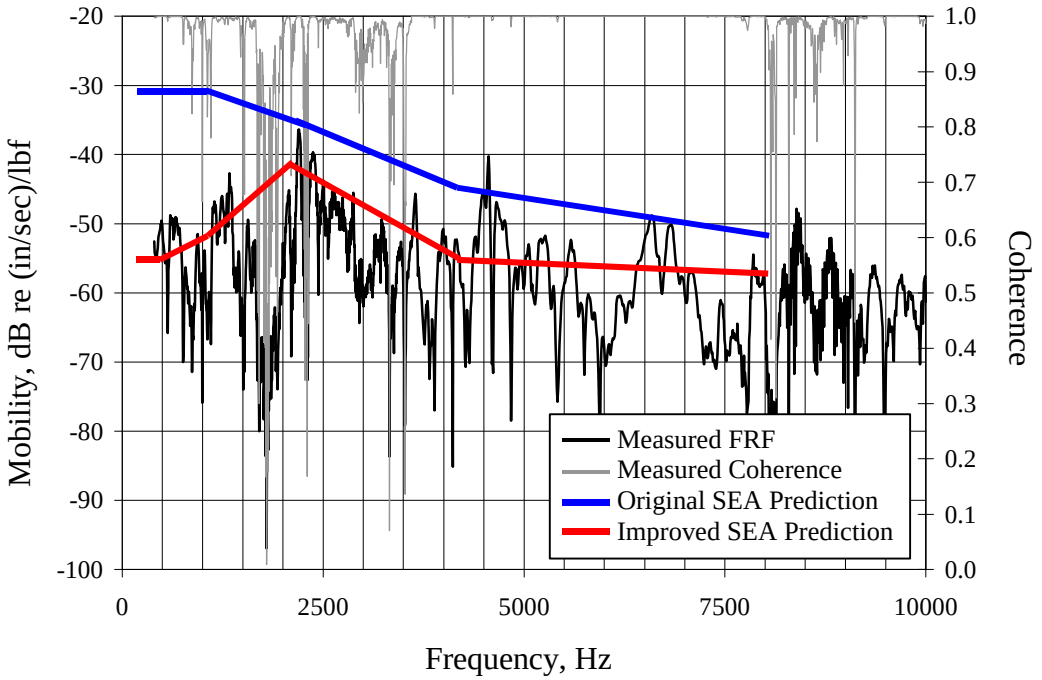

Figure 5.30 Roof Transfer Mobility

Measurement of the transfer mobility to the windshield proved difficult in that the response was very low. However, a measurement/prediction comparison was made in frequency ranges were the measured coherence was best as shown in Figure 5.31.

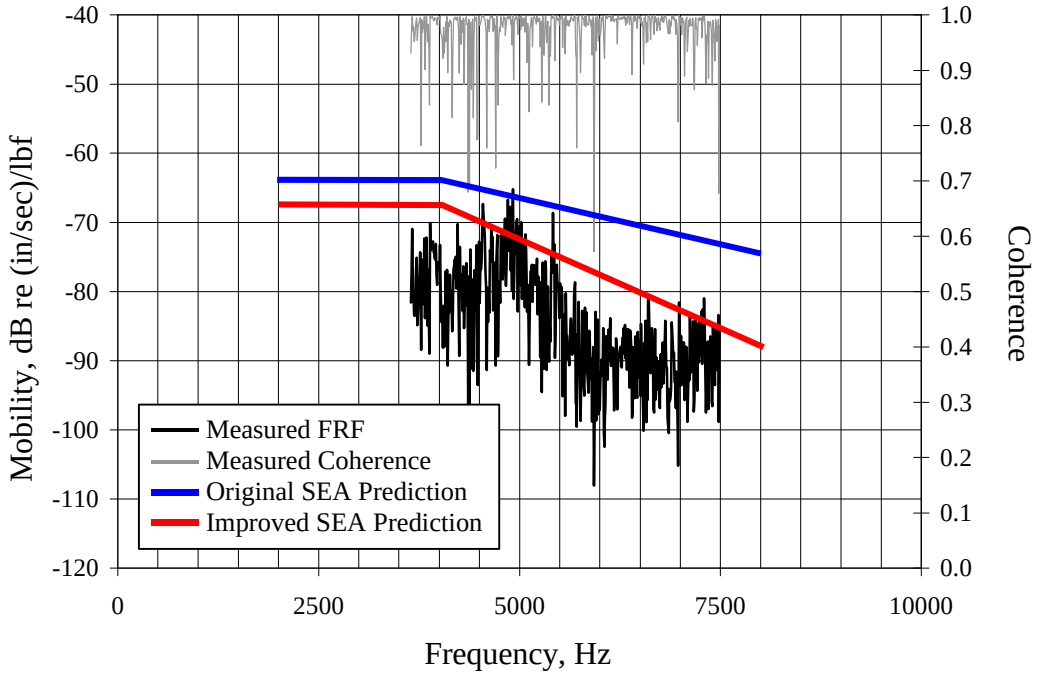

Figure 5.31 Windshield Transfer Mobility

Even in this case the updated SEA model correlates more closely with measured data than does the original model.

5.2.4 SYSTEM IDENTIFICATION AND MODEL IMPROVEMENT

In order to assess the degree to which local parameter discrepancies could be identified using measured data, a structural change was made to the test structure. Specifically, damping tile was applied to the right front body panel. The objective was to see how well the structural change could be identified using the power flow realization and model updating scheme.

After applying the damping treatment, another set of transient measurements (using the same drive point and response locations) was gathered for the 1000 Hz octave band. Again, 10 singular values were used to obtain the PRM model. Updating using SMI resulted in a damping loss factor for the right front body panel that changed from 0.001 in the initial SEA model to approximately 0.013 for the improved model. The normalized coupling change matrix is shown in Figure 5.32.

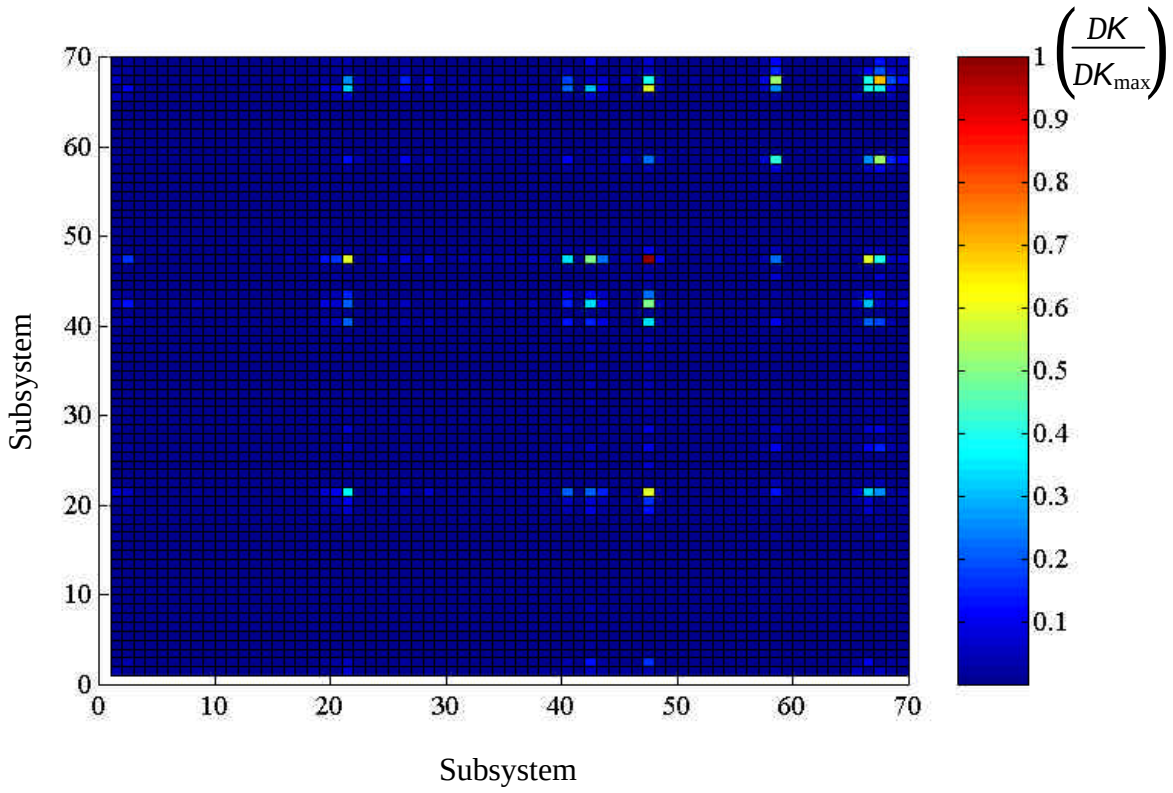

Figure 5.32 Normalized Coupling Change Matrix

Note, the body panel subsystem corresponds to degree of freedom 48 in the plot and, as a result, the element of the change matrix corresponding to row 48 and column 48 is unity as indicated by the red color. A perfect update would involve a change to this element only since the structure was modified at this location alone. However, the true update suffers

from some smearing in that other damping loss factors and some coupling loss factors were modified as well. This effect is minimal as evidenced in the figure. It turns out that the most smearing is limited to 60% of the change to the right front body panel that was actually modified and is seen to occur only to the neighboring subsystems. This can best be illustrated by superimposing the change matrix onto a graphic of the vehicle in the form of a thermogram as shown in Figure 5.33.

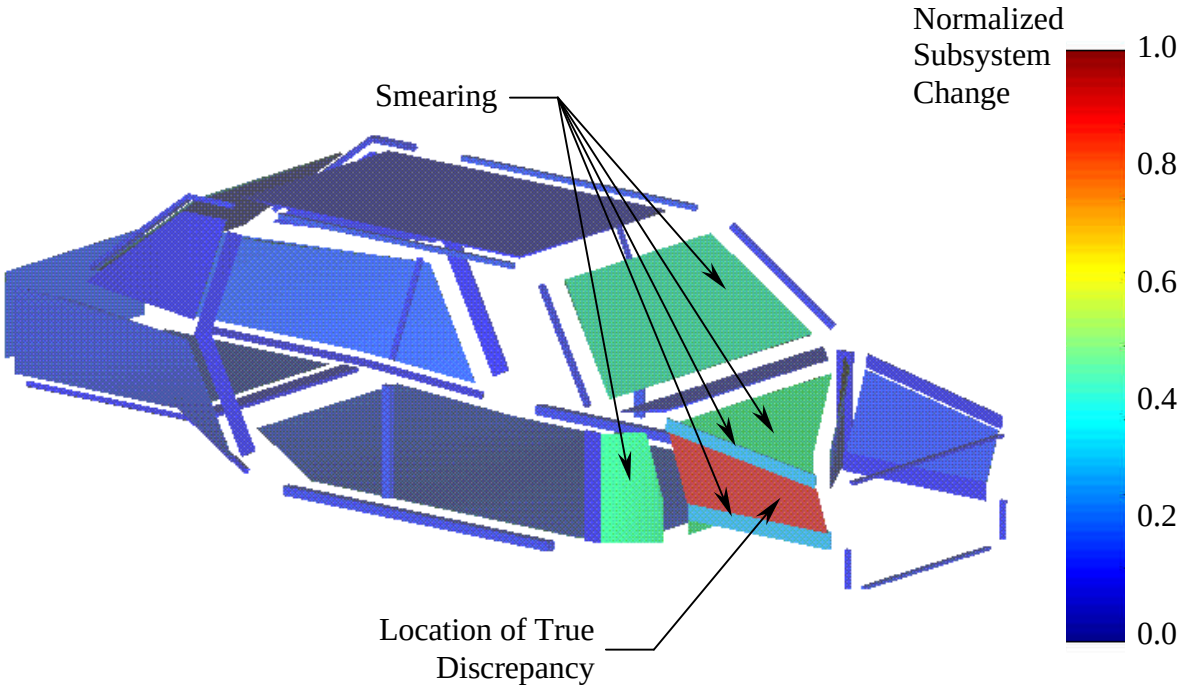

Figure 5.33 Identification of Structural Change

It can be seen that even though some smearing occurs, the PRM/SMI technique successfully identified the location of the structural change.

5.2.5 CONCLUSIONS

The results indicate that the power flow realization method and SEA model improvement procedure can be used to acquire SEA parameters for complex structures provided measurements are made carefully and that a reasonable initial computational SEA model exists. In this study, response was gathered at 20 of the 70 subsystems. Therefore, current methods, such as PIM, would require the acquisition of a 20 input by 20 output measurement matrix totaling 400 measurements per frequency band. For this structure, the PRM/SMI method required only a single column of the full 20 x 20 measurement matrix totaling only 20 measurements per frequency band. This represents a substantial savings in data acquisition and processing time.

6 SUMMARY AND RECOMMENDATIONS

Reliable, established techniques for the prediction of structural dynamic and structural acoustic response exist for frequency regions characterized by relatively long wavelengths and relatively wide natural frequency separations. In general, these regions are usually associated with lower frequencies. Specifically, considerable success has been obtained using finite element analysis (FEA) and boundary element analysis (BEA) methods over a wide range of system complexities.

Over time, experimental methods such as modal testing have evolved such that the current approach to constructing models of dynamic systems at low frequency consists, usually, of merging computational and test based methods. Testing is most often used to confirm and update computational models, ensure that design specifications are met, and to provide details regarding dynamic loads and constraints on motion.

The extension of computational FEA/BEA methods to high frequency regions associated by relatively shorter wavelengths and narrower natural frequency separations has proven difficult. In particular, model size and subsequent solution expense become very large due to the fine mesh required to resolve the response field. Furthermore, physical properties become highly sensitive to small variations in detail and boundary conditions, which increases uncertainty of the solutions. Finally, for very short wavelengths, even typical assumptions regarding ideal components become questionable, such as whether or not beam sections remain plane during deformation.

Predictive statistical energy analysis (SEA) methods have been used for approximately 40 years to overcome this difficulty, however, success has been reported in only a few disciplines and, hence, has yet to reach full acceptance. Similarly, experimental SEA is still considered to be in its infancy. Although some successes have been achieved for simple systems, a considerably limited amount of research has been conducted on the application of experimental SEA to complex systems. Furthermore, existing experimental approaches that can be applied in situ, such as the power injection method (PIM), require the acquisition of a large amount of data and can produce erroneous results.

Lessons learned from the merging of test and computational methods for low frequency systems inspire the techniques presented in this dissertation, the objective of which is to improve standard SEA procedures. In particular, a structured system identification method for obtaining a minimum order power flow model, the power flow realization method (PRM), is derived. It is found that a full matrix of measured inputs and outputs is not required for successful system identification as is the case with current methods such as PIM. Additionally, the method provides useful insight into system dimension and maintains the ability to extract parameters in the presence of measurement noise.

Furthermore, a method of using the PRM results to improve an existing predictive SEA model is derived. This method, given the name SEA model improvement (SMI), can be used to obtain physical parameters from experimental data. This has the potential to overcome the current difficulty, inherent with PIM, of identifying erroneous, non-physical SEA parameters.

It is shown, using a combination of simulations and experiments that the methods derived here are at least as accurate as current methods when applied to simple structures. Although a somewhat reasonable initial SEA model is required, PRM/SMI was found to be successful when applied to data collected from real tests conducted on a complex system. In fact, it was observed that, even with a very limited experimental data set, the techniques developed in this dissertation could quantify and locate a structural change down to the subsystem that was truly modified. This demonstrates a substantial advantage over current methods in data acquisition time alone. Indeed, the full set of measurements, required for PIM, could not even be obtained due the considerable time required to gather the data and the impracticality of positioning inputs at all of the subsystems of interest.

These results indicate that the methodologies presented have the potential to significantly enhance standard experimental SEA procedures. Furthermore, it is believed that these advances, although related to experimental methods, could benefit established and newer applications of predictive SEA by helping to provide insight into the accuracy of modeling techniques and assumptions.

It is recommended that additional effort be made to refine the methods developed here. Although it was not considered here at this early stage, it is also possible that the connectivity of an initial SEA model could be used as an additional constraint during the model improvement process to further reduce the production of erroneous non-physical results that can occur with both PRM/SMI and PIM. Furthermore, additional comparisons of the identification methods using test data on complex systems seem necessary to obtain a deeper understanding of the advantages and disadvantages of each.

REFERENCES

[1] Fahy, F., "Statistical Energy Analysis: A Critical Overview" in Statistical Energy Analysis: An Overview with Applications in Structural Dynamics, Ed. by Keane, A.J. and Price, W.G., Cambridge University Press, 1994.

[2] Sestieri, A., "Vibroacoustics Beyond 2000: Looking for the Sound of Silence" in Structural Dynamics at 2000: Current Status and Future Directions, Ed. by Ewins, D.J. and Inman, D.J., Research Studies Press Ltd., 2001.

[3] DE Langhe, K., "High Frequency Vibrations: Contributions to Experimental and Computational SEA Parameter Identification Techniques," Ph.D. Dissertation, Katholieke Universiteit Leuven, 1996.

[4] Powell, A., "On the Approximation to the 'Infinite' Solution by the Method of Normal Modes for Random Vibration," J. Acoustical Society of America, 30(12), pp. 1136-1139, 1958.

[5] Skudrzyk, E., "Vibration of a System with a Finite or an Infinite Number of Resonances," J. Acoustical Society of America, 30(12), pp. 1140-1152, 1958.

[6] Dowell, E.H., and Kubota, Y., "Asymptotic Modal Analysis and Statistical Energy Analysis of Dynamical Systems," J. Applied Mechanics, 52, pp. 949-957, 1985.

[7] Peretti, L.F., and Dowell, E.H., "Asymptotic Modal Analysis of a Rectangular Acoustic Cavity Excited by Wall Vibration," AIAA Journal, 30(5), pp. 1191-1198, 1992.

[8] Le Bot, A., and Jezequel, L., "Energy Formulation for One-Dimensional Problems," Proc. Acoustica 93, 1993.

[9] Lase, Y., Ichchou, M.N., and Jezequel, L., "Energy Flow Analysis of Bars and Beams: Theoretical Formulations," J. Sound and Vibration, 192(1), pp. 281-305, 1996.

[10] Ichchou, M.N, and Jezequel, L., "Comments on Simple Models of the Energy Flow in Vibrating Membranes and on Simple Models of the Energetics of Transversely Vibrating Plates," J. Sound and Vibration, 195(4), pp. 679-685, 1996.

[11] Le Bot, A., and Jezequel, L., "Energy Methods Applied to Transverse Vibrations of Beams," Proc. 4th Int. Conf. on Intensity Techniques, 1994.

[12] Le Bot, A., and Luzzato, E., "Smooth Energy Formulation for Multi-Dimensional Problems," Workshop on Methods in Medium and High Frequencies: The Alternatives to SEA," 1994.

[13] Sestieri, A., and Carcaterra, A., "An Envelope Energy Model for High Frequency Structural Problems," J. Sound and Vibration, 188(2), pp. 283-295, 1995.

[14] Carcaterra, A., and Sestieri, A., "Envelope versus Envelope-Phase Energy Model for High Frequency Vibrations," Proc. IMAC 13, 1994.

[15] Carcaterra, A., and Sestieri, A., "Complex Envelope Displacement Analysis: A Quasi-Static Approach to Vibrations," J. Sound and Vibration, 201(2), pp. 205-233, 1997.

[16] Pinnington, R.J., and White, R.G., "Power flow Through Machine Isolators to Resonant and Non-Resonant Beams," J. Sound and Vibration, 75(4), pp. 179-197, 1981.

[17] Cushieri, J.M., "Power Flow as a Complement to Statistical Energy Analysis and Finite Element Analysis," ASME Publication, NCA 3 (G00403), 1987.

[18] McCollum, M.D., and Cushieri, J.M., "Thick Plate Bending Wave Transmission Using a Mobility Power Flow Approach," J. Acoustical Society of America, 88(3), pp. 1472-1479, 1990.

[19] Lyon, R.H., Random Noise and Vibration in Space Vehicles, Shock and Vibration Information Center, United States Department of Defense, 1967.

[20] Lyon, R.H., and Maidanik, G., “Power Flow Between Linearly Coupled Oscillators,” J. Acoustical Society of America, 34(5), pp. 623-629, 1962.

[21] Smith, Jr., P.W., “Response and Radiation of Structural Modes Excited by Sound,” J. Acoustical Society of America, 34(5), pp. 640-647, 1962.

[22] Maidanik, G., "Response of Ribbed Panels to Reverberant Acoustic Fields," J. Acoustical Society of America, 34(6), pp. 809-826, 1962.

[23] Lyon, R.H., "Sound Radiation from a Beam Attached to a Plate," J. Acoustical Society of America, 34(9), pp. 1265-1268, 1962.

[24] Manning, J.E., and Maidanik, G., "Radiation Properties of Cylindrical Shells," J. Acoustical Society of America, 36(9), pp. 1691-1698, 1964.

[25] Lyon, R.H., and Eichler, E., "Random Vibration of Connected Structures," J. Acoustical Society of America, 36(7), pp. 1344-1354, 1964.

[26] Scharton, T.D., "Random Vibration of Coupled Oscillators and Coupled Structures," Sc. D. Dissertation, Massachussets Institute of Technology, 1965.

[27] Cremer, L., and Heckl, M., Structure-Borne Sound, Structural Vibrations and Sound Radiation at Audio Frequencies, Translated and Revised by Ungar, E.E., Springer-Verlag, 1973.

[28] Lyon, R.H., and DeJong, R. G., Theory and Application of Statistical Energy Analysis, 2nd Ed., Butterworth-Heinemann, 1995.

[29] Morse, P.M., and Feshback, H., Methods of Theoretical Physics, McGraw-Hill, 1953

[30] Keener, J.P., Principles of Applied Mathematics, Transformations and Approximations, Perseus Books, 1988.

[31] Langley, R.S., "A General Derivation of the Statistical Energy Analysis Equations for Coupled Dynamic Systems," J. Sound and Vibration, 135(3), pp. 499-508, 1989.

[32] Finnveden, S., "A Symmetric Formulation for Experimental Statistical Energy Analysis," J. Sound and Vibration, 223(1), pp. 161-169, 1999.

[33] Norton, M.P, Funamentals of Noise and Vibration Analysis for Engineers, Cambridge University Press, 1989.

[34] Fahy, F., Sound and Structural Vibration, Radiation, Transmission, and Response, Academic Press, 1985.

[35] Hart, F.D., and Shah, K.C., "Compendium of Modal Densities for Structures," NASA Contractor Report, CR-1773, 1971.

[36] Clarkson, B.L., "Experimental Determination of Modal Density" in Random Vibration - Status and Recent Developments, Ed. by Lyon, R.H., Elsevier Press, pp. 59-85, 1986.

[37] Manning, J.E., "Formulation of SEA Parameters Using Mobility Functions" in Statistical Energy Analysis: An Overview with Applications in Structural Dynamics, Ed. by Keane, A.J. and Price, W.G., Cambridge University Press, pp. 47-58, 1994.

[38] Clarkson, B.L., and Pope, R.J., "Experimental Determination of Modal Densities and Loss Factors of Flat Plates and Cylinders," J. Sound and Vibration, 77(4), pp. 535-549, 1981.

[39] Szechenyi, E., "Modal Densities and Radiation Efficiencies of Unstiffened Cylinders Using Statistical Methods," J. Sound and Vibration, 19(1), pp. 65-81, 1971.

[40] Keswick, P.R., and Norton, M.P., "A Comparison of Modal Density Measurement Techniques," Applied Acoustics, 20, pp. 137-153, 1987.

[41] Norton, M.P., and Greenhalgh, R., "On the Estimation of Loss Factors in Lightly Damped Pipeline Systems: Some Measurement Techniques and Their Limitations," J. Sound and Vibration, 105, pp. 397-423, 1986.

[42] Wu, L., Agren, A., and Sundback, U., "Determination of Loss Factors for Statistical Energy Analysis of a Diesel Engine with Geometric Averaging Approach, Acta Acustica, 2, pp. 127-142, 1994.

[43] Bies, D.A., and Hamid, S., "In Situ Determination of Loss and Coupling Loss Factors by the Power Injection Method," J. Sound and Vibration, 91, pp. 187-204, 1980.

[44] Lalor, N., "The Experimental Determination of Vibrational Energy Balance in Complex Structures," Proceedings SIRA Conference on Stress and Vibration, London, 1084-29, 1989.

[45] Ming, R.S., Stimpson, G., and Lalor, N., "On the Measurement of Individual Coupling Loss Factor in a Complex Structure," Proceedings Inter-Noise 90, pp. 961-964, 1990.

[46] Hodges, C.H., Nash, P., and Woodhouse, J., "Measurement of Coupling Loss Factors by Matrix Fitting: An Investigation of Numerical Procedures," Applied Acoustics, 22, pp. 47-69, 1987.

[47] Woodhouse, J., "An Introduction to Statistical Energy Analysis of Structural Vibration," Applied Acoustics, 14, pp. 455-469, 1981

[48] Clarkson, B.L., and Ranky, M.F., "On the Measurement of the Coupling Loss Factor of Structural Connections," J. Sound and Vibration, 94(2), pp. 249-261.

[49] Juang, J.N., and Pappa, R.S., "A Comparitive Overview of Modal Testing and System Identification for Control of Structures," Shock and Vibration Digest, 20(6), pp. 4-15, 1988.

[50] Kennedy, C.C., and Pancu, C.D.P., "Use of Vectors in Vibration Measurement and Analysis," J. Aero. Sci., 14(11), pp. 603-625, 1947.

[51] Lewis, R.C., and Wrisley, D.L., "A System for the Excitation of Pure Natural Modes of a Complex Structure," J. Aero. Sci., 17(11), pp. 705-722, 1950.

[52] Vold, H., Kundrat, J.A., Rocklin, G.T., and Russell, R., "A Multi-Input Modal Estimation Algorithm for Mini-Computers," SAE Paper 820194, 1982.

[53] Leuridan, J.M., "Some Direct Parameter Model Identification Methods Applicable for Multiple Input Modal Analysis," Ph.D. Dissertation, Univ. Cincinnati, 1984.

[54] Craig, Jr., R.R., and Blair, M.A., "A Generalized Multiple-Input, Multiple-Output Parameter Estimation Algorithm," AIAA J., 23(6), pp. 931-937, 1985.

[55] Zhang, L., Kanda, H., Brown, D.L., and Allemang, R.J., "A Polyreference Frequency Domain Method for Modal Parameter Identification," ASME Paper 85-DET-106, 1985.

[56] Prevosto, M., Olagnon, M., and Benveniste, A., “ARMA Modelization: A Solution to Modal Parameter Estimation,” Proceedings 11th International Seminar Modal Analysis, K.U. Leuvan, Paper W1-3, 1986.

[57] Ho, B.L., and Kalman, R.E., “Effective Construction of Linear State-Variable Models from Input/Output Data,” Proceedings 3rd Annual Allerton Conference on Circuit and System Theory, pp. 449-459,1965.

[58] Juang, J.-N., and Pappa, R.S., “An Eigensystem Realization Algorithm for Modal Parameter Identification and Model Reduction,” J. Guidance, Control, and Dynamics, 8(5), pp. 620-627, 1985.

[59] Juang, J.-N., “Mathematical Correlation of Modal-Parameter-Identification Methods Via System Realization Theory,” International J. of Analytical and Experimental Modal Analysis, 2(1), pp. 1-18, 1987.

[60] Berman, A., and Nagy, E.J., “Improvement of a Large Analytical Model Using Test Data,” AIAA J., 21, pp. 1168-1172, 1983.

[61] O’Callahan, J.C., Avitabile, P., and Leung, R., “Development of Mass and Stiffness Matrices for an Analytical Model Using Experimental Modal Data,” Proceedings 2nd International Modal Analysis Conference, pp. 585-589, 1984.

[62] O’Callahan, J.C., and Chou, C.M., “Localization of Model Errors in Optimized Mass and Stiffness Matrices Using Modal-Test Data,” International J. of Analytical and Experimental Modal Analysis, 4(1), 1989.

[63] Van Karsen, C., “Sensitivity Analysis Based on Experimental Modal Parameters,” Proceedings SEM Spring Conference on Experimental Mechanics, pp. 890-894, 1985.

[64] Ljung, L., System Identification: Theory for the User, 2nd Ed., Prentice Hall, 1999.

[65] Manning, J.E., and Lee, K., “Predicting Mechanical Shock Transmission,” The Shock and Vibration Bulletin, 37(4), pp. 65-70, 1968.

[66] Mercer, C.A., Rees, P.L., and Fahy, F.J., “Energy Flow Between Two Weakly Coupled Oscillators Subject to Transient Excitation,” J. Sound and Vibration, 15(3), pp. 373-379, 1971.

[67] Sun, H.B., Sun, J.C., and Richards, E.J., “Prediction of Total Loss Factors of Structures Part III: Effective Loss Factors in Quasi-transient Conditions,” J. Sound and Vibration, 106(3), pp. 465-479, 1986.

[68] Powell, R.E., and Quartarara, L.R., “Statistical Energy Analysis of Transient Vibration,” Statistical Energy Analysis, ASME, NCA-Vol. 3, Winter Annual Meeting of ASME, pp. 3-8, 1987.

[69] Pinnington, R.J., and Lednik, D., “Transient Statistical Energy Analysis of an Impulsively Excited Two Oscillator System,” J. Sound and Vibration, 189(2), pp. 249-264, 1996.

[70] Pinnington, R.J., and Lednik, D., “Transient Energy Flow Between Two Coupled Beams,” J. Sound and Vibration, 189(2), pp. 265-287, 1996.

[71] Hall, H.S., "Exploration into the Validity of Transient Statistical Energy Analysis," M.S. Thesis, North Carolina State University, 2002.

[72] Juang, J.N., Applied System Identification, Prentice Hall, 1994.

[73] Pappa, R.S., and Juang, J.N., "Galileo Spacecraft Modal Identification Using an Eigensystem Realization Algorithm," J. Astronautical Sciences, 33(1), pp. 15-33, 1985.

[74] Juang, J.N., and Pappa, R.S., "Effect of Noise on Modal Parameters Identified by the Eigensystem Realization Algorithm," J. Guidance, Control, and Dynamics, 9(3), pp. 294-303, 1986.

[75] Longman, R.W., and Juang, J.N., "A Variance Based Confidence Criterion for ERA Identified Modal Parameters," Advances in the Astronautical Sciences, 65(1), pp. 581-600, 1987.

[76] Longman, R.W., and Juang, J.N., "Variance and Bias Confidence Criteria for ERA Modal Parameter Identification," Proceedings AIAA/AAS Astrodynamics Conference, pp. 729-739, 1988.

[77] Bergmann, M., Longman, R.W., and Juang, J.N., "Variance and Bias Computation for Enhanced System Identification," Proceedings 28th IEEE Conference on Decision and Control, pp. 155-161, 1989.

[78] Juang, J.N, Cooper, J.E., and Wright, J.R., "An Eigensystem Realization Algorithm Using Data Correlations (ERA/DC) for Modal Parameter Identification," J. Control Theory and Advanced Technology, 4(1), pp. 5-14, 1988

[79] Wagie, D.A., and Skelton, R.E., "A Projection Approach to Covariance Equivalent Realizations of Discrete Systems," IEEE Transactions on Automatic Control, AC-31, pp. 1114-1120, 1986

[80] Anderson, B.D., and Skelton, R.E., "Generation of All Markov Covers," IEEE Transactions on Ciruits and Systems," 35(4), pp. 375-384, 1988.

[81] King, A.M, Desai, U.B., and Skelton, R.E., "A Generalized Approach to Q-Markov Covariance Equivalent Realization of Discrete Systems," Automatica, 24(4), pp. 507-515, 1988.

[82] Longman, R.W., Lew, J.S., Tseng, D.H., and Juang, J.N., "Variance and Bias Computation for Improved Modal Identification Using ERA/DC," 1991 American Control Conference, 1991.

[83] Horta, L.G., and Juang, J.N., "Identifying Approximate Linear Models for Simple Non-linear Systems," J. Guidance, Control, and Dynamics, 9(4), pp. 385-390, 1986.

[84] Juang, J.N., and Suzuki, H., "An Eigensystem Realization Algorithm in Frequency Domain for Modal Parameter Identification," J. Vibration, Acoustics, Stress and Reliability in Design, 110(1), pp. 24-29, 1988.

[85] Juang, J.N., "Mathematical Correlation of Modal Parameter Identification Methods Via System Realization Theory," International J. of Analytical and Experimental Modal Analysis, 2(1), pp. 1-18, 1987.

[86] Longman, R.W., and Juang, J.N., "A Recursive Form of the Eigensystem Realization Algorithm," J. Guidance, Control, and Dynamics, 12(5), pp. 647-652, 1989.

[87] Lew, J.S., Juang, J.N., and Longman, R.W., "Comparison of Several System Identification Methods for Flexible Structures," Paper 91-0947, Proceedings AIAA 32nd Structures, Structural Dynamics and Materials Conference, 1991.

[88] Huang, J.K., Juang, J.N., and Chen, C.W., "Single Mode Projection Filters for Identification and State Estimation of Flexible Structures," J. Guidance, Control, and Dynamics, 12(4), pp. 568-576, 1989.

[89] Phan, M., Juang, J.N., and Longman, R.W., "Identification of Linear Multivariable Systems from a Single Set of Data by Identification of Observers with Assigned Real Eigenvalues," Paper 91-0949, Proceedings AIAA 32nd Structures, Structural Dynamics and Materials Conference, 1991.

[90] Pappa, R.S., and Juang, J.N., "Some Experiences with the Eigensystem Realization Algorithm," Sound and Vibration, 22(1), pp. 30-35, 1988.

[91] Pappa, R.S., "ERA Modal Identification Experiences with Mini-Mast," Proceedings 2nd USAF/NASA Workshop on System Identification and Health Monitoring of Precision Space Structures, 1990.

[92] Juang, J.N., and Lew, J.S., "Integration of System Identification and Robust Controller Designs for Flexible Structures in Space," Paper AIAA-90-3467-CP, Proceedings AIAA Guidance, Navigation, and Control Conference, pp. 1361-1375, 1990.

[93] Phan, M., Juang, J.N., and Longman, R.W., "Recent Developments in Learning Control and System Identification for Robots and Structures," Proceedings 1990 Conference on Dynamics of Flexible Structures in Space, pp. 321-334, 1990.